INFORMATION TO USERS

This material was produced from a microfilm copy of the original document. While the most advanced technological means to photograph and reproduce this document have been used, the quality is heavily dependent upon the quality of the original submitted.

The following explanation of techniques is provided to help you understand markings or patterns which may appear on this reproduction.

1. The sign or "target" for pages apparently lacking from the document photographed is "Missing Page(s)". If it was possible to obtain the missing page(s) or section, they are spliced into the film along with adjacent pages. This may have necessitated cutting thru an image and duplicating adjacent pages to insure you complete continuity.

2. When an image on the film is obliterated with a large round black mark, it is an indication that the photographer suspected that the copy may have moved during exposure and thus cause a blurred image. You will find a good image of the page in the adjacent frame.

3. When a map, drawing or chart, etc., was part of the material being photographed the photographer followed a definite method in "sectioning" the material. It is customary to begin photoing at the upper left hand corner of a large sheet and to continue photoing from left to right in equal sections with a small overlap. If necessary, sectioning is continued again – beginning below the first row and continuing on until complete.

4. The majority of users indicate that the textual content is of greatest value, however, a somewhat higher quality reproduction could be made from "photographs" if essential to the understanding of the dissertation. Silver prints of "photographs" may be ordered at additional charge by writing the Order Department, giving the catalog number, title, author and specific pages you wish reproduced.

5. PLEASE NOTE: Some pages may have indistinct print. Filmed as received.

Xerox University Microfilms
300 North Zeeb Road
Ann Arbor, Michigan 48106

FIELD-ALIGNED AND IONOSPHERIC CURRENTS

A

DISSERTATION

Presented to the Faculty of the

University of Alaska in Partial Fufillment

of the Requirements

for the Degree of

DOCTOR OF PHILOSOPHY

By

Fumihiko Yasuhara, B.S., M.S.

Fairbanks, Alaska

May , 1975

FIELD-ALIGNED AND IONOSPHERIC CURRENTS

RECOMMENDED: _____ *

_____

_____

_____

_____
Chairman, Advisory Committee

APPROVED:

_____ by _____
Director, Geophysical Institute

_____
Date

_____
Vice President for Research

_____
Date

ABSTRACT

This thesis presents a study of the distribution of the electric current ($\vec{I}$), potential (ϕ) and field ($\vec{E}$) in the ionosphere for the 'observed' distribution of field-aligned currents ($j_{\parallel}$). The field-aligned current represents one of the most important aspects of the coupling between the ionosphere and the magnetosphere.

On the basis of magnetic records from the TRIAD satellite, it is found that the poleward field-aligned current is more intense than the equatorward current, the average ratio being 2:1. By using this, together with the known direction of $j_{\parallel}$, the current continuity equation $\vec{\nabla} \cdot \vec{I} = j_{\parallel}$ is solved for several models of the ionosphere with one or two high conductive annular rings. The following results are obtained:

1) The actual field-aligned and ionospheric current system is a complicated combination of current systems proposed in the past. The amount of the N-S closure is determined by the amount of the equatorward $j_{\parallel}$. The amount of the E-W closure depends mainly on the conductivity distribution.

2) The N-S closure current has a large westward deflection, contributing significantly to the westward electrojet. In the evening sector, the eastward electrojet can be totally attributed to a similar, eastward deflection of the N-S closure current. The models with two different conductive annular rings can reproduce the Harang discontinuity.

3) The present models can reproduce the electric field profile across the polar cap, observed by satellites.

4) The degree of the penetration of the high latitude convection electric field into lower latitudes depends significantly on the presence

of the high conductive belt and its location with respect to the field-aligned currents.

5) The distributions of the ionospheric current, potential and electric field during early phases of the substorm are simulated by a series of models, and the results are interpreted in the light of the above conclusions, (1)-(5).

ACKNOWLEDGEMENTS

I wish to express my sincerest gratitude to Prof. Syun-Ichi Akasofu. To him, I am deeply indebted for his guidance, advice, great patience and strongest encouragement in completing this manuscript.

My thanks go to Prof. D. W. Swift for his careful reading of the manuscript and for suggesting the over-all view of the magnetospheric process discussed in Chapter VI. I wish to thank Prof. R. Parthasarathy, Mr. H. C. Stenbaek-Nielsen, Dr. E. W. Wescott and Prof. C. R. Wilson, who are the members of my committee, for their thorough reading of the manuscript. To Prof. T. Neil Davis, I am especially grateful for the careful manner in which he read the manuscript and for pointing out and correcting some obscure passages.

I wish to thank also Prof. H. Maeda, Geophysical Institute, Kyoto University, who suggested I continue my graduate study at the University of Alaska.

The great and various help given by Dr. Y. Kamide in the course of the preparation of this manuscript, as well as his warm friendship, are gratefully acknowledged.

I wish to thank Miss Shirley Liss for her assistance in writing the computer programs.

My thanks also go to my old fellow students Drs. K. Kawasaki and Paul P. Perreault, who willingly continued to help me to live my first life in a foreign country.

The research in this dissertation was supported by the National Science Foundation through Grants GA-36873X and DES74-23832.

TABLE OF CONTENTS

LIST OF ILLUSTRATIONS

LIST OF TABLES

LIST OF SYMBOLS

A(superscript)	value in the auroral oval
B	magnetic induction
$\vec{b}$	unit vector in the direction of the magnetic field
E	electric field
$\vec{e}_r$	unit vector in the radial direction from the center of the earth
H	horizontal component of the earth's magnetic field
I	intensity of the field-aligned current sheets (ampere/unit length)
I	height integrated density of the ionospheric current (ampere/unit length)
I^T	total intensity of the field-aligned currents (ampere)
i	average current density of the field-aligned currents (ampere/unit area)
J	current function
$j_{\parallel}$	field-aligned current density (ampere/unit area)
L	latitudinal thickness of the field-aligned current sheets
M(superscript)	value in the middle- and low-latitude region
MLT	magnetic local time
N(subscript)	quantity related to the poleward field-aligned current
P(superscript)	value in the polar cap
S(subscript)	quantity related to the equatorward field-aligned current
V	plasma velocity
Z	vertical component of the earth's magnetic field
α	azimuthal angle reckoned clockwise from the noon meridian

γ	unit of B ($=10^{-5}$ gauss)
θ	colatitude
λ	latitude
μ	permeability of vacuum
Σ_P	height-integrated ionospheric Pedersen conductivity
Σ_H	height-integrated ionospheric Hall conductivity
τ	characteristic time
ϕ	electric potential
$\Delta\phi$	potential difference across the polar cap along the dawn-dusk meridian
$\Delta\phi(\theta)$	magnitude of the variation of the potential along the circle of colatitude θ
$(\Delta\phi)_t$	total potential difference across the polar cap
χ	inclination
ψ	azimuthal angle reckoned counter-clockwise from the midnight meridian
$\rightarrow$	symbol for a vectorial quantity or operator

CHAPTER I

INTRODUCTION

Various types of three-dimensional current systems associated with the magnetospheric substorm have been proposed in the past. For convenience, these may be classified into six types (a), (b).....(f), as schematically indicated in Figure 1.1. Types (a), (c) and (d) are essentially the same, and were originally proposed by Birkeland. The major feature is a pair of field-aligned currents interconnected by an E-W segment of ionospheric current. Type (b) was proposed by Chapman, and the current system is entirely confined on a spherical shell (the ionosphere). Alfvén type (c) is a combination of two Birkeland types (in fact, Birkeland considered such a combination). Boström type (1) in (d) is essentially the same as (a), but he examined the closure of the field-aligned currents in the magnetotail.

The Boström type (2) in (e) is significantly different from (a)-(d), in that he proposed a pair of field-aligned currents closed by a N-S segment of ionospheric current. Further, an E-W ionospheric current is generated between the feet of the two field-aligned currents and closes across the polar cap and the middle- and low-latitude belt. (Thus, it is a purely two-dimensional current system.) The Zmuda-Armstrong type in (f) consists of two such pairs of field-aligned currents, one in the evening sector and the other in the morning sector.

In determining the relationship between the field-aligned currents and the ionospheric currents, it is vital to know accurately the distribution of the field-aligned currents. Therefore, in the first part of the present thesis (Chapter II), TRIAD satellite data are analyzed.

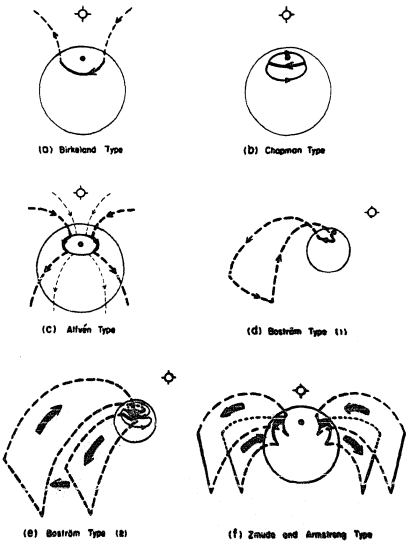

Figure 1.1 Some of the three-dimensional current systems proposed in the pa:

The TRIAD satellite is the first polar orbiting satellite to carry a tri-axial magnetometer. Armstrong and Zmuda (1973) and Zmuda and Armstrong (1974a) have already reported some initial results on the local time dependence (averaged over 3-hour intervals) of the field-aligned current distribution. In their third paper (Zmuda and Armstrong, 1974b), they examined characteristics of the field-aligned currents and showed that downward and upward field-aligned currents appear as a pair at all local times (except in the noon sector).

In this thesis, some new results of the study on TRIAD satellite data are reported. This study began as a joint project with Zmuda and Armstrong in January 1973 by establishing a mobil tracking station at the Geophysical Institute, University of Alaska, Fairbanks. This particular report is based on records of 206 passes along the Alaska meridian (January to May, 1973).

The second part of the thesis (Chapters III, IV and V), examines how the observed distribution of the field-aligned currents is related to ionospheric currents. For this purpose, the ionospheric current distribution $\vec{I}$ is computed by solving the continuity equation

$$\vec{\nabla} \cdot \vec{I} = j_{\parallel}$$

for specific distributions of $j_{\parallel}$ for several model ionospheres. This equation has been studied extensively for various ionospheric models and various 'driving sources' to examine the convection pattern of magnetospheric plasma (Fejer, 1964; Jaggi and Wolf, 1973; Swift, 1967 and 1971; Vasyliunas, 1970 and 1971; and Wolf, 1970). The results will be discussed first in terms of the rotation of the potential distribution in the polar cap and also of the penetration of the polar cap electric

field to lower latitudes. The results will be also discussed in detail by referring to various model calculations of the ionospheric current systems (Iwasaki and Nishida, 1967; Mal'tsev et al., 1973; Maeda and Maekawa, 1973) and three-dimensional current systems which have been proposed in the past. In particular, a set of models are shown to simulate variations of the ionospheric currents during a magnetospheric substorm.

CHAPTER II

DISTRIBUTION OF THE FIELD-ALIGNED CURRENTS

2.1 TYPICAL EXAMPLES OF TRIAD DATA

A complete description of the TRIAD instrumentation can be found in a paper by Armstrong and Żmuda (1973): the orbit of this polar orbiting satellite can be considered to be circular at an altitude of 800 km. Outputs from the three magnetometer axes are sampled sequentially at a rate of 2.25 samples/axes/second to a resolution of 12γ. When the satellite passes over Alaska, the orientation of the magnetometer is such that the three sensors point approximately in the magnetic east-west, north-south, and parallel to the main field directions, respectively, during the period when the data used in the present analysis were obtained.

As has been shown by Armstrong and Żmuda (1973), the largest magnetic perturbation at auroral latitudes is primarily in the magnetic east-west direction. Thus, the total perturbation field arises mainly from field-aligned current sheets which lie extensively in the magnetic east-west direction.

Figure 2.1 provides an example of typical TRIAD data, together with relevant data [such as the orbit projected at a 100 km level along geomagnetic field lines on a geographic map, magnetic records from the standard auroral zone stations (combined to give the AU, AL and AE indices), the H and Z component perturbations along the Alaska meridian]. It can be seen that the east-west component of the TRIAD data shows a large westward deviation after 1022 UT (invariant latitude $\sim 65°$). This particular set of data was examined in detail by Armstrong et al. (1974)

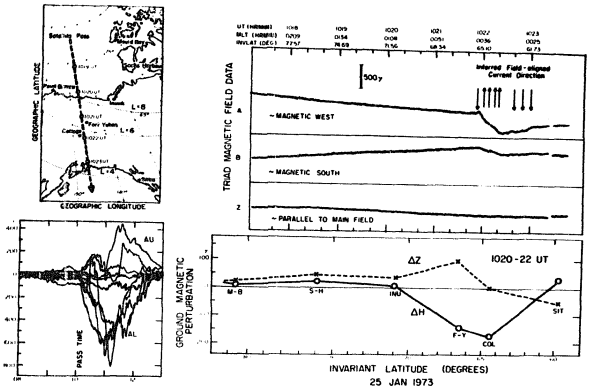

Figure 2.1 An example of typical TRIAD data, together with the relevant circumstantial data. From the top left, clockwise, the orbit projected down to the 100km altitude along geocangnetic field lines, three components of magnetic field perturbation measured by TRIAD, the combined magnetogram from the standard auroral zone stations (Leirvogur, Great Whale River, Fort Churchill, Meanook, College, Tixie Bay, Dixon Island and Kiruna) and the H and Z components of the ground magnetic perturbation at the Alaska meridian chain of stations (Mould Bay, Sachs Harbour, Inuvik, Fort Yukon, College and Sitka).

in conjunction with the simultaneous auroral photographs. The inferred distribution of the field-aligned currents is shown by arrows. This orbit took place during an early epoch of a substorm, and the center of the westward electrojet in the Alaska meridian sector was in the vicinity of College at that time (see the ΔZ component).

In TRIAD data, it is important to note that the westward deviation often does not recover fully at the end of the tracking from Fairbanks (namely, the trace does not merge with the extrapolated line from the poleward trace). This tendency is often apparent even when the tracking was extended to the invariant latitude as low as 55°. Figure 2.2 shows several typical examples of such data. The extrapolation of the poleward and the equatorward traces of each path are shown by dashed lines. These dashed lines do not match. In Section 3, we show that this tendency can be explained by supposing that the intensities of the inflow and the outflow field-aligned currents are not equal.

It should also be noted that the examples (b)-(f) in Figure 2.2 are chosen from the same local time sector (15-16 MLT), but the corresponding magnetic activities (expressed by the Kp index) are quite different. There is a significant equatorward shift of the field-aligned current regions as magnetic activity increases. The last example will be discussed in the next section. The arrow α in the top trace of Figure 2.2 gives the poleward edge of the magnetic perturbation region (at which the east-west component of the perturbation begins to deviate from the extrapolation of the observed poleward field trace). Similarly, the arrow β gives the equatorward edge determined by using the extrapolation of the observed equatorward field trace.

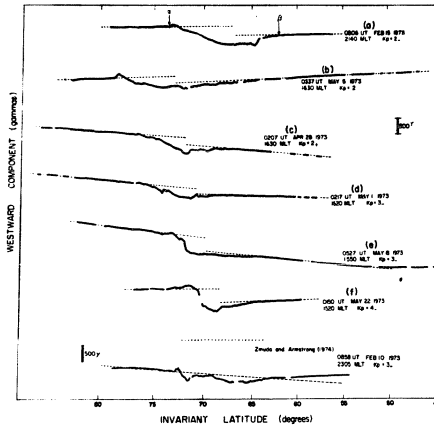

Figure 2.2 Several typical examples of the westward component of the magnetic field perturbations observed by TRIAD. The dashed lines are extrapolation from both the poleward and equatorward portions of the traces. The arrows α and β in the top trace indicate the poleward and equatorward edges of the perturbation regions.

Note that the examples (b)-(f) are chosen from the same local time sector (15-16 MLT), but at the time of different magnetic activities (greater activity toward the bottom). The equatorward shift of the field-aligned current region with magnetic activity can be easily seen. The last trace is one of the examples studied by Zmuda and Armstrong (1974b). The dashed line shows their base-line.

2.2 THE GENERAL DISTRIBUTION PATTERN

In Figures 2.3, 2.4 and 2.5, the distribution of the eastward (a solid line) and the westward (a dotted line) magnetic perturbations approximately along all available orbits are shown in the invariant latitude - magnetic local time coordinates. Question marks shown in these figures indicate either the point α or β is not obtainable due to incomplete data. The TRIAD data are grouped into three, depending on the different degrees of geomagnetic activity when each pass took place, namely Kp $\leq$ 2+ (representing relatively quiet conditions, 3- $\leq$ Kp $\leq$ 4+ (representing moderately disturbed conditions) and Kp $\geq$ 5- (representing disturbed conditions). Each figure includes also an appropriate statistical auroral oval (Q = 2, 5 and 7 for Figures 2.3, 2.4 and 2.5, respectively); the ovals are taken from Feldstein and Starkov (1967). In the following, we describe main results of this study.

As reported by Żmuda and Armstrong (1974b), the direction of the east-west magnetic disturbances is reversed with respect to the noon-midnight meridian, or perhaps more accurately the 13-01 MLT meridian. In the evening sector, the observed magnetic perturbation is mostly directed eastward. This eastward perturbation can be produced by a pair of field-aligned currents, one flowing away from the ionosphere on the poleward side of the auroral oval, and the other flowing into the ionosphere on the equatorward side. In the morning hours, the directions of the current pair are reversed, namely one flowing into the ionosphere on the poleward side of the auroral oval and the other flowing out from the equatorward edge of the oval.

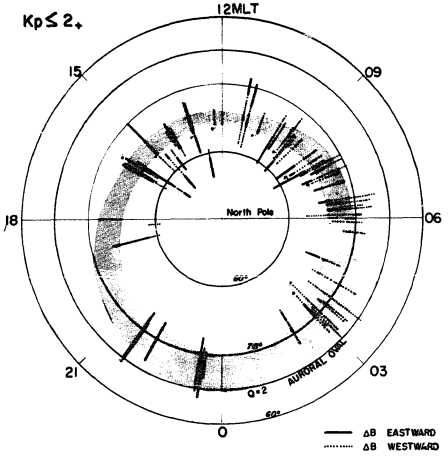

Figure 2.3 The regions of the eastward (a solid line) and westward (a dotted line) magnetic perturbations approximately (within accuracy of ±1 hour) along the orbits of TRIAD for Kp≤2+ (relatively quiet conditions) in invariant latitude-magnetic local time coordinates. They are superposed on the statistical auroral oval of Q=2. A question mark at the end(s) of the lines indicates that the point α or β in Fig. 2.2 is not obtainable because of incomplete data.

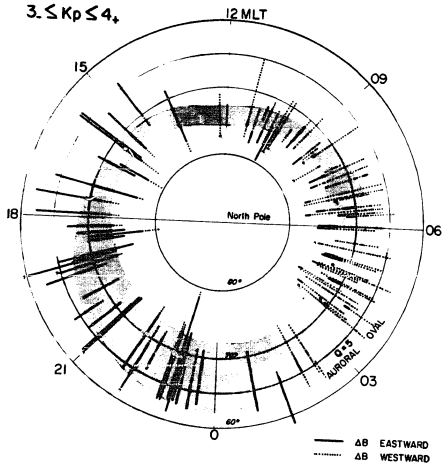

Figure 2.4 Same as Figure 2.3 except for the magnetic condition. This is for 3-≤Kp≤4 (moderately disturbed conditions) and the oval is for Q=5.

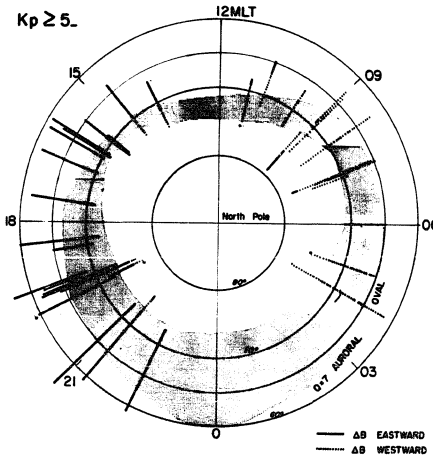

Figure 2.5 Same as Figure 2.3 except for the magnetic condition. This is for Kp.5 (highly disturbed conditions) and the Q=7 oval.

In the pre-midnight sector, an increase of the eastward perturbation is often accompanied by a smaller westward perturbation in a narrow latitudinal region just poleward of it. This can be seen in (a), (b) and (f) in Figure 2.2. Similarly, in the morning sector, an increase of the westward perturbation is sometimes accompanied by a smaller eastward perturbation. These weak variations indicate that there exist weak field-aligned currents flowing toward (in the evening sector) and away from (in the morning sector) the ionosphere near the poleward boundary of the auroral oval. However, these minor currents will not be considered here.

2.3 THE RELATIONSHIP WITH THE STATISTICAL OVAL

There is a reasonable agreement between the region of the field-aligned currents and the statistical oval for each of the three magnetic conditions. The extent of the field-aligned current region, particularly the equatorward boundary, expands with increasing geomagnetic activity.

(i) During relatively quiet periods ($Kp \leq 2+$), the region of the magnetic perturbations associated with the field-aligned currents lies approximately along the statistical oval of $Q = 2$, except for a significant deviation along the poleward boundary in the day sector. There, the magnetic perturbation occurs well poleward of the $Q = 2$ oval.

(ii) During moderately disturbed periods ($3- \leq Kp \leq 4+$), the region of the field-aligned currents coincides reasonably well with the statistical oval of $Q = 5$.

(iii) During disturbed periods ($Kp \geq 5-$), the region of the eastward magnetic perturbation in the evening sector (14-21 MLT) is not confined in the statistical oval and expands well equatorward of the

oval, to as far as the latitude circle of approximately 60°.

2.4 RATIO OF THE INTENSITY OF THE POLEWARD AND EQUATORWARD FIELD-ALIGNED CURRENTS

Consider two infinite current sheets, carrying currents in opposite directions with intensities I_1 and I_2. Here, the intensities I_1 and I_2 are defined as sheet current densities in units of ampere per unit length along the sheets. Then, the relationship between I_1, I_2 and the magnetic field intensity in the three regions (I, II and III as shown in Figure 2.6a separated by the two current sheets) is given by

$$B_1 = B_I - B_{II} = \mu I_1,$$
$$B_2 = B_{III} - B_{II} = \mu I_2 \qquad (2.1)$$

where B_1 denotes the total range of the magnetic deviation across Regions I and II, and B_2 denotes the deviation across Regions II and III and μ is the permeability of a vacuum. Thus, knowing the values of B_1 and B_2, we can obtain the sheet current intensities I_1 and I_2.

This relationship holds among I_1, I_2, B_1 and B_2 even for a pair of infinite current sheets of finite thickness in which the current is distributed. In such a case, the intensities I_1 and I_2 of the two current sheets are the current densities integrated over the thickness of each current sheet, thus their unit is also ampere per unit length along the sheets.

In Figure 2.6b, this relationship for the current sheets of finite thickness is illustrated. In this figure, the lower part shows schematically a typical TRIAD trace of the east-west component of the magnetic

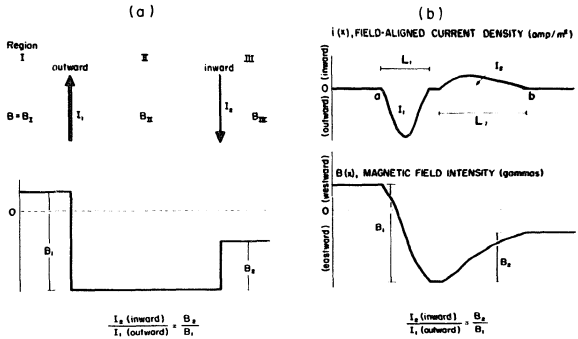

Figure 2.6 The schematic diagrams which show the relationship between the distribution of the two current sheets (of infinite extent in the east-west direction) and of the associated magnetic field. (a) For the two current sheets of infinitesimal thickness. (b) For the two current sheets of a finite thickness. The two points a and b in the upper diagram of Fig. 2.6b correspond to the points a and b in Figure 2.2.

perturbation and the upper part shows schematically the corresponding current distribution. Here the two sheet currents I_1 and I_2 correspond to the poleward and the equatorward field-aligned currents in the evening sector, respectively.

It should be noted that if points a and b in Figure 2.6b are not identified, it is not possible to obtain I_1 and I_2. For the period from January to May, 1973, 29 passes (out of 206) are chosen, in which these two points could be clearly identified. In many other cases, either point a or b was located beyond the limit of the tracking. Note also that all of these 29 passes used here lie in the evening-midnight sector and all data from the midnight-morning sector are so complicated that the method mentioned above is not applicable.

Note also that if the perturbation is assumed to be confined in the region between a and b (namely, if one assumes that the line connecting B(x=a) and B(x=b) is the base-line), it is equivalent to assuming that the intensities of the poleward and the equatorward currents are equal. (See Equation (2.1)). This practice, employed by Żmuda and Armstrong (1974b), for at least a few cases, is illustrated in the last example in Figure 2.2 (a dashed line), although it is quite obvious that the polar and equatorial extrapolation lines (not shown) do not match.

For later use, we define the current densities i_1 and i_2 as follows:

$$i_1 = I_1/L_1$$

$$i_2 = I_2/L_2$$

where L_1 and L_2 are the thickness of the two infinite current sheets as

shown in Figure 2.6. The results deduced from the TRIAD data are shown in Figures 2.7 and 2.8.

Figure 2.7 shows the relationship between I_1 and I_2, together with three lines $I_2/I_1 = 1.0$, $I_2/I_1 = 0.5$ and $I_2/I_1 = 0.2$. Although the ratio varies considerably, most points lie between the two lines $I_2/I_1 = 1.0$ and $I_2/I_1 = 0.2$. It is thus quite clear that I_1 is, in general, greater than I_2.

In the upper part of Figure 2.8, the current intensities (I_1, I_2) are shown as a function of the Kp index. Open circles are for the outflow current and dots for the inflow current. Since these points are all from the evening-midnight sector (for the reasons mentioned in the above), the open circles are also for the poleward sheet current and the dots for the equatorward one. It can be seen that the rate of the increase with Kp is different for the northern and southern sheets. Within the Kp range examined, the intensity of the poleward current sheet increases by an order of magnitude, while that of the equatorward one by a factor of only about 2. Therefore, the poleward current sheet is related more closely with geomagnetic activity than the equatorward current sheet. This can be seen more clearly in the lower part of Figure 2.8, where the average current densities (i_1, i_2) of the two current sheets are plotted as a function of the Kp index. The current density i_1 increases considerably with Kp ($0.5 \sim 2.5 \times 10^{-6}$ amp/m^2), while i_2 is rather constant ($0.4 \pm 0.2 \times 10^{-6}$ amp/m^2), regardless of the values of Kp. This fact suggests that the latitudinal width of the inflow current region increases with Kp.

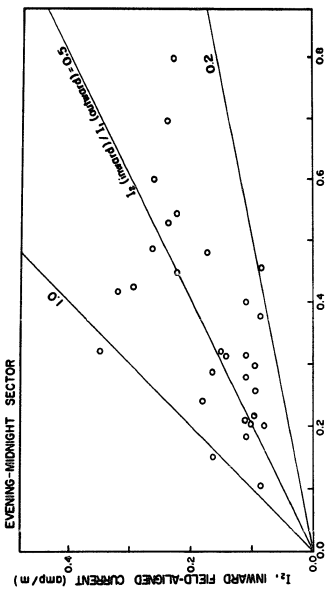

Figure 2.7 Relation between the intensities of the poleward and equatorward field-aligned currents. The lines for the ratio I_2/I_1 of 1.0, 0.5 and 0.2 are shown. The data points are from paths in the evening-midnight sector. Thus, I_1 (outward) is for the poleward current sheet and I_2 (inward) for the equatorward one.

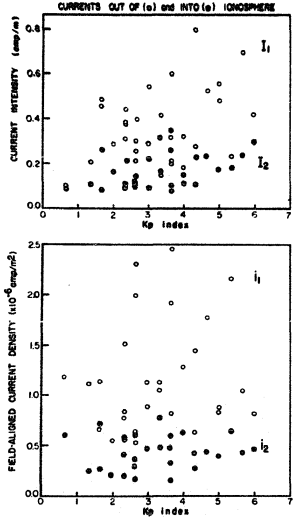

Figure 2.8 (a) The current intensities (I_1, I_2) of the two current sheets as a function of the Kp index. (b) The average current densities (i_1,i_2) of the two current sheets as a function of the Kp index.

The average current densities i_1 and i_2 are obtained by dividing I_1 and I_2 by the latitudinal width of the two current sheets, respectively.

The open circles are for the poleward sheet current (out of the ionosphere) and the closed circles for the equatorward one (into the ionosphere).

CHAPTER III

FORMULATION AND MODELS

The purpose of this chapter and the next chapter is to examine what pattern of the ionospheric potential exists under the 'observed' distribution of the field-aligned currents and how the 'observed' distribution of the field-aligned currents is related to ionospheric currents. More specifically, the distributions of ionospheric potential and currents for a given distribution of field-aligned currents for several model ionospheres are obtained. In this chapter, the formulation of the problem and the description of the models used for the calculations are given.

3.1 FORMULATION

In a steady state, the current continuity equation for the ionosphere is given by

$$\vec{\nabla} \cdot \vec{I} = j_{\shortparallel} \sin \chi \qquad (3.1)$$

Here, $\vec{I}$ is the height-integrated current density (amp/m) in the ionosphere and $j_{\shortparallel}$ is the density of field-aligned current (amp/m^2) (positive for a downward current and negative for an upward current). The inclination angle χ of a geomagnetic field line with respect to the ionosphere is hereafter taken to be 90°; this is a reasonable approximation at latitudes higher than 60°.

Assuming $j_{\shortparallel} = 0$ in the ionosphere, the Ohm's law for ionospheric currents is given by

$$\vec{I} = - \begin{pmatrix} \Sigma_P & \Sigma_H \\ -\Sigma_H & \Sigma_P \end{pmatrix} \cdot \vec{\nabla} \phi \qquad (3.2)$$

where Σ_p and Σ_H denote the height-integrated ionospheric Pedersen and Hall conductivities, respectively, and ϕ is the potential in the frame rotating with the earth. Inserting (3.2) into (3.1) yields

$$-\vec{\nabla} \cdot \left[\begin{pmatrix} \Sigma_p & \Sigma_H \\ -\Sigma_H & \Sigma_p \end{pmatrix} \cdot \vec{\nabla} \phi \right] = j_{\parallel} \qquad (3.3)$$

Equation (3.3) can be solved for ϕ for a given distribution of $j_{\parallel}$ when Σ_p and Σ_H are known as a function of longitude ψ and latitude λ (ψ measured counter-clockwise from the midnight meridian, e.g. ψ=90° corresponds to the 06LT meridian).

In this study, it is assumed that $j_{\parallel}$ has non-zero values only along two latitude circles. Thus, except for those latitude circles,

$$\vec{\nabla} \cdot \vec{I} = 0 \qquad (3.4)$$

Therefore, one may introduce the current function J defined as follows:

$$\vec{I} = \vec{\nabla} J \times \vec{e}_r \qquad (3.5)$$

where $\vec{e}_r$ denotes a unit vector in the radial direction from the center of the earth. Since the gradient of the current function is perpendicular to the current vector $\vec{I}$, contours of J=constant give streamlines of $\vec{I}$.

The relationship between ϕ and J is given by combining equations (3.2) and (3.5);

$$\frac{1}{\sin\theta} \frac{\partial J}{\partial \psi} = -\Sigma_p \frac{\partial \phi}{\partial \theta} - \frac{\Sigma_H}{\sin\theta} \frac{\partial \phi}{\partial \psi}$$

$$\frac{\partial J}{\partial \theta} = \Sigma_H \frac{\partial \phi}{\partial \theta} - \frac{\Sigma_p}{\sin\theta} \frac{\partial \phi}{\partial \psi} \qquad (3.6)$$

where θ denotes the colatitude. The steps which have been chosen to solve this problem are as follows: (i) solve equation (3.3) for ϕ for a given distribution of $j_{\parallel}$ and also for a given distribution of Σ_P and Σ_H; (ii) insert ϕ thus obtained into (3.6) to obtain the current function J; (iii) examine relationships between $j_{\parallel}$ and the stream lines J=constant.

3.2 MODELS

In all models used for the present calculations the ionosphere is divided into three regions, the polar cap, the auroral oval and the middle- and low-latitude belt. Then all the models are grouped into two. In the first group (single ring model), the polar cap is represented by a circular area which is bounded by the latitude circle of λ_1=70°. The auroral oval is represented by a circular belt which is bounded by two latitude circles of λ_1=70° and λ_2=65°. The rest of the ionosphere is the middle- and low-latitude belt. In each region, the conductivity is assumed to be uniform, thus the conductivity models are azimuthally symmetric. In the second group (double ring model), the polar cap is bounded by the latitude circle of λ_1=72°. The auroral oval is bounded by the two latitude circles of λ_1=72° and λ_2=60°. The oval is then divided into two belts by the latitude circle of λ=67°. This is to simulate the two regions of auroras, the oval of discrete auroras and the oval of diffuse auroras. The conductivity in the two belts is different (the conductivity in the oval of discrete auroras is assumed to be twice of that in the oval of diffuse auroras), but is higher than that in the polar cap and the middle- and low-latitude belt. Also for this group, the conductivity is assumed to be uniform in each region,

thus the conductivity models are azimuthally symmetric.

In order to examine the effects of the conductivity in the auroral oval, a number of different combinations of the Pedersen and Hall conductivities in the oval (Σ_P^A and Σ_H^A, respectively) are used. These values are given in Table 3.1. In all these models, the conductivities in the polar cap and in the middle- and low-latitude belt are assumed to be equal, and the ratio of the Hall to Pedersen conductivities is fixed to be 2.0 in these regions (i.e., $\Sigma_P^P = \Sigma_P^M = 1$ mho and $\Sigma_H^P/\Sigma_P^P = \Sigma_H^M/\Sigma_P^M = 2.0$).

The field-aligned currents are assumed to flow into or out only from the circles of λ_1 and λ_2, and thus into or out from the poleward and equatorward edges of the auroral oval in the single ring models and from the two latitude circles of λ=70° and λ=63°, which are imbedded in the discrete and the diffuse auroral ovals respectively, in the double ring models. In the poleward field-aligned current sheet the current flows into the oval in the sector bounded by ψ=0° and ψ=180°, while the current flows out from the oval in the sector bounded by ψ=180° and ψ=0°. In the equatorward current sheet, the directions of the field-aligned currents are reversed with respect to the poleward ones. Three different longitudinal dependences of the field-aligned current intensity are considered for various models of the ionospheric conductivity. Further, in the evening sector, three different ratios of the total inward (equatorward) current (I_S^T) to the total outward (poleward) current (I_N^T) are assumed (i.e., I_S^T/I_N^T=0.2, 0.5 and 1.0). The locations of their peaks, the location with respect to the auroral oval and the longitudinal dependence of the intensity of the field-aligned currents are shown in Figures 3.1a and b. In Table 3.1, the ratio I_S^T/I_N^T and the longitude of

the peaks of the two field-aligned currents are given, together with the values of the conductivity for each model.

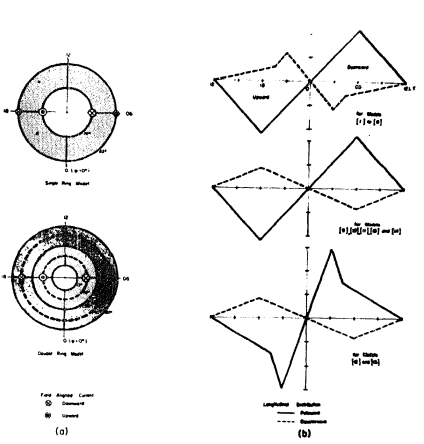

Figure 3.1 (a) The geometry of the high conductivity belt with the locations of the field-aligned currents, and (b) the longitudinal dependence of the field-aligned current intensity for models listed in Table 3.1. The number of the models in which each longitudinal distribution is used is indicated.

		Σ_P^A/Σ_P^P	Σ_H^A/Σ_P^A	I_S^T/I_N^T	LOCATION OF PEAKS I_N	LOCATION OF PEAKS I_S
SINGLE RING MODEL	[1]	1.0	2.0	0.5	90° 270°	45° 315°
	[2]	1.5	"	"	"	"
	[3]	2.0	"	"	"	"
	[4]	5.0	"	"	"	"
	[5]	10.0	"	"	"	"
	[6]	2.0	4.0	"	"	"
	[7]	"	8.0	"	"	"
	[8]	10.0	0.2	"	"	"
	[9]	5.0	2.0	0.2	90° 270°	90° 270°
	[10]	"	"	0.5	"	"
	[11]	"	"	1.0	"	"
	[12]	"	"	0.5	45° 315°	90° 270°
	[13]	10.0	4.0	"	90° 270°	"

DOUBLE RING		REGION OF DISCRETE AURORA		REGION OF DIFFUSE AURORA				
		Σ_P^A/Σ_P^P	Σ_H^A/Σ_P^A	Σ_P^A/Σ_P^P	Σ_H^A/Σ_P^A	I_S^T/I_N^T	LOCATION OF PEAKS I_N	LOCATION OF PEAKS I_S
	[14]	10.0	4.0	5.0	4.0	0.5	90° 270°	90° 270°
	[15]	5.0	3.0	3.0	3.0	0.5	45° 315°	"

TABLE 3.1 List of the parameters of various models used in the present study. The values of the Pedersen and the Hall conductivities in the polar cap and middle- and low-latitudes are fixed to be $\Sigma_P^P = \Sigma_P^M = 1.0$ MHO and $\Sigma_H^P = \Sigma_H^M = 2.0$ MHO, respectively.

CHAPTER IV

RESULTS OF THE CALCULATIONS

4.1 THE IONOSPHERE OF A UNIFORM CONDUCTIVITY

One of the most interesting and important aspects of the field-aligned currents is that their direction is reversed with respect to the noon-midnight meridian, regardless of the degree of auroral and magnetic activity (Żmuda and Armstrong, 1974; see also Figures 2.3 to 2.5). The ratio of the intensity of the equatorward field-aligned current to that of the poleward one (average value of 0.5) is also important.

As a first step, the potential and ionospheric current patterns related to the field-aligned currents which have these important characteristics are examined for a uniform conductivity (model [1] in Table 3.1). Since there is no discontinuity in the ionospheric conductivity in this particular model, the accumulation of the space charge due to the conductivity difference does not arise. The potential is only due to the external source applied through the field-aligned currents. Thus, the potential pattern [1] in Figure 4.1a is symmetric with respect to the midnight-noon meridian, reflecting the effect of the symmetry of the field-aligned current distribution.

One notable feature of this potential pattern is the large difference in the potential distribution between the midnight and the noon sectors. In the noon sector, the equipotential lines spread out radially and densely in the middle-low latitude region, while in the midnight sector, the density of the equipotential lines is very thin. This day-night asymmetry is caused by the fact that the assumed peaks of the

equatorward field-aligned currents are located around the local hours of 21 and 03. The thinness of the equipotential lines (or the weakness of the electric field) on the nightside is due to a greater cancellation, in the night sector than in the noon sector, of the electric field associated with the poleward field-aligned currents by the electric field associated with the equatorward field-aligned currents.

In Figure 4.1b, [1] shows the ionospheric current pattern corresponding to the potential pattern for [1] in Figure 4.1a. (The direction of the current is shown by arrows.)

Although the potential pattern is symmetric with respect to the midnight-noon meridian, the current pattern is asymmetric. This is due to the anisotropy of the conductivity.

4.2 ROTATION OF THE POLAR CAP POTENTIAL PATTERN

4.2.1 Effects of Σ^A/Σ^P (or Σ^A/Σ^M)

In this subsection, the dependence of the distribution of the potential and the electric currents on the relative magnitudes of the conductivities in the polar cap, the auroral oval and the middle- and low-latitude region are examined. Five models from [1] to [5] in Table 3.1 are considered for this purpose.

Figures 4.1a and b show the potential and current patterns for various values of the conductivity in the auroral oval. The number beside each pattern corresponds to the model number.

As seen in Figure 4.1a and as pointed out by several workers, the equipotential lines over the polar cap are rotated when the auroral oval conductivity is enhanced. In all such cases, the rotation is towards

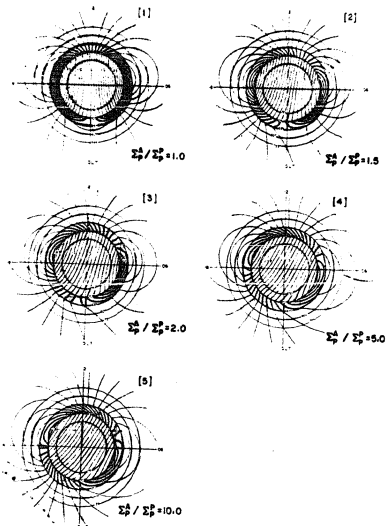

Figure 4.1a The calculated electric potential patterns in the ionosphere for Models [1] to [5]. Σ_E^A/Σ_E^P for each model is indicated by the model number. In all models, Σ_H^P/Σ_P^P = 2.0, $\Sigma_E^M = \Sigma_P^M$. Σ_H^A/Σ_P^A is also fixed to be 2.0. The field-aligned currents are located along the two latitude circles 70° and 65°. The peaks of the field-aligned currents are at 06 and 18LT for the poleward current and at 03 and 21LT for the equatorward current, respectively.

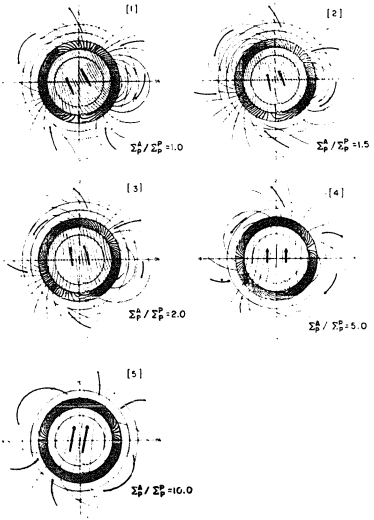

Figure 4.1b The calculated ionospheric electric current patterns corresponding to the potential patterns shown in Figure 4.1a. The direction of the currents is shown by thick arrows.

the pre-noon sector, and the amount of this rotation increases when the conductivities in the auroral oval increase.

When the conductivities in the auroral oval (Σ^A) are higher than those in the polar cap (Σ^P) and the middle-low latitude region (Σ^M), the charge transfer in the auroral oval is faster than in the other two regions. This results in the space charge accumulation at the poleward and equatorward boundaries of the oval. Some portion of these space charges is removed by the field-aligned currents flowing into or out from these boundaries. However, the given magnitude (in the models) of the field-aligned currents limits this charge removal to a certain extent, and the excess charges remain at the boundaries of the different conductivity regions. These charges change the primary potential distribution which was applied from outside the ionosphere. The clockwise rotation of the equipotential lines over the polar cap is caused mainly by this process and is explained as follows.

When there is no enhancement of the conductivities in the oval belt, the positive and the negative peaks of the potential are located at almost 06 and 18LT, respectively; see [1] of Figure 4.1a. The polar cap current flows towards the direction of approximately 14LT (Pattern [1] in Figure 4.1b). In this uniform conductivity model, there is no space charge except for the one given from outside. If the auroral oval conductivities are increased under this situation, the polar cap currents produce a negative charge accumulation around 14LT and a positive charge accumulation around 02LT at the poleward edge of the oval. When the potentials due to these space charges are superposed on the primary potential distribution, the resultant potential distribution rotates

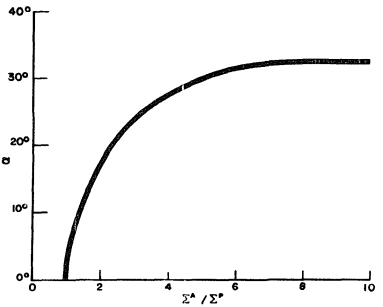

Figure 4.2 The clockwise rotation angle α of the polar cap potential as a function of the ratio of the auroral oval conductivity to the polar cap (and the middle- and low-latitude belt) conductivity Σ^A/Σ^P. This curve is drawn by using results from Models [1] to [5].

clockwise. Then the polar cap currents are deflected toward the same direction according to this new potential distribution and shift the space charge accumulation farther towards earlier local times, and so on. In Figure 4.2 the amount of this clockwise rotation is plotted as a function of the ratio of the conductivity in the auroral oval to the conductivity in the polar cap (or in the middle-low latitude region). As can be seen in this figure, the rotation angle α measured clockwise from the noon meridian increases steeply for small values of the ratio. However, the curve approaches to the asymptotic value ($\sim$33°) when this ratio reaches to about 10. The reason for this can be seen from the ionospheric current patterns (Figure 4.1b). As the conductivity in the auroral oval increases, the ionospheric currents tend to be more concentrated in the oval than in the other regions and the amount of the currents which flow in the polar cap, as well as in the middle-low latitude region, is greatly reduced. This reduction of the polar cap currents results in the reduction of the charge accumulation at the poleward edge of the oval in spite of the fact that the discontinuity of the conductivity becomes greater.

4.2.2 Effects of Σ_H^A/Σ_H^P (or Σ_H^A/Σ_H^M)

In this subsection, effects of the ratio of the Hall conductivity in the auroral oval to the Hall conductivity in the polar cap or middle-low latitude on the rotation of the polar cap electric potential are examined.

The ratio Σ_H^A/Σ_H^P is increased from 2 to 8 by keeping the values of the conductivities in the polar cap and middle-low latitude region constant and by also keeping the value of the Pedersen conductivity in the

auroral oval constant. The models used here are [3], [6] and [7] in Table 3.1. The assumed distribution of the field-aligned currents is the same as the one in the previous section.

The potential pattern and the corresponding ionospheric current pattern for the ratio Σ_H^A/Σ_H^P = 2.0, 4.0 and 8.0 are shown in Figures 4.3a and b, respectively. (For the current direction, see [3] of Figure 4.3b.)

The main effect caused by increased values of the ratio Σ_H^A/Σ_H^P (or Σ_H^A/Σ_H^M) on the potential pattern in the ionosphere is a clockwise rotation.

In the polar cap, the amount of the rotation α increases with Σ_H^A/Σ_H^P (or Σ_H^A/Σ_H^M). The value of α becomes as large as 67° for Σ_H^A/Σ_H^P = 8.0.

This rotation can also be explained by the charge accumulation due to the conductivity discontinuity at the boundary between the polar cap and the auroral oval.

In Figure 4.3a, [3] shows the potential pattern for the ratio Σ_H^A/Σ_H^P = 2.0. The potential pattern indicates also the flow pattern of the Hall current. In the polar cap, the Hall current is deflected towards the morning sector by about 15° from the noon meridian. Therefore, at the poleward boundary of the oval, the centers of the negative space charge and the positive space charge due to the discontinuity of the Hall conductivity are located around 11LT and 23LT, respectively. They shift the locations of the positive and the negative peaks of the potential clockwise. When the discontinuity of the Hall conductivity becomes larger, these peaks are shifted farther towards the earlier local times.

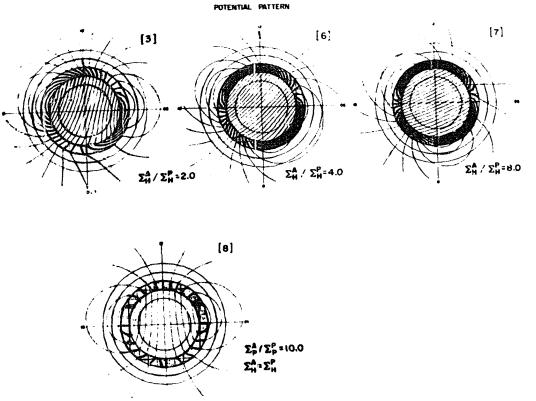

Figure 4.3a The calculated electric potential patterns in the ionosphere for Model [5], [6], [7] and [8]. γ_H^A/γ_H^P for each model is indicated by the model number. In all models γ_H^P/γ_P^P = 2.0 ($\Sigma_H^M = \gamma^P$). For Model [5], [6] and [7], γ_P^A/γ_P^P = 2.0. For Model [8], γ_P^A/γ_P^P = 10.0. The field-aligned currents are located along the two latitude circles 70° and 65°. (The latitudes are shown in Pattern [3].) The peaks of the field-aligned currents are at 06 and 18LT for the poleward currents and at 03 and 21LT for the equatorward current, respectively.

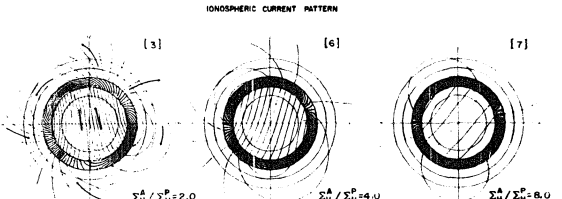

Figure 4.3b The calculated ionospheric electric current patterns corresponding to the potential patterns shown in Figure 4.3a except for [8]. The direction of the currents is shown by thick arrows in Pattern [3].

While the amount of the rotation increases with the increase of the Σ_H^A/Σ_H^P, the rate of the increase becomes smaller for the larger values of this ratio. This tendency is due to the reduction of the ionospheric currents over the polar cap when the ratio of the Hall conductivity in the auroral oval to that in the polar cap becomes large (Figure 4.3b).

4.2.3 Effects of Σ_P^A/Σ_P^P (or Σ_P^A/Σ_P^M)

In the previous section, we examined effects of the Hall conductivity in the auroral oval on the potential pattern in the polar cap. Here, we examine effects of the Pedersen conductivity on the rotation of the pattern.

The result of the previous section shows that the amount of the rotation α increases with Σ_H^A/Σ_H^P. If this ratio is the main factor which determines the angle of the rotation, α should increase monotonically with the ratio of the two Hall conductivities. However, this is not the case. Compare the potential pattern [7] in Figure 4.3a with the pattern in [5] in Figure 4.1a. The amount of rotation is much larger in [7] than in [5], although Σ_H^A/Σ_H^P is larger for the latter than for the former.

One factor which is included in Model [5], but not in Model [7], is an enhancement of the Pedersen conductivity in the auroral oval. In [7] of Figure 4.3a, the Pedersen currents flow towards the direction of post-noon hours. Suppose that the Pedersen conductivity in the auroral oval becomes larger without changing the auroral oval Hall conductivity. Then the negative and positive space charge accumulations arise around 13.5LT and 1.5LT, respectively, due to the discontinuity of the

Pedersen conductivity at the poleward boundaries of the oval. These space charges tend to counter balance the effects of the space charges due to the Hall conductivity discontinuity.

Thus, the enhancement of the Hall conductivity in the auroral oval rotates the polar cap potential pattern clockwise, while the enhancement of the Pedersen conductivity in the oval reduces this rotation. Note that if the Hall conductivity is uniform over the entire ionosphere, the discontinuity of the Pedersen conductivity does not rotate the potential pattern ([8] of Figure 4.3a). This is because the locations of the space charge accumulations due to the discontinuity of the Pedersen conductivity coincide with the locations of the space charges for the primary potential distribution.

4.2.4 Effects of Other Parameters

In the present model calculations, the amount of the rotation of the polar cap potential pattern is also a function of other parameters, as well as of the conductivity (i.e., locations of the peaks of the field-aligned currents, the ratio I_S^T/I_N^T, etc.). Of these parameters, the ratio I_S^T/I_N^T gives the largest effect to α. This dependence is examined by using Models [9], [10] and [11]. The patterns of the potential and ionospheric currents are shown in Appendix I (Figures A1a and b). When I_S^T/I_N^T is increased without changing the conductivities, α gradually increases, 23° for Model [9] ($I_S^T/I_N^T = 0.2$), 33° for Model [10] ($I_S^T/I_N^T = 0.5$), and 81° for Model [11] ($I_S^T/I_N^T = 1.0$). Since the amount of the conductivity discontinuities at the poleward and equatorward boundaries of the oval is the same for the three models,

this rotation is mainly due to the change of the potential distribution associated with the equatorward field-aligned currents. When the intensity of the equatorward field-aligned currents increases, the potential associated with it (the maximum and the minimum at 18 and 06LT, respectively) becomes larger. Since the potential pattern in the polar cap is already rotated clockwise ($0° < \alpha < 90°$), the superposition of this increase of the potential due to the increase of the equatorward field-aligned currents results in larger α. It is interesting to note that α changes rather sharply around $I_S^T/I_N^T = 0.7$. For I_S^T/I_N^T less than this value, the effects of I_S^T/I_N^T on the polar cap potential pattern are small.

The location of the peaks of the field-aligned currents slightly affects the value of α, so long as the distribution of the field-aligned currents is symmetric with respect to the noon-midnight meridian. Instead, it causes non-uniformity in the potential pattern in the polar cap. For example, due to the concentration of the poleward field-aligned currents in the night sector, the equi-potential lines in the polar cap diverge towards the day sector. This is shown by using Models [10], [4] and [12] in Appendix I (Figure A2a). When the field-aligned current distribution is not symmetric with respect to the noon-midnight meridian, α is different from α for the symmetric distribution with the same ionospheric model and I_S^T/I_N^T. However, this effect does not exceed the effect due to the conductivity enhancement in the auroral oval. One example is shown in Appendix I (Figure A3) for the case in which the locations of the maximum and the minimum of the poleward field-aligned currents are at 06 and 21LT, respectively, and the other parameters are the same as Model [10].

4.3 RELATION BETWEEN THE MAGNITUDE OF THE FIELD-ALIGNED CURRENT AND THE IONOSPHERIC CONDUCTIVITY

In the present calculations, the magnitude of the field-aligned currents is assumed to be constant. Thus, the total potential difference $(\Delta\phi)_t$ across the polar cap which is required to provide a given amount of the field-aligned currents, changes with the values of the ionospheric conductivity. In this section, by normalizing $(\Delta\phi)_t$ to 50 k volt, the relationship between the conductivity and the field-aligned current intensity is examined. Some sets of values of the conductivities and the field-aligned currents are given in Table 4.1. These values are obtained by using single ring models (i.e., one high conductive ring with the field-aligned currents at its poleward and equatorward edges).

TABLE 4.1

The values of the ionospheric conductivity and I_N^T for the total potential difference of 50 k volts across the polar cap

	Σ_P^P	Σ_H^P	Σ_P^A	Σ_H^A	I_N^T
(a)	1	2	1	2 MHO	1.33×10^5 AMP
(b)	1	2	2	4	1.85
(c)	1	2	5	10	3.94
(d)	1	2	10	20	7.65
(e)	2	4	10	20	7.88
(f)	5	10	10	20	9.25
(g)	1	2	2	8	3.33
(h)	1	2	2	16	7.15
(i)	1	2	10	2	3.20

When the auroral oval conductivities (Σ_P^A and Σ_H^A) are increased, the field-aligned current intensity is increased almost linearly ((a) to (d) in Table 4.1). On the other hand, when the conductivities in the polar cap (Σ_P^P and Σ_H^P), which are assumed to be equal to those in the middle- and low-latitude belt, are enhanced by a factor of 5 (without changing Σ_P^A and Σ_H^A), the intensity of the field-aligned currents increases only by a factor less than 2 ((d) and (g)). Further, the intensity of the field-aligned currents becomes less sensitive to Σ_P^P and Σ_H^P, when the ratio Σ^A/Σ^P becomes larger. When Σ_H^A is increased, with the other conductivities being fixed, the field-aligned current intensity increases almost proportionally to Σ_H^A ((b), (g) and (h)). However, the increase of Σ_P^A does not contribute much to the increase of the field-aligned currents. From these it can be concluded that the field-aligned currents are mainly closed by the Hall currents through the auroral oval, but not through the polar cap. This will be shown in Section 4.6.

4.4 ELECTRIC FIELD IN THE POLAR REGION

Satellite observations (OGO-6 and INJUN 5) have revealed the presence of a large-scale electric field in the polar cap, the auroral oval and the subauroral zone. The electric field has a dawn-to-dusk component in the polar cap and reverses its direction across the oval. The peaks of the intensity occur, in general, a little equatorward of the reversal and gradually decrease towards lower latitudes. The electric field is fairly uniform in the polar cap, while complicated structures are sometimes observed around the auroral oval. A typical example

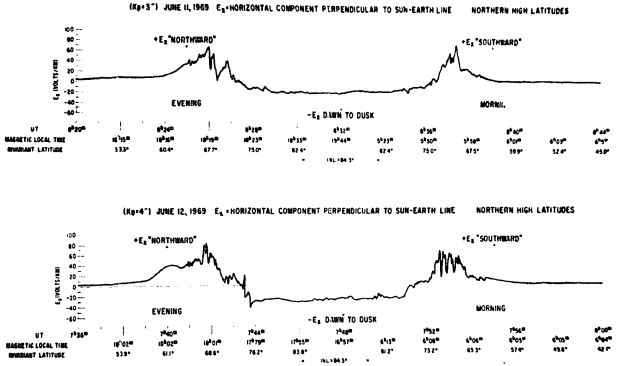

Figure 4.4a The typical horizontal component of the electric field perpendicular to the sun-earth line along two dawn-dusk traverses of OGO-6 across the north polar region (after Heppner, 1972).

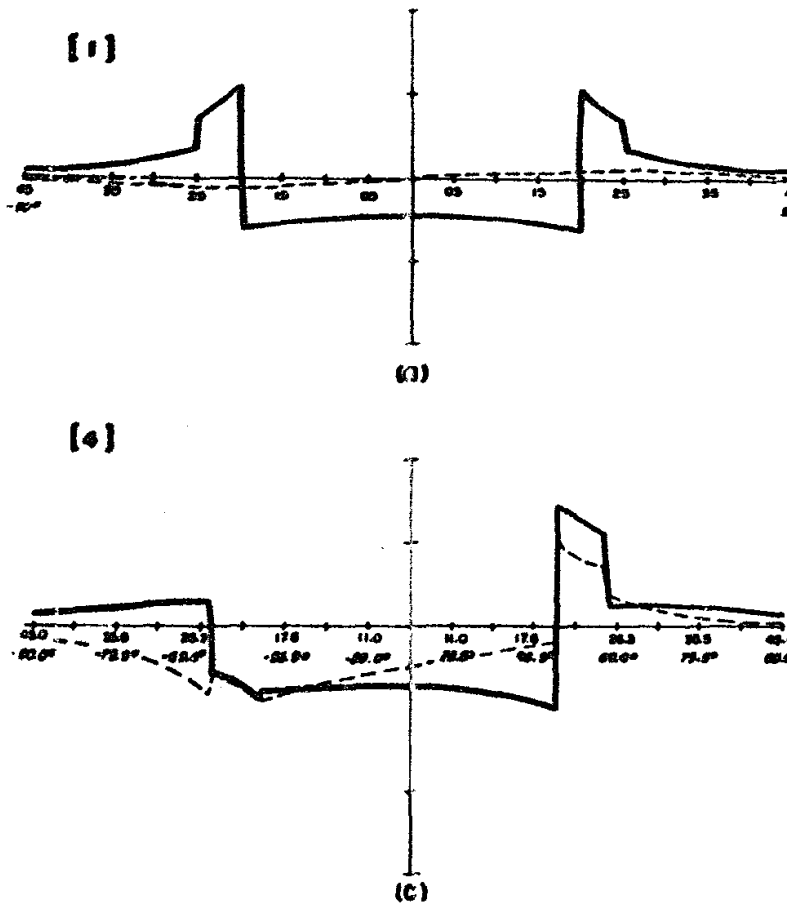

Figure 4.4b The calculated electric fi
component and the dashed lines are for th
colatitude and the local hour angle (0° f
for Model [1] (a uniform conductivity mod
[4] (a single ring model), (c) the profil
(θ=45°, ψ=-80°) and θ=45°, ψ=80°) for Mod
meridian for Model [15] (a double ring mo

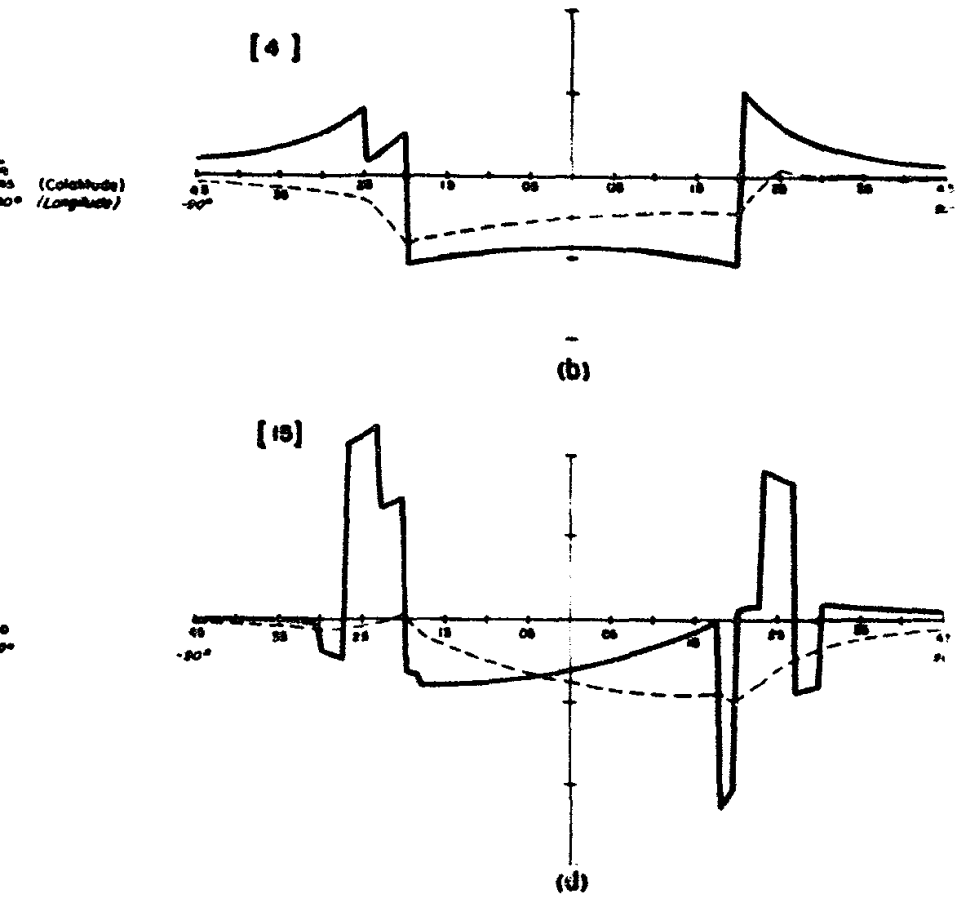

eld profiles. The solid lines are for the dawn-to-dusk
e noon-to-midnight component. The abscissa is the
or 01.T). (a) The profile along the 181.T-061.T meridian
el), (b) the profile along the same meridian for Model
e along the great circle which connects the two points
el [4], and (d) the profile along the 181.T-061.T
del).

of the dawn-to-dusk component of electric field along the dawn-dusk meridian is shown in Figure 4.4a (Heppner, 1972).

In Figure 4.4b, the electric field components calculated for some of the present models are shown. Profile (a) in Figure 4.4b shows the electric field variations along the 18LT (ψ=-90°) and 06LT (ψ=90°) meridian for Model [1] in Table 3.1, Profile (b) along the same meridian for Model [4], and Profile (c) along the great circle which connects the two points (θ=45°, ψ=-80°) and (θ=45°, ψ=80°) for the same model, Profile (d) again along the ψ=-90° and ψ=90° meridian for Model [15]. In these four profiles, the solid lines are for the dawn-to-dusk component (E_y) and the dashed lines are for the noon-to-midnight component (E_x).

As clearly seen, all of the four profiles calculated for the present models show most of the main features of the dawn-dusk electric field profiles observed by OGO-6 satellite. They show very little variation in the polar cap; the sharp changes and the reversal of the direction at the edges of or in the auroral oval and the decrease towards lower latitudes. However, note that the potential patterns for these three models [1], [4] and [15] show different degrees of rotation, and that the patterns are significantly different between Models [1] and [15]. (For Models [1] and [4], see Patterns [1] and [4] in Figure 4.1a. For Model [15], see Pattern [C] in Figure 5.1a. Model [15] is the same as Model [C] in Table 5.1 in Chapter V.) On the other hand, the gross features of the dawn-dusk component profile of the electric field do not change significantly with the potential patterns. Thus, it is difficult

to infer the potential distribution from the electric field distribution along a single meridian.

When Profile (c) is compared with Profile (b), some differences can be noticed. First, in (c), the magnitude of E_y gradually increases towards the dawn sector, while E_y in (b) is almost symmetric with respect to the noon-midnight meridian. In the auroral oval and the low- and middle-latitudes, the E_y profile is more asymmetric in (c) than in (b). Note that the potential pattern is the same for Profiles (b) and (c), but the 'paths' along which E_y is plotted are different. Thus, the electric field profiles depend somewhat on the 'path' along which the electric field is measured.

For the rotated potential pattern, the potential difference $\Delta\phi$ along the dawn-dusk meridian is less than the total difference $(\Delta\phi)_t$ across the polar cap. If $\Delta\phi$ is used as $(\Delta\phi)_t$, the effect of the rotation of the potential pattern by 45° underestimates the value of $(\Delta\phi)_t$ by 24%. It is interesting to compare the apparent change of $(\Delta\phi)_t$ due to the rotation with the change due to other causes, for example, the expansion of the polar cap. Suppose that the polar cap expands from 70° to 65° latitudes without changing the magnitude of the polar cap electric field and that, at the same time, the potential pattern is rotated by 45°. Then the increase of $(\Delta\phi)_t$ due to the expansion is compensated by the effect of the rotation, as long as the 'paths' along which the potential difference is obtained are the same before and after the expansion of the polar cap and the rotation of the potential pattern.

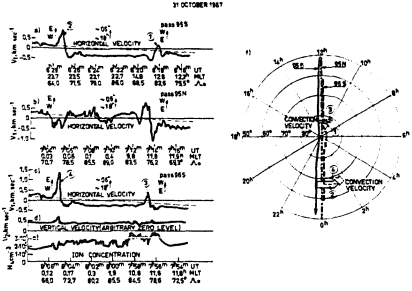

Figure 4.4c Examples for the traverse horizontal drift velocity component $V_\perp$ during a very quiet time (Kp=0+) on Oct. 31, 1967 above the southern hemisphere designated Pass 955 (a) and above the northern hemisphere designated 954 (b). The abscissa gives the universal time, geomagnetic local time and invariant latitude. The dashed line in the correction due to the corotation of the ionosphere: the data taken with this dashed axis as the zero level are measured in the earth's rotating frame. The $V_\perp$ and the vertical drift velocity component V_z for the next southern pass, together with the ion concentration, are also shown in (c), (d) and (e). (f) shows the polar projections of Passes 955 (solid line), 954 (dot-dashed line) and 965 (dashed line) (after Galperin et al., 1974).

The noon-midnight components of the electric field along the dawn-dusk path have not been measured. Thus, they are shown for future reference.

A few measurements of the noon-midnight component of the electric field along the noon-midnight path are available (Gurnett and Frank, 1973; Galperin et al., 1974 (measurement of the plasma velocity)). Figure 4.4c shows an example of the observations of the dawn-dusk component of the plasma convection velocity along the noon-midnight meridian adopted from Galperin et al. (1974). In the passes 95S and 96S, an almost constant dawn-to-dusk component of the velocity (thus constant midnight-to-noon component of the electric field) exists over the polar cap. (Note that a velocity of 1 km/sec corresponds to an electric field of about 50 volt/km.) According to these measurements, the magnitude of this component is, in general, smaller than that of the other component by factor of 2 to 5, but sometimes (even during magnetically quiet time) is comparable (i.e., the potential pattern is rotated). Although the measurements of these two components are not simultaneous, it seems that the noon-midnight component of the electric field cannot be neglected compared with the other component. Thus, when the potential pattern or the plasma convection pattern is studied on the basis of observations of one component of the electric field along a single satellite orbit, great care must be exercised.

4.5 POTENTIAL DISTRIBUTION BELOW THE LATITUDES OF THE OVAL: PENETRATION OF THE CONVECTION ELECTRIC FIELD

As seen in the potential distributions shown in Sections 4.2.2 and 4.2.3, the potential patterns in the middle-low latitude are also rotated

clockwise when the ratio Σ_H^A/Σ_H^P ($\Sigma_H^P = \Sigma_H^M$) is increased. The direction and the amount of the rotation can be explained in the same way as the rotation of the polar cap potential pattern, considering the conductivity discontinuity at the equatorward boundary of the auroral oval.

One of the most important and interesting features about the middle- and low-latitude potential (or electric field) distribution is its magnitude relative to those of the high latitude plasma convection field. This relative magnitude represents the degree of the penetration of the convection electric field into lower latitudes. This problem has been studied extensively by many workers. Particularly, Swift (1971), Vasyliunas (1971) and Jaggi and Wolf (1973) solved a set of equations which allows the coupling between the ionosphere and the magnetosphere through the field-aligned currents, under the self-consistent electric field for particular models of the ionospheric conductivity. In this section, their results and the present results will be compared. In the present study, the field-aligned currents are regarded as an effect of such a coupling. Further, of several observed characteristics of the field-aligned currents, the four features are emphasized. They are (1) the relative location to the high conductive auroral belt, (2) their presence as a pair of the poleward and equatorward at almost all local times, (3) the persistent reversal of the direction with respect to the noon-midnight meridian and (4) the ratio of the intensity of the equatorward field-aligned current to that of the poleward one.

In the present models of the ionosphere, the potential distribution along the equatorward boundary of the oval determines the potential distribution in the middle- and low-latitude belt. Thus, the ratio

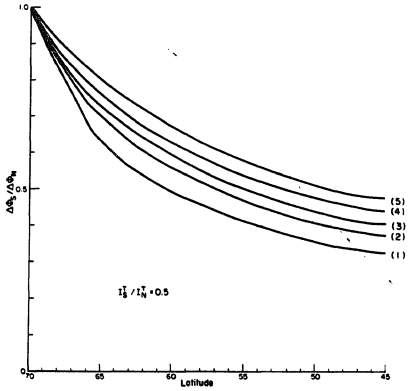

Figure 4.5a The magnitude of the potential along different constant latitude circles ($\Delta\phi(0)$) for different models, [1] to [5] in Table 3.1 ($\Delta\phi(0)$ is normalized to $\Delta\phi_M$, the magnitude of the potential along the poleward boundary of the high conductive belt); these models differ from each other only in conductivity values in the auroral oval. Σ_H^A/Σ_P^A = 1.0 ((1)), 1.5 ((2)), 2.0 ((3)), 5.0 ((4)) and 10.0 ((5)). Σ_H^A/Σ_P^A and Σ_H^P/Σ_P^P are fixed to be 2.0. Σ_H^M/Σ_P^M. I_S^T/I_N^T is also fixed to be 0.5. The peaks of the poleward and the equatorward field-aligned currents are at 06LT and 18LT for the poleward current and at 03LT and 21LT for the equatorward current.

($\Delta\phi_S/\Delta\phi_N$) -- the magnitude of the potential along the equatorward boundary ($\Delta\phi_S$) to that along the poleward boundary ($\Delta\phi_N$) of the oval -- represents the degree of the penetration of the high latitude convection electric field to the low latitude ionosphere. Here, the magnitude of the potential is defined as the sum of the magnitude of the positive and negative peak values along the latitude circles. Note that this definition is allowed only when the relative phase shift of the two potential distributions is small; this will be discussed later.

In Figure 4.5a, the magnitude of the potential along different constant latitude circles ($\Delta\phi(\theta)$) is plotted for different models, [1] to [5] in Table 3.1; note that $\Delta\phi(\theta)$ is normalized to $\Delta\phi_N$. These models differ from each other only in the conductivity values in the auroral oval. The ratio of the total intensity of the equatorward field-aligned current to that of the poleward one is fixed to be 0.5.

In this figure, it can be seen that when the conductivity in the auroral oval increases, the slope of the curves decreases, thus the penetration of the high latitude electric field to the latitudes lower than the equatorward field-aligned current increases. This tendency agrees only qualitatively with that obtained by Vasyliunas (1971). His results show a stronger dependence of the penetration on the ionospheric conductivity.

In his results, as well as those obtained by Swift and Jaggi and Wolf, the potential variation at the latitude just below the latitude of the ring current (or the inner boundary of the plasma sheet) decreases abruptly and becomes much less than $\Delta\phi_N$ by one to three orders of magnitude. On the other hand, the present results show that $\Delta\phi$ decreases

rather smoothly with latitude and that the reduction is at most by a factor of 0.4. There are at least two possible explanations to this difference between the present results and theirs. The first is differences in ionospheric conductivity models. In the ionospheric model adopted by Swift (1971) and Vasyliunas (1971), the enhancement of the auroral oval conductivity was not taken into account. The effects of the ionospheric conductivity were examined only by increasing the conductivity uniformly over the entire ionosphere.

The relationship between the field-aligned currents and the ionospheric currents or the ionospheric electric field and conductivities are given as follows:

$$j_{\parallel} = \vec{\nabla} \cdot \vec{I} = \Sigma_P \vec{\nabla} \cdot \vec{E} + \vec{E} \cdot \vec{\nabla} \Sigma_P + (\vec{b} \times \vec{E}) \cdot \vec{\nabla} \Sigma_H \qquad (4.1)$$

where $j_{\parallel} > 0$ is for an inflow, $\vec{b}$ is a unit vector in the direction of the magnetic field and the ionospheric quantities $\vec{I}$, Σ_P and Σ_H are height-integrated and $\vec{E}$ and $\vec{\nabla}$ are two-dimensional in the horizontal plane.

This relationship shows that there are three possible sources of the field-aligned currents; $\vec{\nabla} \cdot \vec{E}$, $\vec{\nabla} \Sigma_P$ and $\vec{\nabla} \Sigma_H$. Here, $\vec{\nabla} \cdot \vec{E}$ represents the difference in the component of the electric field normal to the boundary between the two regions across the field-aligned currents. When the field-aligned currents flow into or out from regions where there is no gradient of the conductivities, the only source is $\vec{\nabla} \cdot \vec{E}$. This is given mainly from the outside of the ionosphere (except for the ionospheric dynamo). In such a case, a large difference in the electric field between the two regions across the field-aligned currents

could result. However, of course, the magnitude of the difference depends on the magnitude of $j_{\parallel}$. On the other hand, if the field-aligned currents are located at regions where the gradient of the conductivity exists, the second and the third terms of the right-hand side of Equation (4.1) contribute to $j_{\parallel}$.

In the Jaggi and Wolf model, the enhancement of the conductivity in the auroral region, as well as its azimuthal dependence is included. However, since their field-aligned current is also infinitesimally thin while the conductivity variation is continuous, the gradient of the conductivity does not contribute to the field-aligned currents (see their equation 2b).

The second possibility may be that their field-aligned currents differ from the observed one. In particular, the ratio of the intensity of the equatorward field-aligned currents to that of the poleward currents is quite sensitive to the penetration of the high-latitude convection electric field to lower latitudes for the ionosphere with a uniform conductivity.

In order to examine how the ratio I_S^T/I_N^T is related to the degree of the penetration of the electric field below the equatorward boundary of the oval, the magnitude ratio $(\Delta\phi_S/\Delta\phi_N)$ is plotted as a function of I_S^T/I_N^T in Figure 4.5b.

In this calculation, the oval is bounded by two latitude circles $\lambda=70°$ and $\lambda=65°$. The intensity of the field-aligned currents is given by $I_{\parallel}=I_N \sin\psi$ along the $\lambda=70°$ circle and $I_{\parallel}=-I_N \sin\psi$ along the $\lambda=65°$ circle (I_N, $I_S > 0$). The Pedersen and the Hall conductivities in both the polar cap and the middle- and low-latitudes are 1 and 2 (in arbitrary

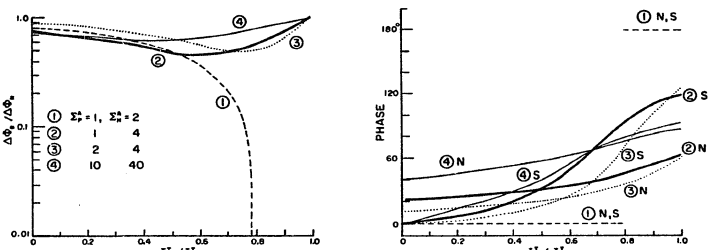

Figure 4.5b $\Delta\phi_S/\Delta\phi_N$, the ratio of the magnitudes of the potential along the equatorward and the poleward boundaries of the high conductive belt as a function of I_S^T/I_N^T (on the left) and the phase of ϕ_N and ϕ_S versus I_S^T/I_N^T (on the right). For each curve Σ_P^A and Σ_H^A are indicated. For all curves, Σ_P^P=1 and Σ_H^P=2. $\Sigma^M = \Sigma^P$. The field-aligned currents are located at the poleward and the equatorward boundaries of the high conductive belt andtheir longitudinal dependences are assumed to be sin ψ and -sin ψ, respectively. In the right diagram, N is for ϕ_N and S is for ϕ_S.

unit), respectively. The Pedersen and the Hall conductivities Σ_P^A and Σ_H^A in the oval are assumed to be

$$\Sigma_P^A = 1 \qquad \Sigma_H^A = 2 \qquad \text{for curve (1)}$$
$$1 \qquad 4 \qquad (2)$$
$$2 \qquad 4 \qquad (3)$$

and

$$\Sigma_P^A = 10 \qquad \Sigma_H^A = 40 \qquad (4)$$

The curve (1) represents the case of a uniform conductivity over the entire ionosphere. Therefore, this is the only case by which the results by Swift and Vasyliunas and present results can be compared. It is important to note that the ratio $\Delta\phi_S/\Delta\phi_N$ decreases sharply between $I_S^T/I_N^T = 0.7$ and 0.8. This indicates that when the conductivity of the ionosphere is uniform, the penetration of the electric field decreases drastically for the ratio $I_S^T/I_N^T > 0.7$. Almost the same relation is obtained for the model in which the equatorward field-aligned currents are located outside the high conductive belt; this model simulates the Jaggi and Wolf model.

Since Swift, Vasyliunas and Jaggi and Wolf showed that their models do not result in a deep penetration of the convection electric field, it may be inferred that the ratio I_S^T/I_N^T resulting from their calculations is of order 0.7 to 0.8, although they did not calculate the distribution of the field-aligned currents.

When a high conductivity belt appears, the penetration of the electric field is drastically improved (Curves (2), (3) and (4) in Figure 4.5b). When the conductivity in the auroral oval becomes higher

than that in the rest of the ionosphere $\Delta\phi_S/\Delta\phi_N$ does not vary much with I_S^T/I_N^T and is larger than 0.45.

For values of I_S^T/I_N^T larger than 0.8, $\Delta\phi_S$ becomes larger than $\Delta\phi_N$. In such cases, ϕ_N cannot be the only source for ϕ_S, and some other mechanisms are required to generate the low latitude electric field. In the case where the relative phase shift between ϕ_S and ϕ_N is larger than 90°, the other mechanisms are also necessary, since the electric field at lower latitudes has a sense opposite to that of the electric field expected from the penetration of the higher latitude convection electric field.

The phase of the poleward and the equatorward field-aligned current distribution may also be another important factor to cause the difference between the previous studies and the present one. At least, in the Vasyliunas calculation, the phase shift of the equatorward field-aligned currents amount to about 90° from the noon-midnight meridian (see his equation (5)).

Up to date, there are only a few observations which show how deep the high latitude convection electric field can penetrate into the latitudes lower than the inner-boundary of the plasma sheet (or the ring current). Swift and Gurnett (1973) compared the location of the equatorward boundary of the electric field region observed by the INJUN 5 satellite with that of the diffuse aurora determined from all-sky photographs during both quiet and disturbed times. They concluded that the two boundaries coincide with each other. This means that the convection electric field is effectively shielded from the lower latitude region by the inner boundary of the plasma sheet (or the ring

current) as predicted by the theories of Swift, Vasyliunas and Jaggi and Wolf, if the diffuse auroral particles originate from there.

In order to compare the present results with the observed electric field variations, the computed dawn-dusk electric field for Models (1)-(5) are compared with the dawn-dusk electric fields observed by OGO-5. It is found that the latitudinal variations of the computed electric field for Models (1) and (2) are similar to the observed electric field variations along the evening and morning passes on June 12 (Figure 4.4a) and along the evening pass on June 11 (Figure 4.4a). However, the observed electric field variations along the morning pass on June 11 are much steeper than what the model calculations (1) and (2) indicate. The computed field variation for Models (4) and (5) is more gradual than any of the observed variations in Figure 4.4a. Therefore, the penetration of the electric field indicated in Models (1) and (2) does not seem to be unreasonable and may occur for a short period during substorms, allowing the injection of ring current particles into the trapping region.

However, the degree of the penetration of the electric field depends greatly on the longitudinal distribution of the field-aligned currents. It may well be that the pre-existing and the newly injected ring current particles respond to the penetrated electric field in such a way to reduce it. This response should occur in variations of the field-aligned currents, but multi-satellite observations are needed for such a study.

The model calculations presented here are simply based on the assumed distributions of the field-aligned currents. Therefore, it is

not possible to include such expected changes in the models and thus the conclusions reached here remain tentative.

4.6 IONOSPHERIC CLOSURE OF THE FIELD-ALIGNED CURRENT

The purpose of this section is to examine quantitatively how the field-aligned currents close in the ionosphere. Three models are chosen for this purpose. They are [10], [13] (a single ring model), [14] (a double ring model) in Table 3. Common to all such models, there are dayside features which appear as the counterpart of nightside features. Therefore, attention will be confined only to nightside features.

Figure 4.6a shows the stream lines of the ionospheric currents for Model [10]. The amount of current flowing between two adjacent flow lines is 20k amp, if the poleward inflow current is assumed to be 7.7×10^5 amperes, and the arrows indicate the direction of the currents. The discontinuity of the stream lines along the latitude circles of $\lambda=70°$ and 65° indicates that there are field-aligned currents from or into those latitude circles.

(i) Model [10]

As a guide for Figure 4.6a, Figure 4.6b is provided to illustrate the relationship between the field-aligned currents (shaded vertical arrows) and the ionospheric currents (thin and thick arrows). A number for each arrow indicates the normalized amount of current with respect to the total amount of the inward flow along the poleward boundary in the morning sector, which is taken to be 100. The reason for grouping the poleward incoming and outgoing field-aligned currents into three

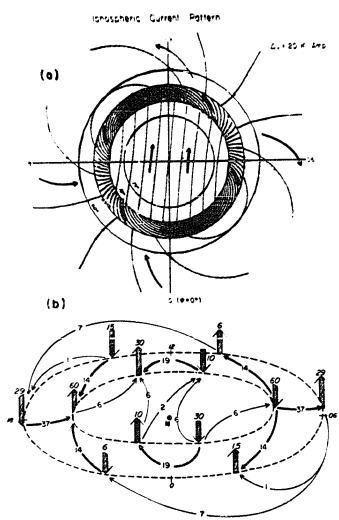

Figure 4.6 (a) The calculated ionospheric current pattern for Model [10] (a single ring model). In this model Σ_P^A/Σ_P^P=5.0, $\Sigma_H^A/\Sigma_P^A = \Sigma_H^P/\Sigma_P^P$ = 2.0 and Σ_P^P = 1 mho. Σ_H^P/Σ_P^P. I_S^T/I_N^T=0.5.

The arrow indicates the direction of the current flow. The amount of current flowing between adjacent flow lines is 20k amp, when I_N^T is assumed to be 7.7×10^5 amp. (b) The schematic illustration of the above current pattern, indicating the various current paths. The ring bounded by the dotted lines represents the auroral oval.

The shaded vertical arrows indicate the field-aligned currents and the solid arrows the ionospheric currents. A number for each arrow indicates the normalized amount of current with respect to the total amount of the poleward field-aligned currents in the evening sector, which is taken to be 100.

parts is self-explanatory. For the equatorward currents, the grouping is made, depending on the direction of the connecting ionospheric currents, flowing approximately in the same meridian (the N-S direction), deflected westward or eastward. The criterion for the deflection is determined by the angle which the stream line makes with respect to the center line of the oval. If the angle is smaller than 45°, the current is considered to be deflected in either westward or eastward direction. Note that three-dimensional divergence of the current is null with accuracy of ± 2. Note also that in order to see only the major features in Figures 4.6a and b, ionospheric currents with the normalized intensity of more than 10 are indicated with thick arrows.

(1) Of the total inflow (100) along the poleward boundary of the oval in the morning sector, about 50% flows across the oval and into the equatorward field-aligned currents. This is called the N-S closure in this thesis. Note that a relatively large part of this component does not close in the same meridian but has a large westward component in the early morning and the late evening hours and also a large eastward component in the late morning and the late afternoon hours.

(2) Only about 10% of this total downward current flows westward along the nightside oval to form the E-W closure. This is because (6+2)% of the westward current (19%) flows across the polar cap.

(3) Of the total inflow, about 20% (=6+6+2+6) flows across the polar cap. However, this is not a direct connection between the field-aligned currents in the opposite sides, as some parts of those circuits lie along the oval, contributing to westward currents in the oval.

(4) The total inflow along the equatorward boundary of the oval in

the evening sector (50) is discharged from the poleward boundary in the evening sector. This is the N-S closure, but again a large part of this does not close in the same meridian, as pointed out in (1).

(5) The amount of current in the mid-low latitude belt is much smaller than that which flows along the oval. The direction of this current is opposite to the expected direction of the low-latitude return current from the auroral electrojet (a purely two-dimensional current).

(ii) Model [13] (Figures 4.7a and b)

Since the distribution of the field-aligned currents is assumed to be the same as that of Model [10], differences in the two current patterns are due to the enhancement of the conductivities in the oval, as well as to the increased ratio of the Hall to the Pedersen conductivities.

(1) All equatorward field-aligned currents are connected to the poleward field-aligned currents, both in the morning and evening sectors. Thus, of the total field-aligned current into or out from the poleward boundary, 50% closes by flowing across the oval. Again this may be called the N-S closure, but it has a large east-west deflection.

(2) The amount of the polar cap current is less in Model [13] than in Model [10], indicating more concentration of the current along the oval.

(3) As a result of (2), the E-W closure increases.

(4) The amount of current in the middle- and low-latitude region is negligibly small.

(iii) Model [14] (Figures 4.8a and b)

(1) Although the total amount of the N-S current is the same as before (namely, 50%), there is no N-S closure in the same meridian.

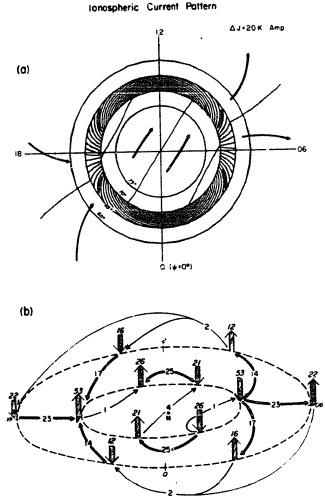

Figure 3.7 a and b (a) Computed current distribution and (b) its schematic illustration for Model [11] (a single ring model). In this model, $\frac{\Delta J}{P}/\frac{P}{P} = 10.0$, $\frac{\Delta J}{H}/\frac{A}{P} = 4.0$, $\frac{P}{H}/\frac{P}{P} = 2.0$ and $\frac{P}{P} = 1$ mho, $\Sigma_H P$

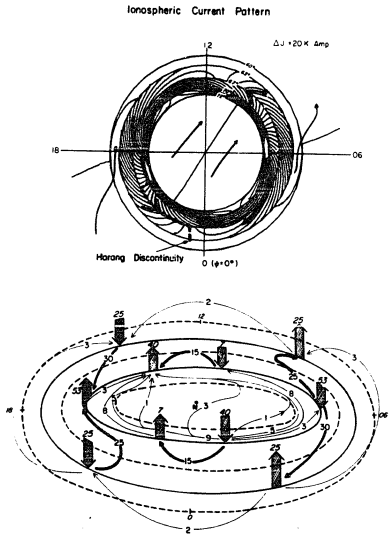

Figure 4.8 a and b (a) Computed current distribution. The thick dashed line shows the Harang discontinuity. (b) Its schematic illustration for Model [14] (a double ring model). In this model, $\Sigma_P^A/\Sigma_P^P = 10.0$, $\Sigma_H^A/\Sigma_P^A = 4.0$ for the region of discrete auroras and $\Sigma_P^A/\Sigma_P^P = 5.0$, $\Sigma_H^A/\Sigma_P^A = 4.0$ for the region of diffuse aurora. $\Sigma_H^P/\Sigma_P^P = 2.0$ and $\Sigma_p = 1$ mho. $\Sigma^M = \Sigma^P$. $I_S^T/I_H^T = 0.5$.

All the currents that contribute to this closure are greatly deflected westward or eastward along the oval. Thus, the N-S closure in Model [14] contributes significantly to the westward electrojet in the early morning sector.

(2) One of the most important differences between Models [13] and [14] is the appearance of the eastward current in the equatorward half (the diffuse auroral region) of the oval in the late evening sector. This is again due to the eastward deflection of the N-S closure current. Note also that this eastward current is deflected at the poleward boundary of the diffuse auroral oval and becomes a westward current. Further, a concentrated westward current flows along the oval of discrete auroras, extending from the westward current in the early morning sector.

(3) Thus, it is possible to delineate the boundary between the regions of the eastward and westward currents in the evening sector. The boundary is shown by a dashed line. This boundary may be identified as the Harang discontinuity.

(4) The ratio of the intensity of the field-aligned currents to that of the ionospheric currents which flow in the region between the poleward and the equatorward field-aligned currents are different before and after midnight. This ratio is larger at pre-midnight hours than at post-midnight hours.

One of the important findings of this study is that the N-S segment of the ionospheric current which connects the pair of field-aligned currents has, in general, an appreciable east-west component. In Model [14] this component has the largest contribution to the westward electrojet.

Another important finding of this study is that the equatorward field-aligned currents in the evening and the morning sectors do not connect to each other. The entire equatorward field-aligned currents are connected with the corresponding fraction of the poleward field-aligned current. This does not seem to depend on models of the ionosphere (which are presently examined) except for the uniform conductivity model, Model [1], and even the relative location of the peaks of the field-aligned currents.

The closure of the remaining fraction of the poleward field-aligned currents greatly depends on the ionospheric conductivity. The direct E-W closure of this current increases when the conductivity is high in the oval compared with that in the other regions. More currents flow in the polar cap and the mid-low latitude region when the auroral oval conductivity is reduced. The deflection of the N-S closure in the westward or eastward direction is also increased with an enhancement of the Hall conductivity in the oval.

The amount of the two-dimensional ionospheric current is surprisingly small for any of the present ionospheric conductivity models. (The purely two-dimensional currents must come from the Hall current if there is no source of the current in the ionosphere. However, when there is gradient (or discontinuity) in the Hall conductivity, the Hall current is not divergence-free, thus not entirely two-dimensional any more.) If this is indeed the case, a magnetic field of the field-aligned current must contribute significantly to the ground magnetic perturbation that have been ascribed to the two-dimensional currents (Fukushima and Kamide, 1973; Leontyev et al., 1974). Thus, the observed magnetic

perturbation in the mid-low latitude belt (positive ΔH in the midnight sector during the magnetospheric substorm) and in the polar cap (S_q^p or DP2) should arise from a net effect of the field-aligned current pair together with the ionospheric currents connected to them.

There have been numerous theoretical studies of ionospheric current patterns, as well as of the magnetospheric current systems. It is of great interest to compare the present results with the earlier studies of ionospheric current patterns, in particular with those studies by Iwasaki and Nishida (1967), Mal'tsev et al. (1973) and Maeda and Maekawa (1973), who obtained ionospheric current patterns or equivalent current patterns under the externally applied 'driving sources'. The three-dimensional current patterns will be discussed later.

The present treatment differs in two essential ways from the earlier treatments. All these authors assumed either a particular charge distribution or potential distribution along specific latitude circles or at points and then solved the Laplace equation for the potential function ϕ for given ionospheric models, while it is assumed here that a particular field-aligned current distribution along specific latitude circles is given. Thus, the present study and the others differ only in the 'driving source'.

A more basic and interesting difference between the study here and the studies by Iwasaki and Nishida (1967) and by Maeda and Maekawa (1973) is that the 'driving source' in the present study is distributed along two latitude circles (as observed), while theirs is distributed along a single latitude circle.

On the other hand, Mal'tsev et al. (1973) assumed the potential distribution along two latitude circles. Thus, the comparison with the earlier studies is possible only for the work by Mal'tsev et al. Further, they assumed a double annular ring which is similar to the one examined in the present work (Model [14]). Unfortunately, however, they showed only the equivalent ionospheric current patterns by including the magnetic field produced by field-aligned currents, making the direct comparison difficult.

One of the most important results in their study is that they reproduced successfully the Harang discontinuity. Thus, the present result is in qualitative agreement with theirs. However, Model [14] reproduced a more realistic current system and the Harang discontinuity than theirs, providing a wide region of the eastward current in the diffuse auroral region in the evening sector and an intense westward current near the poleward boundary of the oval which is the extension of the westward current in the morning sector. These differences may partly be due to the fact that our field-aligned currents are imbedded in the oval, while Mal'tsev et al. assumed the potential distribution (and thus the field-aligned current distribution) along the poleward and equatorward boundaries of the oval.

In summary, this problem can be approached, either from the potential distributions, charge distributions or field-aligned current distributions. However, the electric field observation is, at present, incomplete in obtaining an accurate potential distribution over the entire polar region, as discussed in Section 4.4. On the other hand, even the presently available field-aligned current distribution alone is

extremely useful in studying the ionospheric current pattern. In particular, it is emphasized that the ratio ($\sim$0.5) of the equatorward field-aligned current intensity to the poleward current intensity is of critical importance in this problem. The reversal of the direction of the field-aligned currents with respect to the noon-midnight meridian is also important. Regardless of the methods used, these factors must be included in a model either as results or as required conditions.

As discussed in Chapter I (or see Figure 1.1), various types of three-dimensional current system associated with the magnetospheric substorm have been proposed.

(1) The present result indicates that the real situation appears to be a complicated combination of all these types of current systems. In particular, both the E-W and N-S closures appear always as a combination.

(2) The importance of the E-W closure (the Birkeland type) greatly depends on the ionospheric conductivity distributions. In Model [14] (which simulates realistically the conditions during geomagnetically active times), this closure is a rather minor feature and its contribution to the westward electrojet is not necessarily major in the post-midnight sector.

(3) The pair of field-aligned currents tends to be closed by a N-S segment of the ionospheric current. However, this closure does not occur in the same meridian. For example, for the cases of $I_S^T/I_N^T = 0.5$ 50% of the inflow along the poleward boundary of the oval in the morning sector drives ionospheric currents with a large westward component in the ionosphere, as well as the southward component. Particularly in

the post-midnight sector, the westward electrojet may be identified with this westward component of the current.

(4) This westward component arises obviously from the Hall current. However, this current does not close in the ionosphere by generating the return currents (as indicated in the Boström type (2); Figure 1.1e).

(5) Thus, both the Żmuda-Armstrong type and the Boström type do not represent accurately the real situation.

(6) The present results show that there is only a little two-dimensional current or the so-called 'the return current' (the Chapman type, Figure 1.1b).

The ionospheric closures examined here have a fundamental implication in understanding the coupling between the magnetosphere and the ionosphere. Since the intensities of the poleward and equatorward field-aligned currents are, in general, not equal, the closure by the N-S segment of ionospheric current illustrated in the Boström type (2) and in the Żmuda-Armstrong type does not occur.

For the meridinal N-S closure in the Boström type (2) and in the Żmuda-Armstrong type, it may be necessary to find a radial closure of the currents in the equatorial plane in the magnetosphere (or between the field-lines which 'originate' along the poleward and equatorward boundaries of the auroral oval). The generation mechanism of such a current in the magnetosphere is rather difficult to consider, especially for a steady state, because one may have to rely on currents which arise from the gradient and curvature of the magnetic field (Boström, 1968), but the currents associated with the gradient and curvature drift are mainly azimuthal. However, there is a way to close the ionospheric N-S

connection by the azimuthal currents in the magnetosphere. This is schematically illustrated in Figure 4.9.

It should be noted that a field-aligned current system similar to that illustrated in Figure 4.9 are implied in the studies of the convection of magnetospheric plasma by Fejer (1964), Jaggi and Wolf (1973), Swift (1967, 1971), Vasyliunas (1970, 1971) and others, but they were not calculated. These authors studied the magnetospheric-ionospheric interaction for different driving sources, such as the particle injection into the magnetosphere, the rotation of the earth and the electric field due to the solar wind-magnetosphere interaction. The main emphasis in these studies has been to elucidate the convection pattern or the ring current formation.

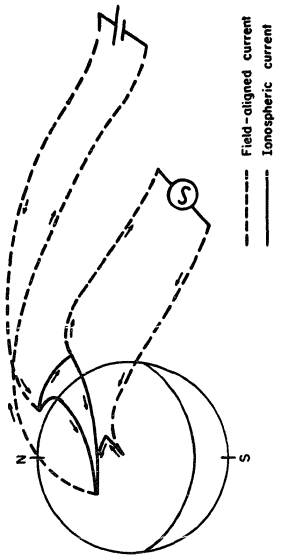

Figure 4.9 The Ionospheric-magnetospheric current system discussed in this thesis.

CHAPTER V

SIMULATION OF THE DEVELOPMENT OF IONOSPHERIC CURRENTS

DURING THE COURSE OF A SUBSTORM

Every quantity in the magnetosphere and in the ionosphere is highly variable both in time and in space during the magnetospheric substorm.

One of the time constants which is important in understanding the ionosphere-magnetosphere system is the induction time constant of the ionosphere τ_i. The entire ionosphere responds to a change of the electromagnetic field within the time τ_i, which is of the order of seconds (Vasyliunas, 1971). The electric field due to time variations of the magnetic field is small enough to be neglected, compared with the static electric field. Thus, if the magnitude and the distribution of the field-aligned currents (which represent the out-puts from the 'black box of the magnetosphere' in the present calculations) are known in the course of a substorm from observations, the distributions of the currents and the electric potential and field in the ionosphere can be obtained, with a good approximation, by using the steady current continuity equation. Further, the azimuthal dependence of conductivity is not included in the present study. With these limitations in mind, it is interesting to try to simulate the distribution of the ionospheric currents, potential and electric field in the course of the substorm by a series of the model calculations.

In this chapter, the results of such an attempt are shown. In Figures 5.1a to c, a series of patterns of the ionospheric electric potential and current, and profiles of the electric field along the

dawn-dusk meridian, are shown. It is assumed that the total intensity of the field-aligned currents varies during the course of the substorm; namely, from the quiet condition to the end of the expansion phase: 10^5, 3×10^5, 7×10^5, 10^6 and 4×10^6 amperes are used for the poleward current. The values of the conductivity, the ratio I_S^T/I_N^T, and the location of the peaks of the poleward and equatorward field-aligned currents are given in Table 5.1. In this Table, the designation for each model corresponds to that of each pattern and profile in Figures 5.1a to c. The reason for assuming the different ratios I_S^T/I_N^T in Models [E] and [F] will be given later. Model [A] represents a quiet condition. This model is similar to Model [2] in Table 3.1 in Section 3.2. The presence of a slightly enhanced conductive belt represents the diffuse precipitation region of the auroral particles which exists even during the quiet periods (see, for example, Winningham et al., 1975). Models [B] to [F] have the two high conductivity rings, representing the discrete and diffuse aurora regions in the auroral oval. These are similar to Model [15] in Table 3.1 in Section 3.2.

The peaks of the poleward field-aligned current are assumed to shift towards the dayside, [C], [D] and [E], because the center line of the field-aligned currents is known to shift during the substorm (Kawasaki et al., 1975). In the following, the simulated progress of the substorm will be examined in detail.

Model [A] represents the quiet condition. The potential pattern for this model ([A] in Figure 5.1a) is slightly rotated clockwise. The potential distribution is uniform in the polar cap. The ionospheric current pattern for this model ([A] in Figure 5.1b) shows a small

			POLAR CAP		AURORAL OVAL				MIDDLE-AND LOW LATITUDES		
	I_N^T	I_S^T/I_N^T	Σ_P	Σ_H/Σ_P	Σ_P	Σ_H/Σ_P	Σ_P	Σ_H/Σ_P	Σ_P	Σ_H/Σ_P	LOCATION OF PEAKS OF $I_{\parallel}$
QUIET TIME ↓ MAXIMUM PHASE	A 10^5	0.5	1	2.0	Σ_P=2.0, Σ_H/Σ_P=2.0				1	2.0	
	B 3 x 10^5	"	"	"	3	2.0	2	2.0	"	"	
	C 7 x 10^5	"	"	"	5	3.0	3	3.0	"	"	
	D 10^6	"	"	"	5	3.0	3	3.0	"	"	
	E 4 x 10^6	0.2	"	"	10	4.0	5	4.0	"	"	
	F 4 x 10^6	0.5	"	"	10	4.0	5	4.0	"	"	

TABLE 5.1 List of the parameters of the models which are used to simulate the substorm. The unit of the conductivity is in MHO and the unit of the total intensity of the field-aligned current is in ampere.

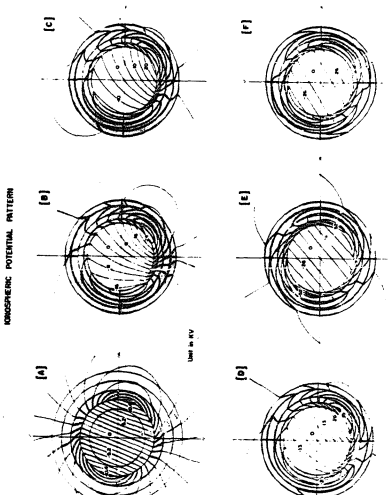

Figure 5.1 The ionospheric potential patterns (a), ionospheric current patterns (b) and the electric field profiles (c) in simulating the magnetospheric substorm by the present model calculations. For the parameters of Models [A] to [F], see Table 5.1.

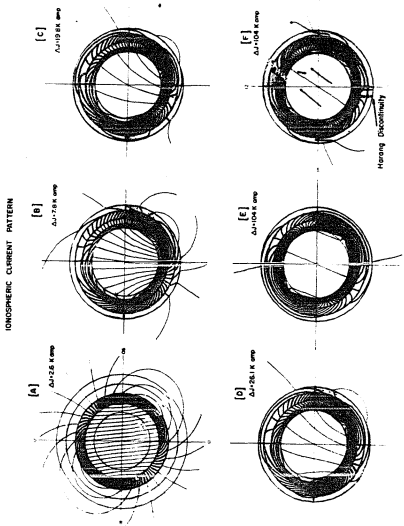

FIGURE 51.1

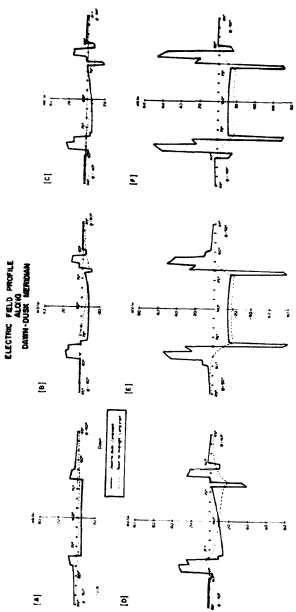

FIGURE 5.1c

counter-clockwise rotation in the polar cap, while the current pattern is rotated clockwise in the auroral oval and the middle- and low-latitudes. The considerable portion of the current fed by the field-aligned currents flows through the polar cap as well as middle- and low-latitudes.

Models [B], [C] and [D] represent the early epoch of the expansive phase. The poleward field-aligned current is suddenly intensified around 21LT and 03LT. It is observed that these peaks of the field-aligned currents start to move towards the dayside. At the same time, an intense precipitation into the discrete auroral region is observed, and the diffuse aurora is also intensified, causing an increase of the ionospheric conductivity. These features are taken into account in Models [B], [C] and [D]. During early epoch, the potential patterns ([B], [C] and [D] in Figure 5.1a) in the polar cap become non-uniform and are rotated clockwise considerably. The non-uniformity is due to the concentration of the net field-aligned currents in the night sector (Section 4.2.4), while the rotation is due to an enhancement of the conductivity in the auroral oval (Section 4.2.1). In the dayside polar cap, effects of the enhancement of the auroral oval conductivity are greater than effects of the location of the peaks of the field-aligned currents. In the nightside polar cap, this relation is reversed. This difference increases the non-uniformity of the potential in the polar cap. The amount of the rotation reaches the peak value at the stage of [D] (about 60°) (Section 4.2.1).

In the nightside auroral oval, the southward component of the electric field begins to increase in the midnight-early-morning sector,

while in the evening sector the region of a large southward component of the electric field appears on the poleward side of the northward component region.

The ionospheric current patterns [B], [C] and [D] in Figure 5.1b (for the direction of the current, see the pattern [F] in this figure) during the early epoch of the expansive phase show a large difference from that of the quiet time. In [B], the polar cap current pattern is almost symmetric with respect to the noon-midnight meridian, and it diverges towards the dayside. In the late evening-midnight sector, a highly concentrated westward current appears along the poleward edge of the oval. In the afternoon-early-evening sector, there appears the region of large eastward currents. In the midnight-early morning sector, a strong westward current prevails over the entire oval. In [C] and [D], all the currents mentioned for [B] are enhanced, except for the polar cap and the middle- and low-latitude currents. In [D], the westward current region with the highly concentrated current along the poleward edge of the late evening oval starts to move towards earlier local hours, penetrating poleward of the strong eastward current region. Thus, a clear demarcation line develops between the regions of the eastward current and the westward current (Section 4.6). The polar cap currents are deflected towards the morning sector. The ratio of the total amount of this current to that of the auroral oval current are considerably reduced, although the absolute intensity is increased a little (94, 99 and 156k amp for [B], [C] and [D], respectively. Compare these amounts with the auroral oval currents, 200, 600 and 850k amp.). The same reduction is also seen for the middle- and low-latitude current. This reduction is

greater in [C] than in [D] because of the different longitudinal distribution of the poleward field-aligned current between these two models (Section 4.6).

Models [E] and [F] may represent the maximum epoch of the expansion phase or the beginning of the recovery phase. The values of the conductivities in the auroral oval, as well as the ratio of the Hall to the Pedersen conductivities, become the largest (for the values of the conductivities used in this chapter, see Brekke et al., 1974). The locations of the maximum and the minimum of the poleward field-aligned currents reach as far as 06 and 18 local times, respectively. Two different ratios $I_S^T/I_N^T = 0.2$ and 0.5 are assumed in Models [E] and [F], respectively. It is implied here that the mechanism, which is responsible for the equatorward field-aligned current, does not respond immediately to the mechanism which caused the enhancement of the poleward field-aligned current. This problem has been studied by a number of workers (Fejer, 1964; Swift, 1967, 1971; Vasyliunas, 1970, 1971; Jaggi and Wolf, 1973), and the time constant in this process (in which the plasma sheet or the ring current plays an important role) is known to be of the order of several tens of minutes to hours, depending on the ionospheric conductivities. Their mechanism will be described in the next chapter.

[E] and [F] in Figures 5.1a and b show the potential and the current patterns for Models [E] and [F]. The two patterns of the potential are almost the same, except for the rotation in the middle- and low-latitudes. The amount of the rotation in the polar cap for these models is almost the same as that for Model [D] (Section 4.2.2). The potential distribution in the polar cap is uniform.

In the current patterns, a drastic decrease of the intensity ratio of the polar cap current to the oval current can be seen (Section 4.2.1). The boundary between the westward and the eastward currents in the evening sector becomes clearer than before. This boundary is shown by thick dashed line in [F] of Figure 5.1b. In model [E], the proportion of the east-west closure of the field-aligned currents is larger than in any other five models, because of the smaller ratio of $I_S^T/I_N^T = 0.2$ instead of 0.5 for the others (Section 4.6) and the east-west closure currents become dominant. However, it should be noted that this value 0.2 of I_S^T/I_N^T is the lower extreme that was observed (Section 2.4).

Figure 5.1c shows the electric field profiles (both the dawn-to-dusk and the noon-to-midnight components, E_y and E_x, respectively), along the dawn-dusk meridian for each model. In this figure, the solid curves are for E_y and the dashed curves for E_x. Here, the latter will not be discussed. The profiles of E_y do not change much with models, except for the variation around the auroral oval (Section 4.4). It is also seen that the magnitude of this component in the polar cap increases by only a factor of 3 or so, although the conductivity in the auroral oval and the intensity of the field-aligned currents (thus of the ionospheric currents, particularly, in the auroral oval) increase by about an order of magnitude. Note that the Hall conductivity in the oval varies from 4 mho in Model [A] to 40 mho in Model [F], while the total intensity of the poleward field-aligned currents increases from 10^5 amperes to 4×10^6 amperes. On the contrary, E_y decreases twice with the 'progress' of the substorm from the stage represented by Model [B] to the stage represented by Model [C] and Model [E] to Model [F].

This insensitive nature of the dawn-to-dusk component of the polar cap electric field to the substorm activity is in agreement with the OGO-6 satellite observation (Heppner, 1972). However, this does not necessarily mean that the total potential difference across the polar cap does not change appreciably; in fact, it increases by about a factor of 5. In Table 5.2, the total intensity of the poleward field-aligned current I_N^T, the total potential difference across the polar cap $(\Delta\phi)_t$, E_y at the pole and the potential difference obtained by integrating E_y along the dawn-dusk meridian $\Delta\phi$ for each model are listed. $(\Delta\phi)_t$ is related to I_N^T better than $\Delta\phi$ is. The reason for this is the rotation of the potential pattern in the polar cap (Section 4.2). The relation between $(\Delta\phi)_t$ and I_N^T depends on the conductivity, the locations of the peak of I_N^T and the ratio I_S^T/I_N^T in a complicated way.

The patterns of the calculated ionospheric currents and the potential shown above, may qualitatively explain some of the magnetic variations observed on the ground during the magnetospheric substorm;

(1) During the substorm, horizontal perturbation vectors $\Delta\vec{H}$ of the magnetic field observed at the polar cap stations are rotated clockwise (Iijima and Nagata, 1972; Kamide et al., 1974). This is explained by the clockwise rotation of the polar cap potential pattern (and thus, of the Hall current direction) due to the enhancement of the auroral oval conductivities. The field-aligned currents also contribute to this clockwise rotation. Indeed, the clockwise deflection of $\Delta\vec{H}$ from the direction of the horizontal perturbation of the magnetic field expected from the Hall current was reported and attributed to the field-aligned currents (Haerendel and Lüst. 1970, Heppner et al., 1971;

	I_N^T	$(\Delta\phi)_t$	E_y at Pole	$\Delta\phi(=\int E_y dy)$
[A]	1×10^5	24kV	4.7 vot/km	23kV
[B]	3×10^5	45	7.8	28
[C]	7×10^5	50	5.8	24
[D]	1×10^6	70	9.0	30
[E]	4×10^6	113	15.7	86
[F]	4×10^6	98	10.4	50

TABLE 5.2 Table of the total potential difference across the polar cap $(\Delta\phi)_t$, the dawn-to-dusk component of the electric field E_y at the pole and the potential difference across the polar cap obtained by integrating E_y along the dawn-dusk meridian in the course of the substorm.

Wescott et al., 1970). During periods of the oval conductivity enhancement, the concentration of the ionospheric currents in the oval occurs and the smaller ratio of the intensity of the polar cap Pedersen current to that of the field-aligned currents makes the magnetic effects of the field-aligned currents larger in the polar cap. (Note that the magnetic effects of the Pedersen current and the field-aligned currents are opposite.) The rotation of $\Delta\vec{H}$ during the substorm may be the combination of these two effects.

(2) The latitudinal distribution of the westward and the eastward ionospheric currents, as well as the Harang discontinuity and its location in local time, can be well reproduced.

(3) The observed spatial relation among the regions of the westward and the eastward currents and the discrete and the diffuse auroras can be also reproduced. Kamide and Akasofu (1975) showed that in the evening sector, the region of the westward current corresponds to that of the discrete aurora and the region of the eastward current to that of the diffuse aurora, while in the morning sector the westward current dominates the entire oval.

(4) The eastward electrojet does not always grow and decay simultaneously with the westward electrojet (Kamide and Fukushima, 1972; Rostoker and Kisabeth, 1973). The eastward jet arises from the eastward deflection of the N-S closure of the field-aligned currents and the westward jet from the westward deflection of the N-S closure, together with their E-W closures as shown by the present calculations. Then the relative intensity of the eastward jet to that of the westward jet depends on the relative importance of the N-S and the E-W closures of the field-

aligned currents, which are, in turn, function of the auroral zone conductivity, the longitudinal distribution of the field-aligned currents and the ratio I_S^T/I_N^T. However, there should be a general tendency of synchronous intensification in the eastward and the westward electrojets, since they are two different branches of one three-dimensional current circuit (see Figure 4.9).

(5) In the evening sector, the signs of the E-W components of the magnetic perturbations observed on the ground and deduced from the observations by the incoherent scatter radar at Chatanika are opposite during substorms. On the other hand, in the morning sector, there is a reasonable agreement between them (Kamide et al., 1975). This may be explained by the difference of the ratio of the ionospheric current intensity to the field-aligned current intensity between the evening and the morning sectors (Section 4.6). To verify this conclusion, however, actual calculations of the magnetic fields due to the ionospheric and the field-aligned currents in the present model are necessary.

CHAPTER VI

GENERAL DISCUSSION AND SUMMARY

6.1 GENERAL DISCUSSION AND SUMMARY

In this thesis, the electric currents, electric potential and electric field in the ionosphere were investigated by model calculations for various models of the ionospheric conductivity with the field-aligned currents as a boundary condition. Since the field-aligned currents represent one of the most important aspects of the coupling between the ionosphere and the magnetosphere, it was intended to gain understanding of some roles of the ionosphere as one end of the magnetosphere-ionosphere feed-back system.

For this purpose, the features of the field-aligned currents are a very important factor. By analyzing magnetic records from the TRIAD satellite, Żmuda and Armstrong (1974b) showed that upward and downward field-aligned currents appear as a pair at all local time (except in the noon sector) and that the direction of such currents is reversed with respect to the noon-midnight meridian, regardless of the degree of geomagnetic activity. In this thesis, by analyzing the same TRIAD data, it was found that the poleward field-aligned currents are more intense than the equatorward currents, the average ratio being 2:1. On the basis of their observed features of the field-aligned currents, the calculations for the ionospheric electric potential, electric currents and electric field were made. The ionospheric models with high-conductive belts but azimuthally uniform were adopted. From these calculations, several new results have been obtained.

The three-dimensional current system has been found to be neither a simple Birkeland type, Boström type nor Zmuda-Armstrong type. Instead, these types almost always co-exist. For example, the field-aligned currents flow into the ionosphere and then flow partly along the auroral oval, partly across the oval and partly across the polar cap before they flow out from the ionosphere.

The present calculations show that the entire equatorward field-aligned current is almost always connected to the same amount of the poleward field-aligned current. Thus, the amount of the N-S closure is determined by the amount of the equatorward field-aligned currents, while that of the E-W closure depends on the other parameters, such as Σ^A/Σ^P, Σ_H^A/Σ_P^A, and the longitudinal dependence of the field-aligned currents. When the enhancement of the conductivity in the auroral oval is small, the amount of the E-W closure is small. When the conductivity in the oval is enhanced, the ionospheric currents are concentrated in the oval and the amount of the E-W closure increases at the expense of the closure through the polar cap or middle- and low-latitude belt. There is no E-W closure between the incoming and the outgoing equatorward field-aligned currents. Since the intensity of the equatorward field-aligned current is about half of the intensity of the poleward one and since the entire equatorward field-aligned current is discharged with the poleward current, the N-S closure is the main closure. However, a large part of the ionospheric currents that constitute this closure are deflected westward or eastward along the oval, contributing to the westward and the eastward electrojets, respectively.

By using the model with two different high-conductive annular rings (simulating the discrete and the diffuse auroral regions) a combination of the various types of the closure has been shown to reproduce the major features of the magnetic perturbations observed on the ground during magnetospheric substorms. Particularly, in the evening sector, an intense westward current flows poleward of the less intense eastward current, while in the morning sector the westward current is dominant over the entire oval. The boundary between the westward and the eastward currents is known as the 'Harang discontinuity', which is well reproduced in the present models.

In the dayside, however, there appears the ionospheric current pattern similar to the nightside one. This may be removed by introducing the azimuthal dependence of the conductivity as suggested by Swift (1967).

Another important conclusion is that the ionospheric current system during the substorm can be reasonably reproduced without invoking a special field-aligned current system which is different from the one during the quiet time.

Instead, changes of the distribution of the ionospheric conductivity, namely appearance of the high conductive region (discrete aurora region) poleward of the existing diffuse aurora region will do this. The present models can reproduce also gross features of the polar region electric field.

When the ionospheric conductivity is uniform, the ionosphere plays only a passive role and acts just as a 'load' or a 'resistance', which discharges the voltage difference imposed from the outside. However, when the conductivity is not uniform, the current flows through the regions

of non-uniform conductivity and builds up the space charges in the region where the gradient (or the discontinuity) of the conductivity is present. Such space charges modify the potential (or the field-aligned current) distribution imposed from outside. Then the ionosphere is no longer a simple resistance. The rotation of the polar cap potential pattern studied in Chapter IV shows this effect. When the Hall conductivity in the auroral oval is enhanced, the potential pattern in the polar cap is rotated clockwise, as long as the field-aligned current distribution is fixed to the sun-earth line. If the potential pattern in the polar cap is considered to represent the convection pattern, driven by the solar wind, the present calculations suggest that the direction of the solar wind is deflected by the magnetosphere. This seems to be unreasonable. How can this unreasonableness be removed?

The first possibility is that the field-aligned current pattern rotates counter-clockwise in such a way that the potential pattern becomes symmetric with respect to the noon-midnight meridian. However, the TRIAD data show that the boundary at which the field-aligned currents change their direction is located around the noon-midnight meridian within the accuracy of $\pm$ 0.5 hrs or so. Further, if the source of the poleward field-aligned current is considered to be the solar wind-magnetosphere dynamo or the neutral line which encircles the earth, as proposed by Akasofu (1974), it is difficult to imagine a large counter-clockwise rotation. The magnetic and the plasma configurations in the outer magnetosphere is known to be reasonably symmetric.

The second possibility is that the longitudinal distribution of the poleward field-aligned current is highly complicated, although the upward

and downward currents are confined in the evening and morning sectors, respectively. The rotation of the polar cap potential pattern is mainly controlled by the enhancement of the Hall conductivity in the auroral oval and the distribution of the poleward field-aligned current. The enhancement of the equatorward field-aligned current intensity makes the rotation angle even larger. A model with the peaks of the poleward field-aligned current at 06 (downward) and 21LT (upward) is examined whether or not the effect of the enhancement of the Hall conductivity in the auroral oval can be compensated by the effect of the asymmetric distribution of the poleward field-aligned current. It is found that this is not possible.

The third possibility is the azimuthal dependence of the conductivity is important in removing the unreasonableness. The day-night asymmetry of the conductivity due to the sunlight does not seem to contribute much to the rotation of the polar cap potential pattern. For simplicity, consider the conductivity discontinuity at 06 and 18 local hours. Then the positive space charges arise at the both local hours since the directions of the ionospheric currents are southwest and northeast at 06 and 18LT, respectively (for example, see the current patterns in Figure 4.1b). These space charges contribute little to the rotation of the polar cap potential pattern, although they may deform it. Further, during mid-summer or mid-winter season, the day-night asymmetry due to the sunlight is considerably reduced. The effects of the conductivity enhancement due to auroral precipitations are different. Suppose that there is a high conductive region between 21LT and 3LT. At 21LT, the current is almost

northward (see the current patterns in Figure 4.1b) and does not produce much space charge due to the conductivity discontinuity, since the current flows almost parallel to this discontinuity. On the other hand, at 3LT, the current flows westward and produces negative space charges at the conductivity discontinuity. This space charge configuration counteracts the clockwise rotation of the polar cap potential pattern. However, the effectiveness of this space charge is not clear.

The fourth possibility is that the polar cap potential pattern in the ionosphere and above the ionosphere is different. This possibility requires, however, further study. In this case, the electric field parallel to the magnetic field must exist over the polar cap.

The importance of the active role of the ionosphere due to the conductivity discontinuity was shown also in Section 4.5. In that section, the degree of the penetration of the high latitude convection electric field into lower latitudes was shown to depend significantly on the location of the equatorward field-aligned current with respect to the location of the gradient of the ionospheric conductivity.

Finally, the probable over-all view of the magnetospheric process is reviewed. A large part of the following over-all view is due to hints by D. W. Swift. It is a well established concept that the solar wind flow around the magnetosphere causes the plasma convection in the magnetosphere. Two energy transfer mechanisms from the solar wind to the anti-sunward flow of the magnetospheric plasma have been proposed; one is the viscous-like interaction (Axford and Hines, 1961) and the other the merging of the earth magnetic field lines with the interplanetary

magnetic field lines (Dungey, 1961). However, in these concepts, the sunward flow of the plasma in the body of the magnetosphere is assumed to be a natural return flow of the anti-sunward flow near the magnetopause. This is equivalent to assuming that the electric field created at the magnetopause can penetrate deep into the magnetosphere. However, there is plasma in the magnetosphere, and this plasma tends to shield out the imposed electric field out of the main body of the magnetosphere. The role of the ionosphere becomes important here. The electric field created by the interaction between the solar wind and the magnetosphere is transferred down to the ionosphere at the poleward edge of the auroral oval through the magnetic field lines. Since the ionosphere acts as a conductor for static or slow varying electric fields, the transferred electric field sets up an electric field distribution over the entire ionosphere. This ionospheric distribution of the electric field is, in turn, mapped back to the magnetosphere. It is this process which introduces the electric field into the main body of the magnetosphere. Then the magnetospheric plasma ExB drift takes place. The direction of this plasma drift can be easily seen when one considers that the equipotential lines in the ionosphere are encircling the space charges associated with the imposed electric field (the positive charges in the morning sector and the negative charges in the evening sector). This ExB drift can be identified with the 'return flow' of the original anti-sunward flow.

Since the magnetospheric plasma (plasma sheet plasma) are not a cold plasma, they drift due to the gradient and the curvature of the magnetic field. They also participate in the corotation drift. The

superposition of the plasma motions due to these drift motions cause the pressure gradient in the direction of the ∇B drift. This results in the space charge accumulation, thus the field-aligned currents (Vasyliunas, 1970). This field-aligned current can be identified with the equatorward field-aligned currents. While these space charges tend to be discharged, to some extent, by the field-aligned currents through the ionosphere, the remaining space charges tends to cancel the primary electric field and modifies the magnetospheric convection. The ionosphere affects the magnetospheric convection in the process of distributing the original electric field and of discharging the space charges resulted from the convection. This whole process is implied in the works by Swift (1971), Vasyliunas (1971) and Jaggi and Wolf (1973). As the plasma particles drift in closer to the earth, the pitch angle distribution of the particles becomes more anisotropic if the first invariant of particle motion is assumed to be conserved. Then the particle precipitation would take place due to the pitch angle diffusion (Kennel, 1969) and cause the diffuse auroral luminosity. The diffuse auroral region would almost coincide with the region of the equatorward field-aligned current.

In the view expressed in the above, the equatorward field-aligned current can be considered as the secondary current, while the poleward one is the primary current. The observation reported in Chapter II in this thesis that the poleward field-aligned current is more intense than the equatorward one, supports this point. One of the results of the present calculations is that the entire equatorward field-aligned current is connected to the same amount of the poleward field-aligned

current. This supports the hypothesis that the driving force from outside the magnetosphere is transferred to the main body of the magnetosphere through the ionosphere. Under the process mentioned in the above, the enhancement of the ionospheric conductivity at the foot of the poleward field-aligned current would result in the substorm ionospheric current system.

Thus, the above theoretical models appear to provide at least qualitiatively the field-aligned currents observed by TRIAD. However, their main emphasis has been to elucidate the convection pattern, and none of them attempted to include a quantitative calculation of the resulting field-aligned currents. Therefore, it is urgent to extend to their study and examine whether or not the resulting characteristic field-aligned currents agree with those of the observed ones.

The present thesis is based on the observed characteristics of the field-aligned currents, and its sole purpose is to elucidate the relationship between the observed field-aligned currents and the induced ionospheric currents. Therefore, the results do not depend on the mechanisms which drive both the primary and secondary currents. However, it is hoped that the whole subject can eventually be treated in a self-consistent way and that the inferred mechanism for the secondary current is proven to be correct.

6.2 FUTURE STUDY

1) The detailed characteristics of the field-aligned currents, such as the longitudinal distribution of the field-aligned currents, the local time dependence of the ratio between the intensities of the poleward and the equatorward field-aligned currents and the relationship of those

quantity with geomagnetic activity, are needed in extending the present study.

2) In the present study, the azimuthal dependence of the ionospheric conductivity was not included. This should be included in future models.

3) The magnetospheric closure and the generation mechanism of the secondary current should be re-examined since the latitudinal width of the equatorward field-aligned current sometimes seems to be too wide (5°) to correspond to the 'Alfvén Layer' or the inner edge of the plasma sheet.

4) It is necessary to calculate magnetic fields due to both the ionospheric and field-aligned currents of the presented models to compare the results in more detail with ground magnetic observations.

APPENDIX I

Figures A1a,b, A2a,b and A3 referred in Section 4.2.4

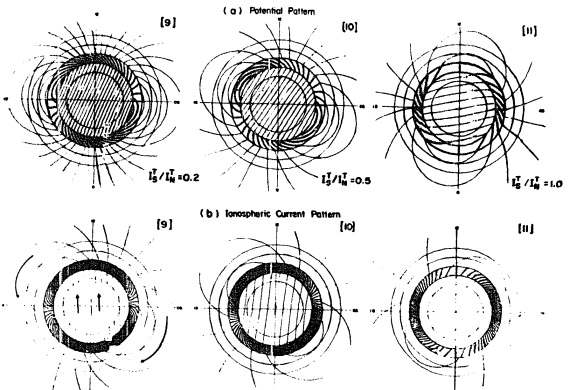

Figure A1 The calculated potential patterns (a) and current patterns (b) in the ionosphere for Models [9], [10] and [11]. For these models, the ratio I_S^T/I_N^T is different. I_S^T/I_N^T = 0.2 for [9], 0.5 for [10] and 1.0 for [11]. In all models χ_P^A/χ_P^P = 5.0, $\chi_H^A/\chi_P^A = \chi_H^P/\chi_P^P$ = 2.0, and $\chi^N = \chi^P$. The field-aligned currents are located along the two latitude circles 70° and 65°. The peaks of the field-aligned currents are at 06 and 18LT. The direction of the ionospheric currents is shown by thick arrows in Pattern [4].

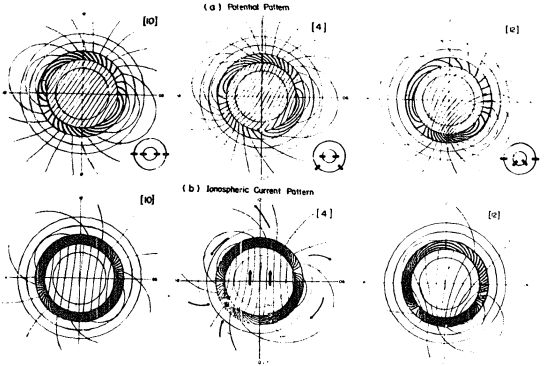

Figure A2 The calculated potential patterns (a) and current patterns (b) in the ionosphere for Models [10], [4] and [12]. For these models, the location of the field-aligned current peak are different. This location is shown schematically for each model. The field-aligned currents are located along the two latitude circles 70° and 65°. $I_S^P/I_N^P = 0.5$. In all models $\lambda_P^A/\lambda_P^P = 5.0$, $\lambda_H^A/\lambda_P^A = \lambda_H^P/\lambda_P^P = 2.0$ and $\lambda^M = \lambda^P$.

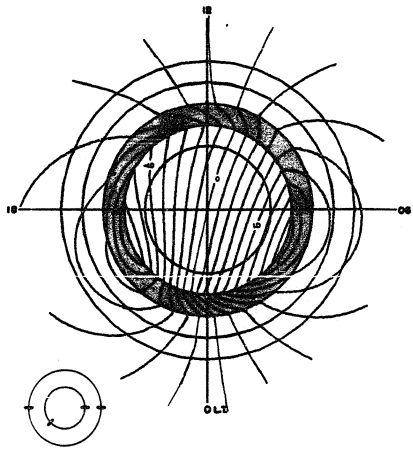

Figure A3 The calculated ionospheric potential pattern for the poleward field-aligned current distribution which is asymmetric with respect to the noon-midnight meridian. The peaks of the field-aligned currents are at 06 and 21LT for the poleward current and at 06 and 15LT for the equatorward current, respectively. $I_S^T/I_N^T = 0.5$. $r_T^A/r_T^P = 5.0$, $r_H^A/r_P^A = r_H^P/r_P^P = 2.0$ and $r^M = r^P$.

APPENDIX II

The computer program used in the present study is listed here. The main routine to calculate potentials ϕ and electric fields E is labeled "POEGEN". In "POEGEN", the two subroutines are used: the one "DCOMP" to obtain the Fourier components of given field-aligned current distributions and the other "KEISUH" to calculate the coefficients P^i, A^i_n's, B^i_n's, C^i_n's and D^i_n's in the equation

$$\phi^i = P^i \ln(\tan\frac{\theta}{2}) + \sum_{n=1}^{n} \left[\left\{ A^i_n (\tan\frac{\theta}{2})^n + B^i_n (\cot\frac{\theta}{2})^n \right\} \sin n\psi + \left\{ C^i_n (\tan\frac{\theta}{2})^n + D^i_n (\cot\frac{\theta}{2})^n \right\} \cos n\psi \right]$$

where i represents the name of the regions.

The current function J is computed by the main program labeled "AMPGEN" which is almost the same as "POEGEN". The plotting of the equi-potential and the equi-current-function contours is done by the main routine labeled "PLCON". The plotting of the electric field is done by the main routine labeled "PLEF".

```
                    MAINPROGRAM    POEGEN
C
C POTENTIAL CONTOUR GENERATION PROGRAM - WITH FIELD-ALIGNED CURRENTS AS
C BOUNDARY CONDITIONS FOR MANY CONDUCTING STRIPS.  NO PHI DEPENDENCE OF
C CONDUCTIVITY. THIS ROUTINE WRITES A DISK FILE WHICH WILL BE PLOTTED
C BY SEPARATE PROGRAMS CUE TO LARGE AMOUNT OF DATA - WHICH WON'T FIT IN
C CORE - AN ARRAY (360, 41, 6) REQUIRES 236K BYTES AND 360-40 HAS ONLY
C 125K AVAILABLE.   THIS VERSION IS ESSENTIALLY SAME AS PROGRAM POTGEN
C WRITTEN BY SHIRLEY LISS.
C
C TO GET COEFFICIENTS, SOLVE 10 BY 10 SIMULTENEOUS EQUATIONS.
C THEN POTENTIAL AND ELECTRIC FIELD CAN BE OBTAINED EASILY.
C UNITS OF POTENTIALS ARE E-FIELD ARE A MULTIPLES OF 25KV ( SEE FAC25K
C I.E. FAC25K * 25KV ) AND  VOLT / KM, RESPECTIVELY.
C
      REAL*8  CHAR(2,5)
      DIMENSION      KLAB(46),
     1   RAY(181),   RAI(181),   PCTS(41,6),   CBCTH(7),
     2   N(6),       ALPHA(6),   BETA(6),      COEFF(4,6,20),  P(5),
     3   RATH(6),    RG(6),      CBCCU(5,20),SBCCU(5,20),
     4   RATHH(6),   CURD(5,5),  CSPH(5,5),    CETH(6),
     5   PATH(181), PAPH(181), CONST(5), SP(20), CP(20)
      DIMENSION      CNEAT(61,3,4)
      EQUIVALENCE    (CBCTH(2),TH1), (DBCTH(2),TH2), (DBCTH(4),TH3),
     1               (CBCTH(5),TH4), (DBCTH(6),TH5), (DBCTH(7),THF)
      EQUIVALENCE    (CNEAT(1,1,1), PAPH(1)),
     1               (CNEAT(1,1,2), PATH(1)),
     2               (CNEAT(1,1,3), RAY(1)),
     3               (CNEAT(1,1,4), RAI(1) )
      DATA     CHAR/ 'MCR.CEN1',
     1               '.(DENS.)',
     2               'MOR.WID.',
     3               '(DENS.) ',
     4               'ROUND.IN',
     5               'EOLT (O)',
     6               'EVE.CEN1',
     7               '.(DENS.)',
     8               'EVE.WID.',
     9               '(DENS.) ' /
      COMMON   R, SIG, NTF, DTR
      BUFF = 99.0
      DTR = 3.1415927 / 180.0
      R = 6488
C
C FORMAT DISK FILE -- REC 1-360 - POTENTIALS FOR EACH PHI, REC 361 FOR
C INPUT PARAMETER LIST, REC 362-363 PHI AND THETA COMP OF RAY( E-FIELD )
C SPECIFIED ON INPUT CARD 1. FOLLOWING GROUPS OF 6 RECORD WILL HAVE
C SIMILAR DATA AS LCAG AS INPUT CARDS REQUESTING RAYS ARE IN INPUT LIST.
C UP TO 10 PROFILES ARE ALL RIGHT, THEN FILE ON DISK IS FULL
C
      CALL  CLROSK(8, 401, 246, 'U', BUFF)
```

```
      DEFINE FILE   8(401, 246, U,  INDEX)
      DO 5  K=1,46
      K(LAB(K) = K -1
    5 CONTINUE
      IDMP = 0
      ISTOP = 0
C
C READ PARAMETERS.
C
      READ(1,101)  SIG, NTF, DPHI, LIST, FAC25K
  101 FORMAT(F10.2, I5, F10.2, I5, F10.2)
      READ(1,102) (DETH(I), I=1,6), (ALPHA(I), I=1,6), (BETA(I),I=1,6)
  102 FORMAT(6F1C.2 / 6F6.2, 5X, 6F6.2 )
      READ(1,103)  ((CURD(I,J), I=1,5), (CURM(IS,J), IS=1,5), J=1,5)
  103 FORMAT(5F6.1, 5E1C.3 )
C
      STEP = 1.
C
      DO  7  I=1,6
      DBETH(I+1) = DETH(I)
    7 CONTINUE
      DBETH(1) = 0.0
C
C LOAD N ARRAYS AND CONVERT TO RADIANS AND HALVE.
C
      DO 9  I=1,6
      N(I) = DBETH(I+1) - DBETH(I)
      RATH(I) = DETH(I)*CTR
      RATHH(I) = RATH(I)/ 2.
    9 CONTINUE
      N(6) = N(6) + 1
C
C WRITE PARAMETERS TO DISK ON REC 361.
      IREC = 361
C
      WRITE(8'IREC)  DETH, ALPHA, BETA, SIG, CURD, CURM, DPHI, NTF,
     1              FAC25K, LIST
      WRITE(3,301)  SIG, DPHI, DETH, ALPHA, BETA, N, NTF, FAC25K
  301 FORMAT('1   INPUT  PARAMETERS ', /
     1    'O       SIGMA =', F4.1, 2X, 'PHC', 10X,
     2'INCREMENT OF PHI =', F5.2, / 1HC, 12X, 'REGION', 19X, 'I', 15X,
     3'II', 13X, 'III', 14X, 'IV', 14X, 'V', 15X, 'VI', /,
     4    '  THI, TH2, TH3, TH4, TH5, THF = ', 6I6X, F10.1), //,
     5    '          ALPHA ( 1 - 6 )          = ', 6(F8.2, 8X),  /,
     6    '          BETA  ( 1 - 6 )          = ', 6(F8.2, 8X),  /,
     7    '          POINTS PER REGION        = ', 5X, 6(I2, 14X), /,
     8    '                NTF                = ', I3, //,
     9    '          UNIT OF POTENTIAL        = ', F10.2, '  * 25 KV', // )
      WRITE(3,304)
  304 FORMAT('  DISTRIBUTION AND MAGNITUDE OF FIELD-ALIGNED CURRENTS',/)
```

```
      WRITE(3,210)
  210 FORMAT(' ',43X, 'TH1', 13X, 'TH2', 13X, 'TH3', 13X, 'TH4', 13X,
     1                'TH5', /)
      WRITE (3,305) ( CHAR(1,I), CHAR(2,I), ( CURD(I,J), CURM(I,J), J=
     1 1,5 ), I=1,5 )
  305 FORMAT ( 5 ( ' ', 10X, 2A8, 11X, 5 ( F4.0, '(', F6.1, ')', 4X ),
     1 / ))
C
C CALL FOR COEFFICIENT AND CALCULATE POTENTIALS.
C
C
      CALL  OCOMP(CURD, CURM, SBCCU, CBCCU, CONST)
C
      CALL  KETSUN(ALPHA, BETA, RATH, SBCCU, CBCCU, COEFF)
C
      WRITE(3,302)  KLAB
  302 FORMAT(///, '   RAY ', T50, ' POTENTIALS ',/,
     1            '   PHI ', 2315, /, '       ', 2315, //)
      ROS = R/SIG
      P(1) = 0.0
      P(6) = 3.0
      DO 10  I=2,5
      P(I) = -0.C0004*(-ALPHA(I-1)*P(I-1)
     1                 + ROS*CCNST(I-1)*SIN(RATH(I-1)) ) / ALPHA(I)
   10 CONTINUE
C LOOP FOR EACH PHI     1 -- 360 DEGREE WITH INCREMENT DPHI  INDEX = IP
C
      INCP = DPHI
      DO 400  IP = 1, 36C, INCP
C
C SET  PMAX = 0  -- MAXIMUM POTENTIAL ALONG RAY.
C
      PMAX = 0.
      DO 8  I=1,NTF
      PHIR = I*IP*DTR
      SP(I) = SIN(PHIR)
      CP(I) = COS(PHIR)
    8 CONTINUE
C
C CALCULATE POTENTIAL IN FOLLOWING LOOPS LOADING RAY ARRAY
C IR = 1 - 6  FOR EACH REGION,  IN = 1 -- N(IR) FOR NUMBER OF POINTS
C IN EACH REGION.
C
      DO 100  IR=1,6
      NN = NUINT
      DO 80  IN=1, NN
      THC = DBOTH(IR) + IN - 1.
      IF( THC .EQ. 0. )  GO TO 15
      THHR = THC*DTR/2.
      JR = THC + 1.
```

```
      CTT = COTAN(THHR)
      TT = TAN(THHR)
C
C GET POTENTIALS.
C
      OI = C.0
      DO 20  NT=1,NTF
      CTTN = CTT**NT
      TTN = TT**NT
      OI = OI + (COEFF(1,IR,NT)*TTN + COEFF(2,IR,NT)*CTTN)*SP(NT)
     1        + (COEFF(3,IR,NT)*TTN + COEFF(4,IR,NT)*CTTN)*CP(NT)
   20 CONTINUE
C
      OI = ( OI + P(IR)*ALOG(TT) )/FAC25K
      GO TO 30
C
   15 JR = 1
      OI = C.0
C
   30 PMAX = AMAX1( PMAX, ABS( OI ) )
      RAY(JR) = OI
   80 CONTINUE
  100 CONTINUE
      WRITE(3,303)  IP, (RAY(I), I=1,46)
  303 FORMAT( ' ', I3, T8, 23F5.2, /, ' ', T8, 23F5.2, / )
C
C AT THIS TIME, WE HAVE A SET OF 46 POTENTIALS ALONG LINE OF PHI=CONST.
C NOW WE MUST INTERPOLATE FOR VALUES WE WANT (-4.0 TO 4.0 IN 0.2 STEPS)
C AND LOAD 'POTS' ARRAY.
C
      PMAX = AMIN1( PMAX, 4.C0 )
      IPMX = PMAX/C.2
      IL = 21 - IPMX
      IH = 21 + IPMX
C
C LOOP THROUGH DESIRED POTENTIALS WE WISH TO FIND.
C
C FIRST SET 'POTS' ARRAY = 99.C
C
      DO 125  I=1,41
      DO 125  J=1,6
      POTS(I,J) = 99.0
  125 CONTINUE
      DO 300  J1=IL,IH
C
C POTENTIAL AT POTS(J1,XX) IS PS.
C
      PS = ( J1 - 21.)*C.2
      DO 130  J=1,6
      RG(J) = 0.
```

```
  130 CONTINUE
C
C LOOP THROUGH CALCULATED VALUES TO FIND OUT WHICH TWO PS IS BETWEEN
C AND SET INDICATORS AS EACH REGION IS LOADED.
C
      DO 200  J2=2,45
      IF( RAY(J2) .LE. PS  .AND. PS .LT. RAY(J2+1) )  GO TO 140
      IF( RAY(J2) .GT. PS  .AND. PS .GE. RAY(J2+1) )  GO TO 150
      GO TO  200
  140 FAC = (PS - RAY(J2)) / (RAY(J2+1) - RAY(J2))
      TVAL = J2 + FAC - 1
      GO TO 160
  150 FAC = (PS - RAY(J2+1)) / (RAY(J2) - RAY(J2+1))
      TVAL = J2 - FAC
  160 DO 170  J3=2,7
      IF( TVAL .GT. CRCT(J3) )   GO TO 170
      IF( RG(J3-1) .EQ. 0.0 )   GO TO 162
      REG = J3 - 1
      WRITE(3,320)  REG, PS, IP
  320 FORMAT('0   MORE THAN ONE POINTS IN REGION ', F5.0,
     1       '   FOR POTENTIAL = ', F6.2, '  ON RAY  ', I6, //)
      IOMP = 1
      GO TO 200
  162 RG(J3-1) = 1
      IXX = J3 - 1
      PCTS(J1,IXX) = TVAL
      GO TO 175
  170 CONTINUE
C
C QUIT WHEN ALL 6 REGIONS LOADED.
C
  175 SSM = RG(1) + RG(2) + RG(3) + RG(4) + RG(5) + RG(6)
      IF( SSM .EQ. 6.0 )  GO TO 300
  200 CONTINUE
  300 CONTINUE
C
C WRITE RECORD TO DISK AND PRINT IF ERROR.
C
      WRITE(8'IP)  PCTS
      IF( IOMP .EQ. 0 )  GO TO 400
      WRITE(3,308)  PCTS
  308 FORMAT( 6(' ', 21F6.2, / , '          ', 20F6.2 /) )
      ISTOP = ISTOP + IOMP
      IOMP = 0
C     IF( ISTOP .GE. 7 )  GO TO 500
  400 CONTINUE
      IF( IST .NE. 1 )  GO TO 425
C
C WRITE OUT ENTIRE DISK FILE WHICH HAS BIG PCTS ARRAY.
C
```

```
      WRITE(3,310)
  310 FORMAT('1  -- ENTIRE FILE FROM DISK -- BIG POTS ARRAY ', //)
      DO 410  J=1,360,INCP
      READ(8'J)  ((POTS(J1,J2),J1=1,411),J2=1,6)
      WRITE(3,312) J
  312 FORMAT( ' ', I5 )
      WRITE(3,308)  POTS
  410 CONTINUE
C
C
C
CCC  0-0-0-0-0      COMPUTE  ELECTRIC  FIELDS.    0-0-0-0-0-0-0-0-0-0-0-
C
C
C CONSTANTS USED ARE ALREADY IN ARRAYS 'CCEFF' AND 'P'.
  425 IREC = 362
C
C READ CARD GIVING STARTING AND ENDING POINTS OF LINE( PART OF GREAT
C CIRCLE ) ALONG WHICH E-FIELD PROFILE IS WANTED.
C PHI1, PHI2, AND THF
      WRITE(3,220)
  220 FORMAT('1', /)
      WRITE(3,221)
  221 FORMAT(' ', 20X, 'PROFILES  OF  ELECTRIC  FIELD' )
C
  428 READ(1,112, END=500) PHI1, PHI2, THF
  112 FORMAT(3F10.1)
      DIF = PHI2 - PHI1
      DIFR = DIF*DTR
      THFR = THF*DTR
      CTHFR = COS(THFR)
      STHFR = SIN(THFR)
      CDIFR = COS(DIFR)
      SDIFR = SIN(DIFR/2.)
      CCGAM = CTHFR*CTHFR + STHFR*STHFR*CDIFR
      SPAN = ARCOS(CCGAM)
      DSPAN = SPAN / DTR
      WSTEP = SPAN / 180.
      DWSTE = WSTEP / DTR
      CANG = (CTHFR*SDIFR) / CCS(SPAN/2.)
      SALON = 0.0
      DO 460  II=1,181
      CSAL = COS(SALON)
      SSAL = SIN(SALON)
      CTH = CTHFR*CSAL + STHFR*SSAL*CANG
      THR = ARCOS(CTH)
      IF( THR  .LT.  0.0003 )  THR = 0.0
      IF( CTH .EQ. 1.) GO TO 116
      STH = SIN(THR)
      APHI = ARCOS( (CSAL - CTH*CTHFR)/(STH*STHFR) )
```

```
      GO TO 114
  116 APHI = 0.0
  114 PHIP = PHI1*DTR + APHI
      IF( ABS(PHIR) .LT. 0.0003 )  PHIP = 0.0
      SPHI = SIN(PHIR)
      CPHI = COS(PHIR)
      THR = THR/CTR
      TT = TAN(THR/2.0)
      IF( THR .LE. TH1 ) GO TO 430
      IF( THR .GE. TH2 )  GO TO 440
      DO 40  I=1,4
      KREG = I + 1
      IF( RATH(I) .LE. THR  .AND. THR .LT. RATH(KREG) )  GO TO 450
   40 CONTINUE
  430 ETHE = 0.0
      EPHI = 0.0
      DO 60  NT=1,NTF
      VAR = NT*PHIR
      SV = SIN(VAR)
      CV = COS(VAR)
      TTN = TT**(NT-1)
      ETHE = NT*( COEFF(1,1,NT)*SV + COEFF(3,1,NT)*CV)*TTN + ETHE
      EPHI = NT*( COEFF(1,1,NT)*CV - COEFF(3,1,NT)*SV)*TTN + EPHI
   60 CONTINUE
      FAC = -12500. / (R*COS(THR/2.)*CCS(THR/2.))
      ETHE = FAC*ETHE
      EPHI = FAC*EPHI
      GO TO 470
  440 ETHE = 0.0
      EPHI = 0.0
      DO 70  NT=1,NTF
      VAR = NT*PHIR
      SV = SIN(VAR)
      CV = COS(VAR)
      TTN = TT**NT
      TTN2 = TTN*TTN
      ETHE = NT*(TTN2 - 1.)*(COEFF(1,6,NT)*SV + COEFF(3,6,NT)*CV)/TTN
     1     + ETHE
      EPHI = NT*(TTN2 + 1.)*(COEFF(1,6,NT)*CV - COEFF(3,6,NT)*SV)/TTN
     1     + EPHI
   70 CONTINUE
      FAC = -25000. / (R*STH)
      ETHE = FAC*ETHE
      EPHI = FAC*EPHI
      GO TO 470
  450 ETHE = 0.0
      EPHI = 0.0
      FAC = -25000. / (R*STH)
      DO 90  NT=1,NTF
      VAR = NT*PHIR
```

```
      SV = SIN(VAR)
      CV = COS(VAR)
      TTN = TT**NT
      TTN2 = TTN*TTN
      ETHE = ETHE + (NT/TTN)*((CCEFF(1,KREG,NT)*TTN2 - CCEFF(2,KREG,NT))
     1       *SV + (CCEFF(3,KREG,NT)*TTN2 - CCEFF(4,KREG,NT))*CV)
      EPHI = EPHI + (NT/TTN)*((CCEFF(1,KREG,NT)*TTN2 + CCEFF(2,KREG,NT))
     1       *CV - (CCEFF(3,KREG,NT)*TTN2 + CCEFF(4,KREG,NT))*SV)
   50 CONTINUE
      ETHE = FAC*( P(KREG) + ETHE )
      EPHI = FAC*EPHI
C
  470 EY = -ETHE*CTH*SPHI - EPHI*CPHI
      CTP = CTH*CPHI
      EMTE = SQRT( ETHE*ETHE*(1.- CTP**2) + 2.*ETHE*EPHI*CTP*SPHI +
     1             EPHI*EPHI*CPHI*CPHI )
      IF( EY .LT. 0.0 )  EMTE = -EMTE
      EMNTN = EPHI*SPHI - ETHE*CTP
      RAY(II) = EMTE
      RAI(II) = EMNTN
      PATH(II) = THD
      PAPH(II) = PHIF/DTR
      SALON = SALON + HSTEP
  480 CONTINUE
C
      WRITE(8*IREC)  PHI1, PHI2, THF, DSPAN, PATH
      IREC = IREC + 1
      WRITE(8*IREC)  PHI1, PHI2, THF, DHSTE, PAPH
      IREC = IREC + 1
      WRITE(8*IREC)  PHI1, PHI2, THF, RAY
      IREC = IREC + 1
      WRITE(8*IREC)  PHI1, PHI2, THF, RAI
      IREC = IREC + 1
      WRITE(3,316)   PHI1, PHI2, THF
  316 FORMAT( / '0PHI = ', F6.1, '       PHI2 = ', F6.1, '       THF = '
     1       , F5.1, //)
      WRITE(3,230)
  230 FORMAT(1H , 3(8X, 'PHI', 2X, 'THETA', 7X, 'EY', 7X, 'EX', 2X), /)
      DO  600  I=1,4
      CNEAT(60,3,I) = 12345678.C
      CNEAT(61,3,I) = 12345678.C
  600 CONTINUE
      WRITE(3,318)  (((CNEAT(I1,I2,I3), I3=1,4), I2=1,3), I1=1,61)
  318 FORMAT(61(' ', 5X, 3(F6.1, 2X, F5.1, 4X, F7.2, 2X, F7.2, 3X, '*',
     1       3X), / ))
      GO TO 428
  900 CALL EXIT
      END
```

```
      SUBROUTINE  DCOMP(CURD, CURP, SBOCU, CBOCU, CONST)
C
C ROUTINE TO GENERATE 'NTF' COEFFICIENTS OF A FOURIER EXPANSION.
C MAXIMUM NTF IS 20. CBOCU ARE 'COSINE' COEFFICIENTS, SBOCU ARE 'SINE'
C COEFFICIENTS. CONST ARE CONSTANT TERMS.C
C  F(PHI) = CONST + SUM( CBCCU(N)*COS(N*PHI) + SBOCU(N)*SIN(N*PHI) )
C
C UP TO 5 FUNCTIONS CAN BE EXPANDED.
C
      DIMENSION   CURD(5,5), CURP(5,5), SBCCU(5,20), CBOCU(5,20),
     1            CONST(5)
      COMMON   R, SIG, NTF, CTR
C
      PI = 3.1415927
C CONVERT ALL DEGREES TO RADIANS.
C
      DO 15  I=1,5
      DO  15  J=1,5
      CURD(I,J) = CURD(I,J)*CTR
   15 CONTINUE
C
C DEFINE MISCELLANEOUS CONSTANTS.
C
      DO 35  IP=1,5
      A1 = CURD(1,IP) - CURD(2,IP)
      A2 = CURD(1,IP) + CURD(2,IP)
      A3 = A2 - CURD(3,IP)
      A4 = CURD(4,IP) - CURD(5,IP) - CURD(3,IP)
      A5 = A4 + CURD(3,IP)
      A6 = CURD(4,IP) + CURD(5,IP)
      A7 = A6 - 2.0*PI
      A8 = CURP(1,IP) - CURP(2,IP)
      A9 = CURP(5,IP) - CURP(4,IP)
      B1 = CURP(2,IP)/ A1
      B3 = CURP(2,IP)/A3
      B4 = CURP(5,IP)/ A4
      B7 = CURP(5,IP)/ A7
C
C LOOP FOR NTF COEFFICIENTS.
C
      DO 25  IN=1,NTF
      S1 = SIN(IN*A1)
      C1 = COS(IN*A1)
      S2 = SIN(IN*A2)
      C2 = COS(IN*A2)
      S5 = SIN(IN*A5)
      C5 = COS(IN*A5)
      S6 = SIN(IN*A6)
      C6 = COS(IN*A6)
C
```

```
      F1 = B1 / IN * ( S1 / IN - A1 * C1 )
      F21 = CURM(2,IP)*CLRD(2,IP)*(C1 - C2)
      F22 = A8/IN * (2.*SIN(IN*CLRD(1,IP)) - S1 - S2)
      F2 = 1./(IN*CURD(2,IP))*(F21 + F22)
      F31 = A3*C2
      F32 = 1./IN * (SIN(IN*CURD(3,IP)) - S2)
      F3 = B3/IN * (F31 + F32)
      F41 = -1. *A4*C5
      F42 = 1./IN *(S5 - SIN(IN*CURD(3,IP)))
      F4 = B4/IN *(F41 + F42)
      F51 = CURM(5,IP)*CLRD(5,IP)*(C5 - C6)
      F52 = A9/IN *(2.*SIN(IN*CURD(4,IP)) - S5 -S6)
      F5 = 1./(CURD(5,IP)*IN) *(F51 - F52)
      F6 = B7/IN *(A7*C6 - S6/IN)
C
      F = F1 + F2 + F3 + F4 + F5 + F6
      SRCCU(IP,IN) = F/PI
C
      G1 = B1/IN *(A1*S1 + 1./IN *(C1 - 1.) )
      G21 = CURM(2,IP)*CLRD(2,IP)*(S2 - S1)
      G22 = A8/IN *(2.*CCS(IN*CURD(1,IP)) - C2 - C1)
      G2 = 1./(IN*CURD(2,IP)) *(G21 + G22)
      G31 = -1.*A3*S2
      G32 = 1./IN *(CCS(IN*CURD(3,IP)) - C2)
      G3 = B3/IN *(G31 + G32)
      G41 = A4*S5
      G42 = 1./IN *(C5 - CCS(IN*CURD(3,IP)))
      G4 = B4/IN *(G41+G42)
      G51 = CURM(5,IP)*CLRD(5,IP)*(S6 - S5)
      G52 = A9/IN *(C6 + C5 - 2.*CCS(IN*CURD(4,IP)))
      G5 = 1./(IN*CURD(5,IP)) *(G51 + G52)
      G6 = -1.*B7/IN *(A7*S6 + 1./IN *(C6 - 1.))
C
      G = G1 + G2 + G3 + G4 + G5 + G6
      CRCCU(IP,IN) = G / PI
C
   35 CONTINUE
C
C COMPUTE CONSTANTS.
C
      H = CURM(1,IP)*CURD(2,IP) + 0.5*CURD(3,IP)*CURM(2,IP)
     1 - 0.5*CURD(3,IP)*CURM(5,IP) + PI*CURM(5,IP)
     2 + CURM(4,IP)*CURD(5,IP)
      CONST(IP) = H/(2.*PI)
   35 CONTINUE
  100 RETURN
      END
```

```
      SUBROUTINE  KEISUU( ALPHA, BETA, RATH, SBCCU, CBOCU, COEFF)
C
C ROUTINE COMPUTES COEFFICIENTS AND PUT THEM INTO ARRAY 'COEFF'.
C ( 'KEISUU' MEANS COEFFICIENT IN JAPANESE.) WE USE 'COEFF' TO CALCULATE
C POTENTIAL AND E-FIELD.
C
      DIMENSION  ALPHA(6), BETA(6), RATH(6), SBCCU(5,20), CBOCU(5,20)
      DIMENSION  COEFF(4,6,20)
C
C FIRST SUBSCRIPT REPRESENTS A, B, C OR D, SECOND, NAME OF REGION, AND
C THIRD, DEGREE IN FOURIER EXPANSION. NTF REPRESENTS THE HIGHEST DEGREE.
C
      DIMENSION   A(1CO), AA(1CO), B(1C), BE(10), SB(10),
     1            DHAL(6,6), DPED(6,6), TI(5), S(5), DT(5,5), ST(5,5),
     2            T(5)
C
      COMMON  R, SIG, NTF, DTR
C
      AL1 = ALPHA(1)
      AL2 = ALPHA(2)
      AL3 = ALPHA(3)
      AL4 = ALPHA(4)
      AL5 = ALPHA(5)
      AL6 = ALPHA(6)
C
      S65 = AL6 + AL5
      S12 = AL1 + AL2
      DAL2 = -2.*AL2
      TAL3 = -2.*AL3
      QAL4 = -2.*AL4
      PAL5 = -2.*AL5
      DO 10  I=2,6
      DO 10  J=1,5
      DHAL(I,J) = ALPHA(I)*BETA(I) - ALPHA(J)*BETA(J)
      DPED(I,J) = ALPHA(I) - ALPHA(J)
   10 CONTINUE
C
      DO 5  I=1,4
      DO 5  J=1,6
      DO 5  K=1,20
      COEFF(I,J,K) = 0.0
    5 CONTINUE
C
      DO 15  I=1,5
      S(I) = SIN(RATH(I))
   15 CONTINUE
      DO 200  NT=1,NTF
      DO 20  I=1,5
      T(I) = TAN( RATH(I)/2.0 )**NT
      TT(I) = T(I)*T(I)
```

```
      20 CONTINUE
C
      DO 30  I=2,5
      DO 30  J= 1,4
      DT(I,J) = TT(I) - TT(J)
      ST(I,J) = TT(I) + TT(J)
      30 CONTINUE
C
      DO 40  K=1,5
      SB(K) = 0.000064895*S(K)/(SIG*NT)
      B(2*K-1) = SB(K)*SBOCU(K,NT)
      B(2*K)  = SB(K)*CBOCU(K,NT)
      40 CONTINUE
C
      B(1) = B(1)/T(1)
      B(2) = B(2)/T(1)
      DO 50  K=2,4
      KK =2*K
      B(KK-1) = B(KK-1)*T(K)
      B(KK) = B(KK)*T(K)
      50 CONTINUE
C
      B(9) = B(9)*(T(5)+1.)
      B(10) = B(10)*(T(5)+1.)
C
C LOADING OF ARRAY B HAS BEEN DONE.  LOAD ARRAY A.  SINCE ARRAY A IS
C DESTROYED IN COMPUTATION, PUT IT IN ARRAY AA AND KEEP.
C FIRST CLEAR OUT ARRAY A.
      DO 55  I=1,100
      A(I) = 0.0
      55 CONTINUE
C
      A(1) = S12
      A(2) = -DHAL(2,1)
      A(3) =  DPED(3,2)*TT(1)
      A(4) = -DHAL(3,2)*TT(1)
      A(5) =  DPED(4,3)*TT(1)
      A(6) = -DHAL(4,3)*TT(1)
      A(7) =  DPED(5,4)*TT(1)
      A(8) = -DHAL(5,4)*TT(1)
      TER1 =  DPED(6,5) - S65*TT(5)
      TER2 = -DHAL(6,5)*( 1. + TT(5) )
      A(9) = TER1 * TT(1)
      A(10) = TER2 * TT(1)
      A(11) = DAL2
      A(13) =  AL3*DT(2,1) + AL2*ST(2,1)
      A(14) = -DHAL(3,2)*DT(2,1)
      A(15) =  DPED(4,3)*DT(2,1)
      A(16) = -DHAL(4,3)*DT(2,1)
      A(17) =  DPED(5,4)*DT(2,1)
```

```
      A(18) = -DHAL(5,4)*DT(2,1)
      A(19) =  TER1*DT(2,1)
      A(20) =  TER2*DT(2,1)
      A(23) = TAL3*YT(2)
      A(25) =  AL4*DT(3,2) + AL3*ST(3,2)
      A(26) = -DHAL(4,3)*DT(3,2)
      A(27) =  DPEDE(5,4)*DT(3,2)
      A(28) = -DHAL(5,4)*DT(3,2)
      A(29) =  TER1*DT(3,2)
      A(30) =  TER2*DT(3,2)
      A(35) = QAL4*TT(2)
      A(37) =  AL5*DT(4,3) + AL4*ST(4,3)
      A(38) = -DHAL(5,4) * DT(4,3)
      A(39) =  TER1*DT(4,3)
      A(40) =  TER2*DT(4,3)
      A(47) = PAL5*YT(4)
      A(49) = AL6*DT(5,4) + AL5*ST(5,4) - ( AL6*DT(5,4) - AL5*ST(5,4))*
     1        TT(5)
      A(50) =  TER2*DT(5,4)
      DO 51  K=2, 50, 2
      A( K+49 ) = -A( K)
      A( K+50 ) =  A( K-1 )
   51 CONTINUE
C
      DO 60  I=1,100
      AA(I) = A(I)
   60 CONTINUE
C
      DO 61  I=1,10
      BB(I) = B(I)
   61 CONTINUE
C
C SOLVE SIMULTENUOUS EQUATIONS BY USING SUBRCUTINE 'SIMQ'.
C
      CALL SIMQ(A,B,10,KS)
C
      DO 70  I=1,10
      SB(I) = B(I)
   70 CONTINUE
C
      DO 68  I=1,10
      B(I) = 0.0
      DO 68  K=1,10
      B(I) = B(I) + AA(K*10+I-10)*SB(K)
   68 CONTINUE
C
      DO 69  I=1,10
      B(I) = BB(I) - B(I)
   69 CONTINUE
C SECOND CALL FOR SIMQ  --  HIGHER STEP BY ONE ORDER
```

```
      CALL  SIMQ( AA,B, 10, KS )
C
      DO 71  I=1, 10
      SB(I) = SB(I) + B(I)
   71 CONTINUE
C
C CALCULATE OTHER COEFFICIENTS AND PLT THEM INTO ARRAY COEFF.
C
      DO 72  K=1,5
      COEFF(1,K,NT) = SB(K)
      COEFF(3,K,NT) = SB(K+5)
   72 CONTINUE
      COEFF(1,6,NT) = (CCEFF(1,1,NT)*TT(1)+COEFF(1,2,NT)*DT(2,1)+COEFF(1
     1,3,NT)*DT(3,2)+COEFF(1,4,NT)*DT(4,3)+COEFF(1,5,NT)*DT(5,4))/(1.+
     2TT(5))
      COEFF(3,6,NT) = (COEFF(3,1,NT)*TT(1)+CCEFF(3,2,NT)*DT(2,1)+COEFF(3
     1,3,NT)*DT(3,2)+COEFF(3,4,NT)*DT(4,3)+CCEFF(3,5,NT)*DT(5,4))/(1.+
     2TT(5))
C
      DO 73  K=2,4,2
      COEFF(K,2,NT) = (COEFF(K-1,1,NT)-CCEFF(K-1,2,NT))*TT(1)
      COEFF(K,3,NT) = COEFF(K-1,1,NT)*TT(1)+COEFF(K-1,2,NT)*DT(2,1)
     1-COEFF(K-1,3,NT)*TT(2)
      COEFF(K,4,NT) = CCEFF(K-1,1,NT)*TT(1)+COEFF(K-1,2,NT)*DT(2,1)
     1+COEFF(K-1,3,NT)*DT(3,2)-CCEFF(K-1,4,NT)*TT(3)
      COEFF(K,5,NT) = CCEFF(K-1,1,NT)*TT(1)+COEFF(K-1,2,NT)*DT(2,1)
     1+COEFF(K-1,3,NT)*DT(3,2)+CCEFF(K-1,4,NT)*DT(4,3)-CCEFF(K-1,5,NT)*
     2TT(4)
   73 CONTINUE
C
      COEFF(2,6,NT) = COEFF(1,6,NT)
      COEFF(4,6,NT) = COEFF(3,6,NT)
  200 CONTINUE
C
      RETURN
      END
```

```
                    MAINPROGRAM  PLCON
C
C  ROUTINE READS BIG POTENTIAL FILE -- ONE REGION AT A TIME AND DRAWS
C  CONTOURS LABELING EVERY MULTIPLE OF 0.4.  POTENTIALS ARE ON DISK
C  IN 246 WORD RECORDS FOR EACH VALUE OF PHI.  246 WORDS RECORDS HAVE
C  41 WORDS FOR EACH REGION.
C  41 WORDS ARE THETA VALUES WHERE POTENTIALS -4.0, -3.8, -------- 3.8,
C  4.0 OCCURE. FILL CHARACTER WAS 99.0, SO THOSE VALUES ARE NON-DATA ITEMS.
C  NOTE -- THERE IS NOT ENOUGH RCSP IN CORE FOR ALL DATA AT ONE TIME.
C  SCALE USED FOR PLOTS IS 10 DEG/INCH.
C
      REAL*4              NFAC
      DIMENSION           LR(3)
      DIMENSION      PA(41,36),    DEN(2C5),     TH(6),
     1               AL(6),        BE(6),        PARM(69),    RAY(46),
     2               CURC(5,5),    CURP(5,5)
      DIMENSION      SUB(15),      TSW(15),      CUL(5),      CUM(5)
      EQUIVALENCE    (PARM(1),TH(1)), (PAPP(7),AL(1)),(PARM(13),BE(1)),
     1               (PARM(19),SIG),
     2               (PAPP(2C),CURD(1,1)), (PARM(45),CURM(1,1))
      EQUIVALENCE    (RAY(1),CUP(1))
C
      DATA   SUB/ '1  ',' 11  ',' 111 ',' IV ',' V  ',' VI ',' 1  ',' 11 ',' 111',
     1       'IV ', 'V  ','VI ','1  ','2  ','3  ','4  ','5  ','F  ',
     2       'P  ' /
      DATA   ISW/ 6*3, 6*2, 6*6,  48 /
      DATA   CUL/ 'COM', 'WCM', 'BDC', 'CCE', 'WDE' /
      DATA   CUM/ 'PCM', 'FCM', 'BCS', 'PDE', 'FCE' /
      WRITE(3,66C)
  66C FORMAT ( '     ENTERED PLCON CM    ' )
      DTR = 3.1415927/ 18C.
C     DEFINE FILE 8 (401, 246, U, INDEX)
      DEFINE FILE 8 (760, 246, U, INDEX)
      WRITE(3,661)
  661 FORMAT ( '  DEFINED THE FILE CK    ' )
      LR(1) = 2
      LR(2) = 4
      LR(3) = 6
C  READ WHICH REGIONS TO LOAD DEFAULT = 2,4,6
      READ ( 1, 101, END=5 ) ( LR(ILR), ILR=1,3)
  101 FORMAT ( 3I1)
    5 SCL = 10.
      CALL  PLOTST
      CALL  PLOT(6.,  5., -3)
      CALL  OFFSET(0., SCL, C., SCL)
C
      ISV = 8
C
C  READ RECORD 361 TO GET REGIONS, CONSTANTS USED IN CALCULATION OF
C  POTENTIALS AND E-FIELDS.
C
```

```
      IREC = 361
      READ(ISY'IREC) (TH(I), I=1,6), (AL(I), I=1,6), (BE(I), I=1,6), SIG
     1                ,((CLRD(I,J), I=1,5), J=1,5),
     2                 ((CURM(I,J), I=1,5), J=1,5), DPHI, NTF, NFAC, LTST
      WRITE(3,662)
  662 FORMAT ( '  READ PARM RECORD CK ' )
      INCP = DPHI
C
C DRAW 5 CIRCLES OF RADIUS THETA1 TO THETA5. EACH IS REALLY 2 CIRCLES
C WITH RADII 0.02 INCH APART TO MAKE THEM SEEM DARKER THAN CONTOURS.
C
      DO 50  I=1,5
      ILOOP = 1
      RR = TH(I)
      ANG = 0.
      DANG = 10.*DTR
   30 CALL  PLOT(0., RR, 13)
      DO 40  J=1,37
      XP = RR*SIN(ANG)
      YP = RR*COS(ANG)
      CALL  PLOT(XP, YP, 12)
      ANG = ANG + DANG
   40 CONTINUE
      IF( ILOOP .EQ. 2 )  GO TO 50
      ILOOP = 2
      RR = RR + 0.02
      GO TO 30
   50 CONTINUE
      CALL  PLOT(-4.5, 0., 3)
      CALL  PLOT(+4.5, 0., 2)
      CALL  PLOT(0., 4.5, 3)
      CALL  PLOT(0., -4.5, 2)
      CALL  SYMBOL(-0.1, -4.7, 0.14, 'C', 0.0, 1)
      CALL  SYMBOL(-0.0, -4.6, 0.07, 'C', 0.0,1)
      DO 325 IPPP = 1, 2
      INCP = 0
      IF ( IPPP .EQ. 2 ) INCP = 400
C
C FIRST SET OF PLOTTING IS FOR CONTOURS-- LOOP ONCE FOR EACH REGION.
C
      DO 300  I=1,6
C
C READ IN REGION I INTO PA ARRAY.
C
      DO 100  J=1,360, INCP
C     IREC = J
      IREC = J + INCP
      GO TO (60, 70, 80, 90, 110, 120),  I
   60 READ(ISY'IREC)  (PA(K,J), K=1,41),   (CUM(K), K=1,205)
      GO TO 100
```

```
      70 READ(ISY*IREC)  (DUM(K), K=1,41),    (PA(K,J), K=1,41),
     1                   (DUM(K), K=1,164)
        GO TO 130
      80 READ(ISY*IREC)  (DUM(K), K=1,82),    (PA(K,J), K=1,41),
     1                   (DUM(K), K=1,123)
        GO TO 130
      90 READ(ISY*IREC)  (DUM(K), K=1,123),   (PA(K,J), K=1,41),
     1                   (DUM(K), K=1,82)
        GO TO 100
     110 READ(ISY*IREC)  (DUM(K), K=1,164),   (PA(K,J), K=1,41),
     1                   (DUM(K), K=1,41)
        GO TO 100
     120 READ(ISY*IREC)  (DUM(K), K=1,205),   (PA(K,J), K=1,41)
     100 CONTINUE
C
C PLOT CONTOURS FOR REGION 1 -- LABELING CONTOURS MULTIPLE OF 0.4
C IN REGIONS 2, 4, AND 6.  OR WHATS BEEN RECLESTED
C
         ILABL = ( 1 - LR(1) ) * ( 1 - LR(2) ) * ( 1 - LR(3) )
         DO 250  J=1,41
         VLB = (J-21)*0.2
         ILB = -1
         IF( MOD(J-1,2) .EQ. 0 )  ILB = 1
C
C SEARCH ALL RAYS FOR WHICH  HAS CHOSEN POTENTIAL. A VALUE OF 99.0 MEANS
C NO CALCULATION ATTEMPTED OR THAT POTENTIAL DESIRED IS NOT ON PARTI-
C CULAR RAY IN PARTICULAR REGION.
C
         IFP = 0
         DO 200  K=1, 37C, IACP
         KKK = K
         IF( KKK .GT. 360 )  KKK = KKK - 360
         IF( PA(J,KKK) .EQ. 99.0 )  GO TO 175
         ANG = KKK*DTR
         PR = PA(J,KKK)
         XP = PR*SIN(ANG)
         YP = -PR*COS(ANG)
         IF(IFP .EQ. 0  .OR. ILB .EC. 1)  CALL  PLOT(XP, YP, 13)
         IFP = 1
         CALL  PLOT(XP, YP, 12)
         CALL  PLOT(XP, YP-C.1, 12)
         IF(ILB .LE. 0)  GC TO 200
         ILB = 0
         XN = XP/SCL - 0.03
         YN = YP/SCL - C.03
         IF(      ILABL       .EQ. C)  CALL NUMBER(XN, YN, 0.07, VLB, 0.0,
     1 1)
         CALL  PLOT(XP, YP, 13)
         GO TO 200
     175 IFP = C
```

```
      IF(ILB .EQ. -1) GO TO 200
      ILB = 1
  200 CONTINUE
  250 CONTINUE
  300 CONTINUE
  325 CONTINUE
C
C PLOT OF CONTOURS FINISHED -- NOW LIST OUT ALL PARAMETERS USED IN
C CALCULATING CONTOURS -- ALPHAS, BETAS, THETAS, ETC. SO THEY WILL
C BETWEEN CONTOURS AND E-FIELD PROFILES.
C
      YS = 4.2
      XS = 6.0
      DO  350  I=1,15
      CALL  SYMBOL(XS, YS, 0.28, ISP(I), 0.0, -1)
      CALL  SYMBOL(-0.0, YS-0.05, 0.10, SUB(I), 0.0, 3)
      CALL  SYMBOL(-C.0, YS, 0.28, ' = ', C.0, 3)
      CALL  NUMBER(-C.0, -0.0, 0.28, PARP(I), 0.0, 2)
      YS = YS - 0.5
  350 CONTINUE
      YS = 4.2
      XS = 9.0
      DO  36C  I=1,5
      CALL  SYMBOL(XS, YS, 0.28, CLL(I), 0.0, 3)
      CALL  SYMBOL(-0.0, YS, 0.28, ' = ', C.0, 3)
      YS = YS - C.5
  360 CONTINUE
      YS = YS - 1.0
      DO  370  I=1,5
      CALL  SYMBOL(XS, YS, 0.28, CUP(I), 0.0, 3)
      CALL  SYMBOL(-0.0, YS, 0.28, ' = ', C.0, 3)
      YS = YS - C.5
  370 CONTINUE
      CALL  SYMBOL(10.40, 4.7, 0.28,'I    II   III  IV   V  ', 0.0, 23)
      XS = 10.40
      DO  39C  K=1,5
      YS = 4.2
      KST = 14 + 5*K
      DO  380  J=1,5
      JJ = KST + J
      CALL  NUMBER(XS, YS, 0.28, PARP(JJ), 0.0, -1)
      YS = YS - 0.5
  380 CONTINUE
      XS = XS + 1.2
  390 CONTINUE
      YST = YS - 1.0
      XS = 10.40
      DO 392  K=1,5
      YS = YST
      KST = 39 + 5*K
```

```
      DO  394  J=1,5
      JJ = NST + J
      CALL  NUMBER(XS, YS, 0.28, FARR(JJ), 0.0, -1)
      YS = YS - C.5
394 CONTINUE
      XS = XS + 1.2
392 CONTINUE
375 CALL  PLOT(2C., 0.C, -3)
400 CALL  PLOT(19., -9., 1C0)
      CALL  EXIT
      END
```

MAINPROGRAM PLEF

```
C
C ROUTINE READS AND PLOTS E-FIELD PROFILES.
C BOTH X- AND Y-COMPS ( MIDNIGHT TO NOON AND DAWN TO DUSK COMPS ) ARE
C PLOTTED ALONG PART OF GREAT CIRCLES WHOSE BEGINNING POINTS ARE READ
C FROM FILE.
C SCALE IS IC DEG/INCH IN X AND VARIABLE IN Y.
C
      DIMENSION      TH(6),   AL(6),   BE(6),   CURD(5,5),   CURM(5,5),
     1               PARM(69)
      DIMENSION      SUB(19), ISM(19), CLL(5),  CUM(5),      RAY(181),
     1               CMP(2),  PATH(181),  PAPH(181)
      EQUIVALENCE    (PARM(1), TH(1)), (PARM(7),AL(1)), (PARM(13),BE(1)),
     1               (PARM(19),SIG), (PARM(2C),CURD(1,1)),
     2               (PARM(45),CURM(1,1))
C
      DATA  SUB/ '1  ','2  ','3  ','4  ','5  ','F  ','I  ','II ','III',
     1           'IV ','V  ','VI ','I  ','II ','III','IV ','V  ','VI ',
     2           'P  ' /
      DATA  ISM/ 6*37, 6*42, 6*66, 48 /
      DATA  CUL/ 'CCM', 'WOB', '80C', 'CCE', 'WOE' /
      DATA  CUM/ 'PCM', 'FCM', '8DS', 'PCE', 'FCE' /
      DATA  CMP/ 'Y',  'X' /
      DTP = 3.1415927/ 1EC.
      DEFINE  FILE 8 (401, 246, L, INDEX)
      CALL  PLOTST
      CALL  PLOT(2., 5., -3)
   10 READ(1,103, END=7CC)  YFAC
  103 FORMAT( F5.1 )
      CALL  OFFSET(0., 1C., C., YFAC)
      ISY = 8
C
C READ RECORD 361 TO GET REGIONS AND CONSTANTS USED.
C
      IREC = 361
      READ(ISY'IREC) (TH(I), I=1,6), (AL(I), I=1,6), (BE(I), I=1,6), SIG
     1              ,((CURD(I,J), I=1,5), J=1,5),
     2               ((CURM(I,J), I=1,5), J=1,5),   DPHI,  NTF,  LIST
C
C LIST ALL PARAMETERS USED IN CALCULATION.
C
      YS = 4.2
      XS = 0.0
      DO 350  I=1,19
      CALL  SYMBOL(XS,YS,0.28,ISM(I),0.0,-1)
      CALL  SYMBOL(-C.0, YS-C.C5, 0.10, SUB(I), 0.0, 3)
      CALL  SYMBOL(-C.0, YS, 0.28, ' = ', 0.0, 3)
      CALL  NUMBER(-C.0, -0.0, C.28, PARM(I), C.0, 2)
      YS = YS - C.5
  350 CONTINUE
      YS = 4.2
```

```
      XS = 3.0
      DO 360  I=1,5
      CALL  SYMBOL(XS, YS, 0.28, CUL(I), C.C, 3)
      CALL  SYMBOL(-C.C, YS, 0.28, ' = ', C.C, 3)
      YS = YS - C.5
  360 CONTINUE
      YS = YS - 1.0
      DO 370  I=1,5
      CALL  SYMBOL(XS, YS, 0.28, CUP(I), C.C, 3)
      CALL  SYMBOL(-C.C, YS, 0.28, ' = ', C.C, 3)
      YS = YS - C.5
  370 CONTINUE
      CALL  SYMBOL(4.40, 4.7, 0.28, 'I   II   III  IV   V  ', 0.0, 23)
      XS = 4.40
      DO 390  K=1,5
      YS = 4.2
      KST = 14 + 5*K
      DO 380  J=1,5
      JJ = KST + J
      CALL  NUMBER(XS, YS, 0.28, PARM(JJ), C.C, -1)
      YS = YS - 0.5
  380 CONTINUE
      XS = XS + 1.2
  390 CONTINUE
      YST = YS - 1.0
      XS = 4.40
      DO 392  K=1,5
      YS = YST
      KST = 39 + 5*K
      DO 394  J=1,5
      JJ = KST + J
      CALL NUMBER(XS, YS, 0.28, PARM(JJ), C.C, -1)
      YS = YS - 0.5
  394 CONTINUE
      XS = XS + 1.2
  392 CONTINUE
      CALL  PLOT(15., 0.C, -2)
C
C PLOT X AND Y COMPONENTS OF E-FIELD ON SAME DIAGRAM.
C
      REC = 362
C
C SEE DESCRIPTION IN POEGEN FOR LOCATIONS OF DATA ON FILE.
C LOOP FROM 1--10 BELOW IS FOR POSSIBLE LINES WHICH FIT ON FILE
C     DO 1000  L=1,10  IS POSSIBLE.
C
      DO 1000  L=1,10
C
C DRAW AXES AND DO OTHER SET- UPS.
C
```

```
      CALL  AXIS(0.0, -5.0, ' ', -1, 10., 90.0, -5.*YFAC, YFAC, 10. )
      IREC = REC
      READ(ISY'IREC) PHI1, PHI2, THF, DSPAN, (PATH(I), I=1,181)
      JREC = REC + 1.
      READ(ISY'JREC) PHI1, PHI2, THF, DWSTE, (PAPH(I), I=1,181)
      IF( THF .EQ. 55.0 ) GO TO 10
      HSPAN = DSPAN/2.
      CALL  PLOT(-HSPAN, 0.0, 13)
      CALL  PLOT( HSPAN, 0.0, 12)
      Y = YFAC/20.
      DO 100  J=1,19
      X = -HSPAN + (J-1)*DSPAN/18.
      CALL  PLOT(X, Y, 13)
      CALL  PLOT(X, -Y, 12)
      IF(MOD(J,2) .EQ. 0)  GO TO 100
      JP = 10*J - 9
      X = X/10. - 0.2
      CALL  NUMBER(X, -0.2, 0.12, PATH(JP), 0.0, 1)
      X = X - 0.07
      CALL  NUMBER(X, -0.4, 0.12, PAPH(JP), 0.0, 1)
  100 CONTINUE
C
C THO LOOPS BELOW ARE FOR DAWN-DUSK(Y) AND MIDNIGHT-NOON(X) COMPONENTS -
C LABLE EVERY 20TH POINT ALONG PATH.
C
C
C NOTE THAT ON PLOT, POSITIVE VALUES OF Y-COMP( DAWN-DUSK) ARE PLOTTED
C DOWNWARD( I.E. AS NEGATIVE ).
C
C
      IREC = REC + 2
      DO 500  IC=1,2
      READ(ISY'IREC)  PHI1, PHI2, THF, (RAY(I), I=1,181)
      X = -HSPAN
      CALL  PLOT(X, -RAY(1), 13)
      DO 415  JC=1,181
      Y = -RAY(JC)
      CALL  PLOT(X, Y, 12)
      IF(MOD(JC-1), 20) .NE. 0)   GO TO 413
      CALL  SYMBOL(X/10., Y/YFAC, 0.07, CMP(IC), 0.0, 1)
      CALL  PLOT(X, Y, 13)
  413 X = X + DWSTE
  415 CONTINUE
      IREC = REC + 3.
  500 CONTINUE
      CALL  PLOT(10., 0.0, -3)
      REC = REC + 4.
 1000 CONTINUE
      GO TO 10
C
```

```
C END PLOT AND SET NEW ORIGIN.
C
  700 CALL   PLOT(6.C, -5.0, 100)
      CALL   EXIT
      END
```

```
                    MAINPROGRAM   AMPGEN
C
C CURRENT CONTOUR GENERATION PROGRAM - IGNORE REFERENCES TO POTENTIAL
C CONTOURS
C
C POTENTIAL CONTOUR GENERATION PROGRAM - WITH FIELD-ALIGNED CURRENTS AS
C BOUNDARY CONDITIONS FOR MANY CONDUCTING STRIPS.  NO PHI DEPENDENCE OF
C CONDUCTIVITY. THIS ROUTINE WRITES A DISK FILE WHICH WILL BE PLOTTED
C BY SEPARATE PROGRAMS CLE TO LARGE AMOUNT OF DATA - WHICH WON'T FIT IN
C CORE - AN ARRAY (360, 41, 6) REQUIRES 236K BYTES AND 360-40 HAS ONLY
C 125K AVAILABLE.   THIS VERSION IS ESSENTIALLY SAME AS PROGRAM PCTGEN
C WRITTEN BY SHIRLEY LISS.
C
C TO GET COEFFICIENTS, SOLVE 10 BY 10 SIMULTENEOUS EQUATIONS.
C THEN POTENTIAL AND ELECTRIC FIELD CAN BE OBTAINED EASILY.
C UNITS OF POTENTIALS AND E-FIELD ARE A MULTIPLES OF 25KV ( SEE FAC25K
C I.E. FAC25K * 25KV ) AND  VOLT / MK, RESPECTIVELY.
C UNIT OF CURRENT = 10 * NFAC K AMPS
C
      REAL*4                NFAC
      REAL*8  CHAR(2,5)
      DIMENSION             PCTS2(41,6),   RG2(6)
      DIMENSION             KLABES(1),
     1   RAY(181),  RA(181),  PCTS(41,6),   CBOTH(7),
     2   N(6),      ALPHA(6),  BETA(6),     COEFF(6,6,20),  P(6),
     3   RATH(6),   RG(6),     CECCU(5,2C),SECCU(5,20),
     4   RATHM(6),  CURD(5,5), CURM(5,5),   DETM(6),
     5   PATH(181), PAPH(181), CONST(5), SP(20), CP(20)
      DIMENSION             CNEAT(61,3,4)
      EQUIVALENCE           (CBOTH(2),TH1), (CBOTH(3),TH2), (CBOTH(4),TH21,
     1                      (CBOTH(5),TH4), (CBOTH(6),TH5), (CBOTH(7),THF)
      EQUIVALENCE           (CNEAT(1,1,1), PAPH(1)),
     1                      (CNEAT(1,1,2), PATH(1)),
     2                      (CNEAT(1,1,3), RAY(1)),
     3                      (CNEAT(1,1,4), PZ(1) )
      COMMON    R, SIG, NTF, DTR
      DATA   P / 6 * C.0 /
      DATA      CHAR/ 'MOR.CENT',
     1                '.(DENS.)',
     2                'MOR.MID.',
     3                '(DENS.) ',
     4                'ROUND.IN',
     5                'COLT (0)',
     6                'EVE.CENT',
     7                '.(DENS.)',
     8                'EVE.MID.',
     9                '(DENS.) ' /
      BUFF = 99.0
      DTR = 3.1415927 / 180.C
      R = 6480
C
```

```
C FORMAT DISK FILE -- REC 1-360 = POTENTIALS FOR EACH PHI, REC 361 FOR
C INPUT PARAMETER LIST, REC 363-364 PHI AND THETA COMP OF RAY( E-FIELD )
C SPECIFIED ON INPUT CARD 1, FOLLOWING GROUPS OF 4 RECORDS WILL HAVE
C SIMILAR DATA AS LONG AS INPUT CARDS REQUESTING RAYS ARE IN INPUT LIST.
C UP TO 10 PROFILES ARE ALL RIGHT, THEN FILE ON DISK IS FULL
C  REC 401 TO 760 CONTAIN THE SECANT POTS2 ARRAY
C
      CALL  CLRDSK(8, 760, 246, 'U', BUFF)
      DEFINE FILE   8(760, 246, U,  INDEX)
C     CALL  CLRDSK(8, 401, 246, 'U', BUFF)
C     DEFINE FILE   8(401, 246, U,  INDEX)
      IDMP = 0
      ISTOP = 0
C
C READ PARAMETERS.
C
C     READ(1,101)  SIG, NTF, DPHI, LIST, FAC25K
      READ(1,101)  SIG, NTF, DPHI, LIST, NFAC
  101 FORMAT(F10.2, I5, F10.2, I5, F10.2)
      READ(1,102)  (DETH(I), I=1,6),  (ALPHA(I), I=1,6), (BETA(I),I=1,6)
  102 FORMAT(6F10.2 / 6F6.2, 5X, 6F6.2 )
      READ(1,103)  ((CURD(I,J), I=1,5), (CURM(I,J), I=1,5), J=1,5)
  103 FORMAT(5F6.1, 5F10.3 )
C
C
      STEP = 1.
      DO  7  I=1,6
      DBOTH(I+1) = DETH(I)
    7 CONTINUE
      DBOTH(1) = 0.0
C
C LOAD N ARRAYS AND CONVERT TO RADIANS AND HALVE.
C
      DO  9  I=1,6
      N(I) = DBOTH(I+1) - DBOTH(I) + 1
      RATH(I) = DETH(I)*DTR
      RATHH(I) = RATH(I)/ 2.
    9 CONTINUE
C
C WRITE PARAMETERS TO DISK ON REC 361.
      IREC = 361
C
C     WRITE(8'IREC)  DETH, ALPHA, BETA, SIG, CURD, CURM, DPHI, NTF,
C    1                FAC25K, LIST
      WRITE(8'IREC)  DETH, ALPHA, BETA, SIG, CURD, CURM, DPHI, NTF,
     1               NFAC, LIST
C     WRITE(3,301)  SIG, DPHI, DETH, ALPHA, BETA, N, NTF, FAC25K
      WRITE(3,301)  SIG, DPHI, DETH, ALPHA, BETA, N, NTF, NFAC
  301 FORMAT('1    INPUT  PARAMETERS ', /
     1   '0       SIGMA =', F4.1, 2X, 'MHO',  10X,
```

```
     2*INCREMENT OF PHI =', F5.2, / 1H0, 12X, 'REGION', 19X, 'I', 15X,
     3'II', 13X, 'III', 14X, 'IV', 14X, 'V', 15X, 'VI', /,
     4    ' THI, TH2, TH3, TH4, TH5, THF = ', 6(6X, F10.1), //,
     5    '       ALPHA ( 1 - 6 )       = ', 6(F8.2, 8X), /,
     6    '       BETA  ( 1 - 6 )       = ', 6(F8.2, 8X), /,
     7    '       POINTS PER REGION     = ', 5X, 6(I2, 14X), /,
     8    '                 NTF         = ', I3, //,
     9    '       UNIT OF CURRENT       = ', F10.2, '  * 10 K AMP ',///)
C    0    '       UNIT OF POTENTIAL     = ', F10.2, '  * 25 KV', // )
      WRITE(3,304)
  304 FORMAT(' DISTRIBUTION AND MAGNITUDE OF FIELD-ALIGNED CURRENTS',/)
      WRITE(3,210)
  210 FORMAT(' ',43X, 'TH1', 13X, 'TH2', 13X, 'TH3', 13X, 'TH4', 13X,
     1    'TH5', /)
      WRITE (3,305) ( CHAR(I,1), CHAR(2,1), ( CURD(I,J), CURM(I,J), J=
     1 1,5 ), I=1,5 )
  305 FORMAT ( 5 ( ' ', 1CX, 2A8, 11X, 5 ( F4.0, '(', F6.1, ')', 4X ),
     1 / ))
C
C CALL FOR COEFFICIENT AND CALCULATE POTENTIALS.
C
      CALL  DCOMP(CURD, CURP, SBCCU, CBCCU, CONST)
C
      CALL  KEISLM(ALPHA, BETA, RAT, SBCCL, CBCCU, COEFF)
C
      IKL = 1
      DO 5 I = 1, 6
      NN = N(I)
      DO 5 IZN = 1, NN
      KLAB(IKL) = DBCTH(I) + IZN - 1
      IKL = IKL + 1
    5 CONTINUE
      WRITE(3,302)  KLAB
  302 FORMAT(///, '   RAY ', T50, ' POTENTIALS ',/,
     1          '    PHI ', 1717, /, 2 ( '        ', 1717, / ) , //  )
      ROS = P/SIG
C
C *****  T H E   W A Y   I T   W A S   ********
C
C     P(1) = 0.0
C     P(6) = 0.0
C     DO 10  I=2,5
C     P(I) = -0.000C4*(-ALPHA(I-1)*P(I-1)
C    1                + ROS*CONST(I-1)*SIN(RAT(I-1)) )/ ALPHA(I)
C  10 CONTINUE
C
C LOOP FOR EACH PHI     1 -- 360 DEGREE WITH INCREMENT DPHI  INDEX = IP
C
      INCP = DPHI
      DO 400  IP = 1, 360, INCP
```

```
C
C SET  PMAX = 0  -- MAXIMUM POTENTIAL ALONG RAY.
C
      PMAX = 0.
      DO 8  I=1,NTF
      PHIR = I*PHDTR
      SP(I) = SIN(PHIR)
      CP(I) = COS(PHIR)
    8 CONTINUE
C
C CALCULATE POTENTIAL IN FOLLOWING LOOPS LOADING RAY ARRAY
C IR = 1 - 6  FOR EACH REGION,  IN = 1 -- N(IR) FOR NUMBER OF POINTS
C IN EACH REGION.
C
      DO 100  IR=1,6
      NN = N(IR)
      DO 80  IN=1, NN
      THR = CBOTH(IR) + IN - 1.
      IF( THR .EQ. 0. )  GO TO 15
      THHR = THR*DTR/2.
      JR = JR + 1
      CTT = COTAN(THHR)
      TT = TAN(THHR)
C
C GET POTENTIALS.
C
      OI = 0.0
      DO 20  NT=1,NTF
      CTTN = CTT**NT
      TTN = TT**NT
      TTN2 = TTN * TTN
      GO TO ( 510, 520, 520, 520, 520, 530 ), IR
  510 OI = OI + TTN*( ( COEFF(1,1,NT) - BETA(1) * COEFF ( 3,1,NT) ) *
     1       CP(NT) - ( BETA(1) * CCEFF(1,1,NT) + COEFF(3,1,NT) ) *
     2       SP(NT) )
      GO TO 20
  520 OI = OI + ( 1. / TTN) * ( ( CCEFF(1,IR,NT) * TTN2 - COEFF(2,IR,NT)
     1      -BETA(IR) * ( COEFF(3,IR,NT) * TTN2 + COEFF(4,IR,NT) ) ) *
     2  CP(NT) -  ( BETA(IR) * ( CCEFF(1,IR,NT) * TTN2 + COEFF(2,IR,NT))
     3  + CCEFF(3,IR,NT) * TTN2 - CCEFF(4,IR,NT) ) * SP(NT) )
      GO TO 20
  530 OI = OI + ( 1. / TTN ) * ( ( ( TTN2 - 1. ) * COEFF(1,6,NT) -
     1       BETA(6) * ( TTN2 + 1. ) * COEFF(3,6,NT) ) * CP(NT) - ( (
     2       TTN2 - 1. ) * CCEFF(3,6,NT) + BETA(6) * ( TTN2 + 1. ) *
     3      COEFF(1,6,NT) ) * SP(NT) )
   20 CONTINUE
C
      OI = OI * 2.5 / NFAC * ALPHA(IR) * SIG
      IF ( IR .EQ. 1  .OR. IR .EQ. 6 ) GO TO 30
      OI = OI + ( -P(IR) * ( IP * DTR * BETA(IR) *ALOG ( ABS ( TTN ))))
```

```
     1          * 2.5 * ALPHA(IR) * SIG / NFAC
      GO TO 30
C
   15 JR = 1
      C1 = 0.0
C
   30 PMAX = AMAX1( PMAX, ABS( C1 ) )
      RAY(JR) = C1
   80 CONTINUE
  100 CONTINUE
      WRITE(3,303)  IP, (RAY(I), I=1,51)
  303 FORMAT ( ' ', I3, T8, 17F7.2, /, 2 ( ' ', T8, 17F7.2, / ) , / )
C
C AT THIS TIME, WE HAVE A SET OF 46 POTENTIALS ALONG LINE OF PHI=CONST.
C NOW WE MUST INTERPOLATE FOR VALUES WE WANT (-4.0 TO 4.0 IN 0.2 STEPS)
C AND LOAD 'POTS' ARRAY.
C
      PMAX = AMIN1( PMAX, 4.CC )
      IPMX = PMAX/0.2
      IL = 21 - IPMX
      IH = 21 + IPMX
C
C LOOP THROUGH DESIRED POTENTIALS WE WISH TO FIND.
C
C FIRST SET 'POTS' ARRAY = 99.0
C
      DO 125  I=1,41
      DO 125  J=1,6
      POTS(I,J) = 99.0
      POTS2(I,J) = 99.0
  125 CONTINUE
      DO 300  J1=IL,IH
      SSM = 0
      SSM2 = 0
C
C POTENTIAL AT POTS(J1,XX) IS PS.
C
      PS = ( J1 - 21.)*0.2
      DO 130  J=1,6
      RG(J) = 0.
      RG2(J) = 0.
  130 CONTINUE
C
C LOOP THROUGH CALCULATED VALUES TO FIND OUT WHICH TWO PS IS BETWEEN
C AND SET INDICATORS AS EACH REGION IS LOADED.
C
      DO 200  J2=1,50
      IF ( KLAB(J2) .EQ. KLAB(J2+1) ) GO TO 200
      IF( RAY(J2) .LE. PS  .AND. PS .LT. RAY(J2+1) )  GO TO 140
      IF( RAY(J2) .GT. PS  .AND. PS .GE. RAY(J2+1) )  GO TO 150
```

```
      GO TO  200
  140 FAC = (PS - RAY(J2)) / (RAY(J2+1) - RAY(J2))
      TVAL = KLAB(J2) + FAC
      GO TO 160
  150 FAC = (PS - RAY(J2+1)) / (RAY(J2) - RAY(J2+1))
      TVAL = KLAB(J2+1) - FAC
  160 DO 170 J3=2,7
      IF( TVAL .GT. CBOTM(J3) )   GO TO 170
      IF( RG(J3-1) .EQ. 0.0 )   GO TO 162
      IF ( RG2(J3-1) .EQ. 0.0 ) GO TO 163
      REG = J3 - 1
      WRITE(3,320)  REG, PS, IP
C 320 FORMAT(*0    MORE THAN ONE PCINTS IN REGION *, F5.0,
  320 FORMAT(*0    MORE THAN TWO PCINTS IN REGION *, F5.0,
     1       *   FOR POTENTIAL = *, F6.2, *  ON RAY  *, I6, //)
      IDMP = 1
      GO TO 200
  162 RG(J3-1) = 1
      IXX = J3 - 1
      PCTS(J1,IXX) = TVAL
      GO TO 175
  163 RG2(J3-1) = 1.
      IXX = J3-1
      PCTS2(J1,IXX) = TVAL
      GO TO 176
  170 CONTINUE
C
C QUIT WHEN ALL 6 REGIONS LOADED.
C
  175 SSM = RG(1) + RG(2) + RG(3) + RG(4) + RG(5) + RG(6)
  176 SSM2 = RG2(1) + RG2(2) + RG2(3) + RG2(4) + RG2(5) + RG2(6)
      SSSS = SSM + SSM2
      IF (SSSS .EQ. 12. ) GO TO 300
  200 CONTINUE
  300 CONTINUE
C
C WRITE RECORD TO DISK AND PRINT IF ERROR.
C
      WRITE(8*IP)  PCTS
      IP2 = 400 + IP
      WRITE( 8*IP2 ) PCTS2
  325 IF( IDMP .EQ. 0 )  GO TO 400
      WRITE(3,308)  PCTS
      WRITE(3,308) PCTS2
  308 FORMAT( 6(* *, 21F6.2, / , *          *, 20F6.2 /) )
      ISTOP = ISTOP + IDMP
      IDMP = 0
C     IF( ISTOP .GE. 7 )  GO TO 900
  400 CONTINUE
      IF( LIST .NE. 1 )  GO TO 425
```

```
C
C WRITE OUT ENTIRE DISK FILE WHICH HAS BIG POTS ARRAY.
C
      WRITE(3,310)
  310 FORMAT('1  -- ENTIRE FILE FROM DISK -- BIG POTS ARRAY ', //)
      DO 410 J=1,2*CTRCP
      READ(8'JJ  ((PCTS(J1,J2),J1=1,41),J2=1,6)
      WRITE(3,312) J
  312 FORMAT( ' ', I5 )
      WRITE(3,308)  PCTS
      JJ = J + 400
      READ(8'JJ) ((PCTS2(J1,J2),J1=1,41),J2=1,6)
      WRITE(3,308) PCTS2
  410 CONTINUE
C
C
C
CCC   *-*-*-*-*       COMPUTE  ELECTRIC  FIELDS.      *-*-*-*-*-*-*-*-*-*-*-
C
C
C CONSTANTS USED ARE ALREADY IN ARRAYS 'COEFF' AND 'P'.
      425 IPEC = 363
C
C READ CARD GIVING STARTING AND ENDING POINTS OF LINE( PART OF GREAT
C CIRCLE ) ALONG WHICH E-FIELD PROFILE IS WANTED.
C PHI1, PHI2, AND THF
      WRITE(3,220)
  220 FORMAT('1', /)
      WRITE(3,221)
  221 FORMAT(' ', 2CX, 'PROFILES  OF  ELECTRIC  FIELD' )
C
  428 READ(1,112, END=5CC) PHI1, PHI2, THF
  112 FORMAT(3F10.1)
      DIF = PHI2 - PHI1
      DIFR = DIF*CTR
      THFR = THF*DTR
      CTHFR = COS(THFR)
      STHFR = SIN(THFR)
      CDIFR = COS(DIFR)
      SDIFR = SIN(DIFR/2.)
      COGAM = CTHFR*CTHFR + STHFR*STHFR*CDIFR
      SPAN = ARCCS(CCGAM)
      DSPAN = SPAN / DTR
      WSTEP = SPAN / 18C.
      DWSTE = WSTEP / DTR
      CANG = (CTHFR*SDIFR) / COS(SPAN/2.)
      SALCN = 0.C
      DO 460  II=1,181
      CSAL = COS(SALCN)
      SSAL = SIN(SALCN)
```

```
      CTH = CTHFR*CSAL + STHFR*SSAL*CANG
      THR = ARCOS(CTH)
      IF( THR  .LT.  C.CCC3 )  THR = 0.0
      IF( CTH .EQ. 1.)  GC TC 116
      STH = SIN(THR)
      APHI = ARCOS( (CSAL - CTH*CTHFR)/(STH*STHFR) )
      GO TO 114
  116 APHI = C.C
  114 PHIP = PHI1*DTR + APHI
      IF( ABS(PHIR)  .LT.  C.3CC3 )  PHIR = C.0
      SPHI = SIN(PHIR)
      CPHI = COS(PHIR)
      THD = THR/CTR
      TT = TAN(THR/2.0)
      IF( THD .LE. TH1 )  GC TC 430
      IF( THD .GE. TH5 )  GO TC 440
      DO 40  I=1,4
      KREG = I + 1
      IF( RATH(I) .LE. THR  .AND. THR .LT. RATH(KREG) )  GO TO 450
   40 CONTINUE
  430 ETHE = 0.0
      EPHI = 0.0
      DC 60  NT=1,NTF
      VAR = NT*PHIR
      SV = SIN(VAR)
      CV = COS(VAR)
      TTN = TT**(NT-1)
      ETHE = NT*( COEFF(1,1,NT)*SV + COEFF(3,1,NT)*CV)*TTN + ETHE
      EPHI = NT*( COEFF(1,1,NT)*CV - COEFF(3,1,NT)*SV)*TTN + EPHI
   60 CCNTINUE
      FAC = -125CO. / (R*COS(THR/2.)*COS(THR/2.))
      ETHE = FAC*ETHE
      EPHI = FAC*EPHI
      GC TO 470
  440 ETHE = 0.0
      EPHI = 0.0
      DC 70  NT=1,NTF
      VAR = NT*PHIR
      SV = SIN(VAR)
      CV = COS(VAR)
      TTN = TT**NT
      TTN2 = TTN*TTN
      ETHE = NT*((TTN2 - 1.)*(COEFF(1,6,NT)*SV + COEFF(3,6,NT)*CV)/TTN
     1     + ETHE
      EPHI = NT*((TTN2 + 1.)*(COEFF(1,6,NT)*CV - COEFF(3,6,NT)*SV)/TTN
     1     + EPHI
   7C CONTINUE
      FAC = -25000. / (R*STH)
      ETHE = FAC*ETHE
      EPHI = FAC*EPHI
```

```
      GO TO 470
  450 ETHE = 0.0
      EPHI = 0.0
      FAC = -25CC0. / (ROSTH)
      DO 90  NT=1,NTF
      VAR = NT*PHIR
      SV = SIN(VAR)
      CV = COS(VAR)
      TTN = TT**NT
      TTN2 = TTN*TTN
      ETHE = ETHE + (NT/TTN)*((CCEFF(1,KREG,NT)*TTN2 - CCEFF(2,KREG,NT))
     1        *SV + (COEFF13,KREG,NT)*TTN2 - COEFF(4,KREG,NT))*CV)
      EPHI = EPHI + (NT/TTN)*((CCEFF(1,KREG,NT)*TTN2 + COEFF(2,KREG,NT))
     1        *CV - (CCEFF3,KREG,NT)*TTN2 + COEFF(4,KREG,NT))*SV)
   90 CONTINUE
      ETHE = FAC*( P(KREC) + ETHE )
      EPHI = FAC*EPHI
C
  470 EY = -ETHE*CTH*SPHI - EPHI*CPHI
      CTP = CTH*CPHI
      EMTE = SQRT( ETHE*ETHE*(1.- CTP**2) + 2.*ETHE*EPHI*CTP*SPHI +
     1             EPHI*EPHI*CPHI*CPHI )
      IF( EY .LT. 0.C )  EMTE = -EMTE
      EMNTN = EPHI*SPHI - ETHE*CTP
      RAY(II) = EMTE
      RAI(II) = EMNTN
      PATH(II) = THD
      PAPH(II) = PHIR/DTR
      SALON = SALON + WSTEP
  460 CONTINUE
C
      WRITE(8*IREC)  PHI1, PHI2, THF, DSPAN, PATH
      IREC = IREC + 1
      WRITE(8*IREC)  PHI1, PHI2, THF, DWSTE, PAPH
      IREC = IREC + 1
      WRITE(8*IREC)  PHI1, PHI2, THF, RAY
      IREC = IREC + 1
      WRITE(3,316)   PHI1, PHI2, THF
  316 FORMAT( / *OPHI = *, F6.1, *        PHI2 = *, F6.1, *       THF = *
     1        , F5.1, // )
      WRITE(3,230)
  230 FORMAT(1H  3(8X, *PHI*, 2X, *THETA*, 7X, *EY*, 7X, *EX*, 2X), /)
      DO  600  I=1,4
      ONEAT(60,3.I) = 12345678.0
      ONEAT(61,3.I) = 12345678.0
  600 CONTINUE
      WRITE(3,318)  (((ONEA(I61,I2,I3), I3=1,4), I2=1,3), (I=1,61)
  318 FORMAT(61(* *, 5X, 3(F6.1, 2X, F5.1, 4X, F7.2, 2X, F7.2, 3X, *0*,
```

```
     1          3X), / ))
        GO TO 420
   900 CALL EXIT
       END
```

REFERENCES

Akasofu, S.-I., The aurora and the magnetosphere: The Chapman memorial lecture, Planet. Space Sci., 22, 885, 1974.

Armstrong, J. C., S.-I. Akasofu and G. Rostoker, A comparison of satellite observations of Birkeland currents with ground observations of visible aurora and ionospheric currents, J. Geophys. Res., in press, 1975.

Armstrong, J. C. and A. J. Zmuda, Triaxial magnetic measurements of field-aligned currents at 800km in the auroral region: Initial results, J. Geophys. Res., 78, 6802, 1973.

Axford, W. I. and C. O. Hines, Aunifying theory of high-latitude geophysical phenomena and geomagnetic storms, Can. J. Phys., 39, 1433, 1961.

Brekke, A., J. R. Doupnik and P. M. Banks, Incoherent scatter measurements of E region conductivities and currents in the auroral zone, J. Geophys. Res., 79, 3773, 1974.

Boström, R., Currents in the ionosphere and magnetosphere, Ann. Geophys., 24, 681, 1968.

Dungey, J. W., Interplanetary magnetic field and the auroral zones, Phys. Rev. Letters, 6, 47, 1961.

Fejer, J. A., Theory of the geomagnetic disturbance variations, J. Geophys. Res., 69, 123, 1964.

Feldstein, Y. I. and G. V. Starkov, Dynamics of auroral belt and polar geomagnetic disturbances, Planet. Space Sci., 15, 209, 1967.

Fukushima, N. and Y. Kamide, Partial ring current models for worldwide geomagnetic disturbances, Rev. Geophys. Space Phys., 11, 795, 1973.

Galperin, Yu. I., V. N. Ponomarev and A. G. Zosimova, Plasma convection in polar ionosphere, Ann. Geophys., 30, 1, 1974.

Gurnett, D. A. and L. A. Frank, Observed relationship between electric fields and auroral particle precipitation, J. Geophys. Res., 78, 145, 1973.

Haerendel, G. and R. Lüst, Electric fields in the ionosphere and magnetosphere, in particle and fields in the magnetosphere, edited by B. M. McCormac, p. 213, D. Reidel, Dordrecht, Netherlands, 1970.

Heppner, J. P., Electric field variations during substorms, Planet. Space Sci., 20, 1475, 1972.

Heppner, J. P., J. D. Stolarik and E. M. Wescott, Field-aligned continuity of Hall current electrojets and other consequences of density gradients in the auroral ionosphere, in the radiating atmosphere, edited by B. M. McCormac, p. 407, D. Reidel, Dordrecht, Netherlands, 1971.

Iijima, T. and T. Nagata, Signatures for substorm development of the growth phase and expansion phase, Planet. Space Sci., 20, 1095, 1972.

Iwasaki, N. and A. Nishida, Ionospheric current system produced by an external electric field in the polar cap, Rep. Ionos. Space Res., Japan, 21, 17, 1967.

Jaggi, R. K. and R. A. Wolf, Self-consistent calculation of the motion of a sheet of ions in the magnetosphere, J. Geophys. Res., 78, 2852, 1973.

Kamide, Y. and N. Fukushima, Positive geomagnetic bays in evening high-latitudes and their possible connection with partial ring current, Rep. Ionos. Res. Space Res., Japan, 26, 79, 1972.

Kamide, Y., S.-I. Akasofu, S. E. Deforest and J. L. Kisabeth, Weak and intense substorms, Planet. Space Sci., in press, 1975.

Kamide, Y. and S.-I. Akasofu, The auroral electrojet and global auroral features, J. Geophys. Res., in press, 1975.

Kamide, Y., F. Yasuhara, S.-I. Akasofu and A. Brekke, Ionospheric current obtained from the Chatanika radar and ground magnetic perturbation at auroral latitudes, in preparation, 1975.

Kawasaki, K., C.-I. Meng and Y. Kamide, The development of three-dimensional current system during a magnetospheric substorm, Planet. Space Sci., 22, 1471, 1974.

Kennel, C. F., Consequences of a magnetospheric plasma, Rev. Geophys., 7, 379, 1969.

Leont'sev, S. V., V. B. Lyatskiy and Y. P. Mal'tsev, DP2 current system in its place in the development of a substorm, Geomag. Aeronomy, 14, 91, 1974.

Maeda, H. and K. Maekawa, A numerical study of polar ionospheric currents, Planet. Space Sci., 21, 1287, 1973.

Mal'tsev, Yu. P., S. V. Leont'yev and V. B. Lyatskiy, Electric fields and currents in the boundary region of electrojets, Geomagn. and Aeronomy, 13, 910, 1973.

Rostoker, G. and J. L. Kisabeth, Response of the polar electrojets in the evening sector to polar magnetic substorms, J. Geophys. Res., 78, 5559, 1973.

Swift, D. W., Possible consequences of the asymmetric development of the ring current belt, Planet. Space Sci., 15, 835, 1967.

Swift, D. W., Possible mechanisms for formation of the ring current belt, J. Geophys. Res., 76, 2276, 1971.

Swift, D. W. and D. A. Gurnett, Direction comparison between satellite electric field measurements and the visual aurora, J. Geophys. Res., 78, 7306, 1973.

Vasyliunas, V. M., Mathematical models of magnetospheric convection and its coupling to the ionosphere, in particles and fields in the magnetosphere, edited by B. M. McCormac, p. 60, D. Reidel, Dordrecht, Netherlands, 1970.

Vasyliunas, V. M., The relationship of magnetospheric process in Earth's magnetospheric process, edited by B. M. McCormac, p. 29, D. Reidel, Dordrecht, Netherlands, 1971.

Wescott, E. M., J. D. Stolarik and J. P. Heppner, Auroral and polar cap electric fields from barium releases, in particle and fields in the magnetosphere, edited by B. M. McCormac, p. 229, D. Reidel, Dordrecht, Netherlands, 1970.

Winningham, J. D., F. Yasuhara, S.-I. Akasofu and W. Heikkila, The precipitation pattern of electrons (50eV - 10keV) during a quiet and substorm times in the 22-03 MLT sector, J. Geophys. Res., in press, 1975.

Wolf, R. A., Effects of ionospheric conductivity on convective flow of plasma in the magnetosphere, Geophys. Res., 75, 4677, 1974.

Żmuda, A. J. and J. C. Armstrong, The diurnal variation of the region with vector magnetic field changes associated with field-aligned currents, J. Geophys. Res., 79, 2501, 1974a.

Żmuda, A. J. and J. C. Armstrong, The diurnal flow pattern of field-aligned currents, J. Geophys. Res., 79, 4611, 1974b.